

## What can galaxy shapes tell us about physics beyond the standard model?

Oliver H. E. Philcox<sup>1,2,\*</sup>, Morgane J. König,<sup>3</sup> Stephon Alexander,<sup>4,5</sup> and David N. Spergel<sup>6</sup>

<sup>1</sup>*Simons Society of Fellows, Simons Foundation, 160 5th Avenue, New York, New York 10010, USA*

<sup>2</sup>*Center for Theoretical Physics, Columbia University, New York, New York 10027, USA*

<sup>3</sup>*Department of Physics, Massachusetts Institute of Technology, 77 Massachusetts Avenue, Cambridge, Massachusetts 02139, USA*

<sup>4</sup>*Brown Theoretical Physics Center and Department of Physics, Brown University, 182 Hope Street, Providence, Rhode Island, 02903, USA*

<sup>5</sup>*Center for Computational Astrophysics, Flatiron Institute, 162 5th Ave, New York, New York 10010, USA*

<sup>6</sup>*Simons Foundation, 160 5th Ave, New York, New York 10010, USA*



(Received 17 November 2023; accepted 22 February 2024; published 28 March 2024)

The shapes of galaxies trace scalar physics in the late-Universe through the large-scale gravitational potential. Are they also sensitive to higher-spin physics? We present a general study into the observational consequences of vector and tensor modes in the early and late Universe, through the statistics of cosmic shear and its higher-order generalization, flexion. Higher-spin contributions arise from both gravitational lensing and intrinsic alignments, and we give the leading-order correlators for each (some of which have been previously derived), in addition to their flat-sky limits. In particular, we find nontrivial sourcing of shear  $EB$  and  $BB$  spectra, depending on the parity properties of the source. We consider two sources of vector and tensor modes: scale-invariant primordial fluctuations and cosmic strings, forecasting the detectability of each for upcoming surveys. Shear is found to be a powerful probe of cosmic strings, primarily through the continual sourcing of vector modes; flexion adds little to the constraining power except on very small scales ( $\ell \gtrsim 1000$ ), though it could be an intriguing probe of as-yet-unknown rank-three tensors or halo-scale physics. Such probes could be used to constrain new physics proposed to explain recent pulsar timing array observations.

DOI: [10.1103/PhysRevD.109.063541](https://doi.org/10.1103/PhysRevD.109.063541)

### I. INTRODUCTION

Through current observational projects such as DES, KiDS, and HSC (e.g., [1–4]), and forthcoming experiments such as Rubin and Roman (e.g., [5,6]), we will measure the apparent shapes of hundreds of millions of galaxies across a wide range of redshifts. The technical barriers associated with such measurements are huge; thanks to decades of computational, observational, and theoretical work, we are now in a regime where they can be made robustly, facilitating their use in modern cosmological analyses.

The principal use of galaxy shape catalogs is as a probe of the underlying matter density of the Universe (e.g., [7–11]). Due to gravitational lensing, photons emitted from some distant galaxy are continuously deflected by matter as they traverse the vast expanses of space before reaching our telescopes; as such, their deflection angle encodes the gravitational potential,  $\Phi$ , projected along the line of sight. For coherent sources such as galaxies, the net effect of lensing is to distort the shape of the galaxies, such that an initially circular projection is distorted to an ellipse

(at leading order). Furthermore, the intrinsic shape of the galaxy is itself a probe of  $\Phi$  (which itself can contain novel physics [e.g., [12–14]]), through tidal interactions as the galaxy forms (e.g., [15–20]). Collating the distortions measured from millions of objects (accounting for their significant noise) yields a large-scale map of  $\Phi$ , or, through the Poisson equation, the matter density,  $\rho_m$ .

*a. Vectors and tensors* A full description of gravitational lensing involves not just the scalar part of the metric,  $h_{00} \propto \Phi$ , but also vector and tensor parts,  $h_{0i}$  and  $h_{ij}$  (e.g., [21–24]). The same holds also for the intrinsic shapes of galaxies, again through the tidal tensor,  $t_{ij}$  [25], though these have been little discussed for vector modes. As such, the shapes of galaxies provide a window into the vector and tensor sectors of the Universe that are hard to observe in other probes (such as galaxy density, at leading order [26,27]). In the standard cosmological model, we expect such contributions to be trivially small; however, nonstandard cosmological models can source vector and tensor modes, and thus be probed using galaxy shapes.

There exist a large number of theoretical models capable of generating vector and tensor modes in the late Universe. Many such scenarios are rooted in inflation, principally

\*ohep2@cantab.ac.uk

from the appearance of vector and tensor fields, for example in vector inflation and axionic models optionally including Chern-Simons interactions [28–35]. They can also be sourced from single field inflation; whilst primordial vectors decay quickly, primordial gravitational waves (tensor modes) are a signature of many canonical scenarios (see e.g., [36] for recent constraints). An array of late-time sources are also possible, driven by old and new fields. Many of these are motivated by our lack of understanding of dark energy; modified gravity scenarios such as quintessence, vector dark energy, and Chern-Simons general relativity, could lead to a spectrum of new perturbations which become relevant at late times, thereby evading constraints from the cosmic microwave background (e.g., [29,37–41]). A network of cosmic strings (arising from some symmetry breaking scenario, such as GUT models) would also lead to continuous production of vector and tensor modes, and thus distortion of galaxy shapes (e.g., [24,42,43]). These are of particular current relevance (e.g., [44]) given their plausibility as a model for explaining the recent detection of a stochastic gravitational wave background from pulsar timing array experiments [45–48]. Finally, such physics could conceivably break parity symmetry; to some extent, this is expected from primordial phenomena such as baryogenesis (e.g., [32,49,50]), and is of particular current interest given the potential detections on the CMB and distribution of galaxies [51–58] (though see the no-go theorems in [59,60]).

*b. Shear and flexion* To make use of the tranche of cosmological information contained within galaxy shapes, we require some way of distilling this information. Conventionally, this is performed by considering the “shear” of galaxies,  $\gamma_{ij}$ , which measures their ellipticity (e.g., [7,9]). Since this is a rank-two tensor, it is sensitive to rank-two components of the metric, including  $\partial_i \partial_j h_{00}$ ,  $\partial_i h_{0j}$ ,  $h_{ij}$ , i.e., scalars, vectors, and tensors. In general, the shear is computed for each galaxy of interest, which are combined to make full-sky maps, usually expressed in terms of electric and magnetic components,  $\gamma^E$  and  $\gamma^B$ . By measuring the two-point correlation functions, particularly  $\langle \gamma^E \gamma^{E*} \rangle$ , we can probe the power spectrum of matter, and thus constrain parameters such as the matter density and clustering amplitude, as well as more esoteric physics such as primordial non-Gaussianity from higher-spin particles [12]. For vectors and tensors, there is information also in the  $B$ -mode spectra, such as  $\langle \gamma^B \gamma^{B*} \rangle$ , with parity-violating physics appearing in the cross-spectra  $\langle \gamma^E \gamma^{B*} \rangle$ . Further information may also arise in higher-order correlators and cross-spectra, which probe bispectra and beyond (cf. [61] for scalar physics, and [12,62–64] for other applications including [anisotropic] primordial non-Gaussianity and higher-spin inflationary phenomena).

The gravitational distortions of galaxies are not fully encapsulated by the shear tensor,  $\gamma_{ij}$ . At next order, one

can define the “flexion” components,  $\mathcal{F}_{ijk}$ , and  $\mathcal{G}_{ijk}$ , which parametrize the octopole moments of an image (e.g., [65–71]). This is a rank-three tensor, and thus sensitive of scalar, vector, and tensor physics.<sup>1</sup> It may also be a probe of new physics sourced by some irreducible rank-three tensor, such as torsion. In this case, the field can be written in terms of “gradient” and “curl” modes; only the latter is sourced by standard model physics, e.g.,  $\langle \mathcal{F}^{g*} \mathcal{F}^g \rangle$ . Flexion has been discussed in a range of previous works, with the general conclusion being that it becomes useful in scalar analyses only on very small scales (e.g., [66,70]); here, we include the flexion in a complete manner, and assess whether the above conclusions remain true for vector and tensor physics.

In the remainder of this work, we will present an in-depth overview of the effects of vector and tensor physics on shear and flexion, considering both intrinsic and extrinsic (lensing) contributions, providing a general dictionary of novel phenomena to galaxy shapes. To this end, we will first set out our conventions for new physics in Sec. II via their impact on the metric tensor, and give two motivating examples of beyond- $\Lambda$ CDM physics, before presenting a pedagogical overview of galaxy shape observables in Sec. III. In Sec. IV, we will discuss the sourcing of shear and flexion by scalars, vectors, and tensors, before giving the associated power spectra in Sec. V, including their small-scale limiting forms. To put our results in context, Sec. VI considers the ability of upcoming cosmic shear surveys to detect vector and tensor modes using the two fiducial models discussed in Sec. II (sourced by inflation and cosmic strings). Finally, we conclude in Sec. VII. Appendix A provides a brief summary of the two-sphere mathematics used in this work, with Appendix B outlining our cosmic string tensor model. Finally, Appendices C and D derive full-sky power spectra associated with intrinsic and extrinsic vector modes, and Appendix E lists the mathematical kernels appearing in the power spectra.

## II. SCALARS, VECTORS, AND TENSORS

### A. General formalism

Weak gravitational interactions induce a distortion in the background (FRW) metric of the Universe, which takes the form

$$ds^2 = a^2(\eta)(\eta_{\mu\nu} + h_{\mu\nu})dx^\mu dx^\nu, \quad (1)$$

where  $\eta$  and  $x^i$  are conformal time and comoving space,  $\eta_{\mu\nu}$  is the flat-space metric, and  $a(\eta)$  is the scale factor (e.g., [72–74]). In the weak field limit, the perturbation  $h_{\mu\nu}$  can be

<sup>1</sup>Whilst one can go further still and define a rank-four tensor, it is not of interest to this work (though it can enable constraints on spin-four primordial non-Gaussianity transferred to the scalar sector [12]).

decomposed into independent scalar, vector, and tensor modes, with the scalar part taking the form

$$h_{00}^S = -2\Psi(\mathbf{x}, \eta), \quad h_{0i}^S = h_{i0}^S = 0, \quad h_{ij}^S = -2\Phi(\mathbf{x}, \eta)\delta_{ij}^K, \quad (2)$$

in the conformal-Newtonian gauge, where  $\Phi$  and  $\Psi$  are the Bardeen potentials. In the absence of anisotropic stress,  $\Phi = \Psi$ ; this will be assumed below. In the presence of vector modes, we can write

$$h_{00}^V = 0, \quad h_{0i}^V = h_{i0}^V = B_i(\mathbf{x}, \eta), \quad h_{ij}^V = \partial_j H_i + \partial_i H_j, \quad (3)$$

for divergence-free vectors  $B_i$  and  $H_i$ . Again working in the conformal-Newtonian gauge, we can set  $H_i = 0$  and consider only  $B_i$  (equivalent to working with the gauge-invariant potential  $-\sigma_{g,i} = B_i - \partial_\eta H_i$  [24]). Finally, the tensor degrees of freedom can be written in the form (again working in the conformal-Newtonian gauge)

$$h_{00}^T = 0, \quad h_{0i}^T = h_{i0}^T = 0, \quad h_{ij}^T = h_{ij}, \quad (4)$$

where  $h_{ij}$  (not to be confused with  $h_{\mu\nu}$ ) is the transverse-traceless rank-two tensor associated with gravitational wave propagation.

In the discussion below, we will find it useful to expand the metric perturbations in Fourier-space via the relations (e.g., [75,76])

$$\begin{aligned} \Phi(\mathbf{x}, \eta) &= \int_{\mathbf{k}} e^{i\mathbf{k}\cdot\mathbf{x}} \Phi(\mathbf{k}, \eta), \\ B_i(\mathbf{x}, \eta) &= \int_{\mathbf{k}} e^{i\mathbf{k}\cdot\mathbf{x}} \sum_{\lambda=\pm} e_i^{(\lambda)}(\hat{\mathbf{k}}) B_\lambda(\mathbf{k}, \eta), \\ h_{ij}(\mathbf{x}, \eta) &= \int_{\mathbf{k}} e^{i\mathbf{k}\cdot\mathbf{x}} \sum_{\lambda=\pm} e_{ij}^{(\lambda)}(\hat{\mathbf{k}}) h_\lambda(\mathbf{k}, \eta), \end{aligned} \quad (5)$$

where  $\int_{\mathbf{k}} \equiv \int d\mathbf{k}/(2\pi)^3$ . Here, we have decomposed the vector and tensor modes in *helicity states*, defined as

$$e^{(\pm)}(\hat{\mathbf{k}}) \equiv (\hat{\mathbf{e}}_1 \mp i\hat{\mathbf{e}}_2)/\sqrt{2}, \quad e_{ij}^{(\pm)}(\hat{\mathbf{k}}) \equiv e_i^{(\pm)}(\hat{\mathbf{k}})e_j^{(\pm)}(\hat{\mathbf{k}}), \quad (6)$$

where  $\{\mathbf{e}_1, \mathbf{e}_2, \hat{\mathbf{k}}\}$  is a locally orthonormal basis set. As such, the impact of scalar, vector, and tensor modes on the metric, and thus gravitational lensing, is controlled by the (scalar) helicity components  $\{\Phi, B_\pm, h_\pm\}$ .

Most metric perturbations of interest in cosmology are controlled by stochastic processes such as inflationary quantum mechanical fluctuations, and are thus random fields. As such, their properties can be encapsulated by correlation functions, the simplest of which are power spectra:

$$\begin{aligned} \langle \Phi(\mathbf{k}, \eta)\Phi^*(\mathbf{k}', \eta') \rangle &= P_\Phi(k, \eta, \eta') \times (2\pi)^3 \delta_D(\mathbf{k} - \mathbf{k}') \\ \langle B_\lambda(\mathbf{k}, \eta)B_{\lambda'}^*(\mathbf{k}', \eta') \rangle &= \delta_{\lambda\lambda'}^K \times P_{B_\lambda}(k, \eta, \eta') \times (2\pi)^3 \delta_D(\mathbf{k} - \mathbf{k}') \\ \langle h_\lambda(\mathbf{k}, \eta)h_{\lambda'}^*(\mathbf{k}', \eta') \rangle &= \delta_{\lambda\lambda'}^K \times P_{h_\lambda}(k, \eta, \eta') \times (2\pi)^3 \delta_D(\mathbf{k} - \mathbf{k}'), \end{aligned} \quad (7)$$

(noting that the mean of each field can be set to zero according to the equivalence principle). Here, we have assumed that the relevant physics is homogeneous (leading to the Dirac delta) and isotropic (such that the correlators depend only on  $|\mathbf{k}|$ ); furthermore, the different helicity states are uncorrelated. Finally, we may optionally assert parity conservation (i.e., symmetry under point reflections): this enforces  $P_{B_+} = P_{B_-}$  and  $P_{h_+} = P_{h_-}$ , though this is not generically required.<sup>2</sup>

Additional information on the metric perturbations is provided by the Einstein equations, which specify the time evolution of fluctuations. For the scalar sector, their linearization leads to the well-known form  $\Phi(\mathbf{k}, \eta) \equiv T_S(\eta)\Phi(\mathbf{k}, \eta_0)$ , where the transfer function  $T_S(\eta)$  is constant in matter domination, and we normalize to the value of the spectrum today (at  $\eta = \eta_0$ ). From the  $ij$  part of the perturbed Einstein equation, we obtain the following equations for the evolution of vector and tensor modes (e.g., [77,78]):

$$\begin{aligned} B'_i(\mathbf{x}, \eta) + 2\mathcal{H}(\eta)B_i(\mathbf{x}, \eta) &= -16\pi G a^2(\eta) \frac{\partial^j}{\nabla^2} \delta T_{ij}^V(\mathbf{x}, \eta) \\ h''_{ij}(\mathbf{x}, \eta) + 2\mathcal{H}(\eta)h'_{ij}(\mathbf{x}, \eta) - \nabla^2 h_{ij}(\mathbf{x}, \eta) &= 16\pi G a^2(\eta) \delta T_{ij}^T(\mathbf{x}, \eta). \end{aligned} \quad (8)$$

Here, primes denote derivatives with respect to conformal time,  $\mathcal{H}(\eta) \equiv a'(\eta)/a(\eta)$  is the conformal Hubble parameter, and  $\delta T_{ij}^{V,T}$  are the vector and tensor parts of the perturbed stress-energy tensor. From this equation, it is clear that vector and tensor modes can be either (a) primordial, evolving under the homogeneous equations, or (b) dynamically sourced by phenomena contributing to the nonscalar stress-energy tensor (such as cosmic strings and neutrino free-streaming). In the next section, we will consider examples of each form.

## B. Motivating examples

### 1. Inflationary perturbations

In the standard paradigm, quantum fluctuations in inflation source scalar perturbations to the metric, which seed structure formation in the late Universe. A variety of models also predict a primordial spectrum of vector and tensor modes, for example due to gauge fields active in

<sup>2</sup>In gravitational wave literature, the total gravitational wave power spectrum is often denoted  $P_h = P_{h_+} + P_{h_-}$ .

inflation or large excursions of the inflaton. Conventionally, such spectra are parametrized as power laws:

$$P_B(k) = r_V(k_0) \times \frac{2\pi^2}{k^3} \Delta_\zeta^2(k_0) \left(\frac{k}{k_0}\right)^{n_V-1},$$

$$P_h(k) = r_T(k_0) \times \frac{2\pi^2}{k^2} \Delta_\zeta^2 \left(\frac{k}{k_0}\right)^{n_T}, \quad (9)$$

where  $k_0 = 0.002 \text{ Mpc}^{-1}$  is a fiducial scale,  $n_X$  is a slope, and  $r_X$  specifies the amplitude relative to the scalar power spectrum amplitude,  $\Delta_\zeta^2$ . For  $n_V = 1$ ,  $n_T = 0$ , we find a scale-invariant form. Observations of the CMB place strong constraints on tensors, with  $r_T(k_0) \lesssim 0.03$  [36,79] with a fiducial value  $n_T = -r_T/8$ . In some scenarios, the primordial perturbations can violate parity symmetry (as discussed in Appendix B of [25]); in this case, there is a different amplitude for the two parity states, with

$$P_{B_\pm}(k) = (1 \pm \epsilon_V) P_B(k), \quad P_{h_\pm}(k) = (1 \pm \epsilon_T) P_h(k), \quad (10)$$

for chirality parameter  $\epsilon_X$ .

To model vector and tensor modes in the late Universe, we require the evolution of  $B_i$  and  $h_{ij}$  as well as the primordial form. This is obtained by solving the homogeneous version of (9), yielding (e.g., [78]):

$$B_i(\mathbf{k}, \eta) = T_V(\eta) B_i(\mathbf{k}, \eta_*), \quad T_V(\eta) = \left(\frac{a(\eta_*)}{a(\eta)}\right)^2$$

$$h_{ij}(\mathbf{k}, 0) = T_T(k, \eta) h_{ij}(\mathbf{k}), \quad T_T(k, \eta) \approx \frac{3j_1(k\eta)}{k\eta}, \quad (11)$$

where  $\eta_*$  is some reference scale and we give the approximate form for the tensor transfer function in matter domination. In this regime, the vector modes decay away quickly, whilst the tensor modes evolve much more slowly, and propagate as a damped wave. For this reason, vector modes are rarely considered in cosmology, since those produced only by inflation are vanishingly small at late times.

Incorporating these transfer function definitions, we can write the power spectra in separable form:

$$\langle \Phi(\mathbf{k}, \eta) \Phi^*(\mathbf{k}', \eta') \rangle = T_S(\eta) T_S(\eta') P_\Phi(k) \times (2\pi)^3 \delta_D(\mathbf{k} - \mathbf{k}')$$

$$\langle B_\lambda(\mathbf{k}, \eta) B_{\lambda'}^*(\mathbf{k}', \eta') \rangle = \delta_{\lambda\lambda'}^K \times T_V(\eta) T_V(\eta') P_{B_\lambda}(k) \times (2\pi)^3 \delta_D(\mathbf{k} - \mathbf{k}')$$

$$\langle h_\lambda(\mathbf{k}, \eta) h_{\lambda'}^*(\mathbf{k}', \eta') \rangle = \delta_{\lambda\lambda'}^K \times T_T(k, \eta) T_T(k, \eta') P_{h_\lambda}(k) \times (2\pi)^3 \delta_D(\mathbf{k} - \mathbf{k}'); \quad (12)$$

this holds true in the linear regime for any primordial perturbations in the early Universe.

## 2. Cosmic strings

An example of late-time new physics that could generate detectable vector and tensor modes is cosmic strings (e.g., [24,41–43,80–82]). These are one-dimensional topological defects that are a generic prediction of any grand unification model, sourced by phenomena such as spontaneous symmetry breaking or from superstring theory. A network of strings will contribute to the late-time energy momentum tensor through anisotropic stress, and thus act as a non-decaying source for both vector and tensor metric perturbations  $B_i$  and  $h_{ij}$ . These source photon-baryon vorticity,

and thus generate CMB  $B$ -modes, allowing them to be indirectly constrained [41]. They could also be a possible source of the signal detected in recent pulsar timing array experiments [44].

Full modeling of the cosmic string correlators is non-trivial, and beyond the scope of this work. For our purposes, we consider only a simple prescription (known as the “velocity-dependent one-scale” model), which posits a Poissonian sample of string segments with some tension  $G\mu$  and intercommuting (i.e., reconnecting) probability  $P$  (following [e.g., [24]]). Each Nambu-Goto string segment can be described by a position  $\sigma$  and a (conformal) time  $\eta$  on the string world sheet, and give the following contribution to the stress-energy tensor in the transverse gauge [43]:

$$\delta T^{\mu\nu}(\mathbf{x}, \eta) = \mu \int d\sigma \begin{pmatrix} 1 & -\partial_\eta x^i \\ -\partial_\eta x^j & \partial_\eta x^i \partial_\eta x^j - \partial_\sigma x^i \partial_\sigma x^j \end{pmatrix} \delta_D(\mathbf{x} - \mathbf{x}(\sigma, \eta)). \quad (13)$$

Using the Einstein equations (8), we can compute the vector and tensor metric perturbations arising from the strings, and thus the associated power spectrum of  $B_i$  and  $h_{ij}$ . For the vector modes, an explicit calculation can be found in [24]; for tensors, we provide a derivation in Appendix B. Following a number of simplifying assumptions (detailed in Appendix B), we obtain the following forms for the equal-time power spectrum of vector and tensor modes:

$$\begin{aligned}
P_{B_{\pm}}(k, \eta, \eta) &= (16\pi G\mu)^2 \frac{2\sqrt{6}\pi v_{\text{rms}}^2}{3(1-v_{\text{rms}}^2)} \frac{4\pi\chi^2 a^4}{H} \left(\frac{a}{k\xi}\right)^5 \operatorname{erf}\left[\frac{k\xi/a}{2\sqrt{6}}\right], \\
P_{h_{\pm}}(k, \eta, \eta) &= (16\pi G\mu)^2 \frac{\sqrt{6}\pi}{9(1-v_{\text{rms}}^2)} \frac{4\pi\chi^2 a^4}{H} \left(\frac{a}{k\xi}\right)^5 \operatorname{erf}\left[\frac{k\xi/a}{2\sqrt{6}}\right] [v_{\text{rms}}^4 + (1-v_{\text{rms}}^2)^2],
\end{aligned} \tag{14}$$

where  $v_{\text{rms}}$  and  $\xi$  are the average string velocity and length,  $H$  is the Hubble parameter, and  $a$  is the scale factor (dropping the  $\eta$ -dependence for clarity). As in [24], we will assume the fiducial values  $\xi = 1/(H\gamma_s)$ ,  $v_{\text{rms}}^2 = (1 - \pi/3\gamma_s)/2$ , with correlation length  $\gamma_s = (\pi\sqrt{2}/3\tilde{c}P)^{1/2}$  for  $\tilde{c} \approx 0.23$  and  $P \approx 10^{-3}$  [82]. Notably, the spectra do not depend on the helicity state, thus the effects are parity-conserving. These forms will be used in Sec. VI to forecast the detectability of the cosmic string tension parameter  $G\mu$  from galaxy shape statistics.

### III. GALAXY SHAPE OBSERVABLES

#### A. Shear and flexion: Single sources

A photometric galaxy dataset consists of a large number of two-dimensional galaxy images, sorted into redshift bins. As discussed above, our main interest is not the images themselves, but their distortions; this can be parametrized in terms of the image moments (defined in some locally orthogonal basis  $\{\hat{e}_1, \hat{e}_2\}$ ; e.g., [9]):

$$Q_{i_1 \dots i_n} \equiv \frac{\int d\vec{\theta} I(\vec{\theta}) \Delta\theta_{i_1} \dots \Delta\theta_{i_n}}{\int d\vec{\theta} I(\vec{\theta})}, \quad i \in \{1, 2\}. \tag{15}$$

This depends on the observed brightness profile  $I(\vec{\theta})$ , and the position vector  $\Delta\vec{\theta}$ , relative to some suitably defined image center. Noting that the first moment  $Q_i$  vanishes (due to the definition of  $\Delta\vec{\theta}$ ), the simplest way to parametrize the image distortions is via the dimensionless *shear parameters*:

$$\gamma_1 \equiv \frac{1}{2} \frac{Q_{11} - Q_{22}}{\zeta_2}, \quad \gamma_2 \equiv \frac{1}{2} \frac{Q_{12} + Q_{21}}{\zeta_2}, \tag{16}$$

for  $\zeta_2 \equiv Q_{11} + Q_{22}$ . The complex shear,  $\gamma_1 \pm i\gamma_2$ , is a spin- $\pm 2$  quantity; under rotation of the  $\hat{e}_i$  basis vectors by an angle  $\varphi$ , it transforms as  $(\gamma_1 \pm i\gamma_2) \rightarrow e^{\pm 2i\varphi}(\gamma_1 \pm i\gamma_2)$ . Analysis of almost all current photometric surveys proceeds by measuring the shear of each galaxy, combining them to produce redshift-binned maps, then using the statistics of these to place constraints on cosmology, through a theoretical model of lensing and intrinsic effects [1–4,83].

Whilst the shear fully encapsulates the quadrupolar distortions of the image, there is more information to be found if one looks also to the octopole moments, through the fully symmetric tensor  $Q_{ijk}$  [12,68,69]. Much as the

image quadrupole can be used to form spin- $\pm 2$  quantities ( $\gamma_1 \pm i\gamma_2$ ), the image octopole can be used to form spin- $\pm 1$  and spin- $\pm 3$  quantities, known as flexion of the first and second kind:

$$\begin{aligned}
\mathcal{F}_1 &\equiv \frac{4}{9} \frac{Q_{111} + Q_{122}}{\xi}, & \mathcal{F}_2 &\equiv \frac{4}{9} \frac{Q_{112} + Q_{222}}{\zeta_3}, \\
\mathcal{G}_1 &\equiv \frac{4}{3} \frac{Q_{111} - 3Q_{122}}{\zeta_3}, & \mathcal{G}_2 &\equiv \frac{4}{3} \frac{3Q_{112} - Q_{222}}{\zeta_3},
\end{aligned} \tag{17}$$

where the normalization is given in terms of the image hexadecapole;  $\zeta_3 \equiv Q_{1111} + 2Q_{1122} + Q_{2222}$ . Under rotation by  $\varphi$ , the complex-valued flexions transform as  $(\mathcal{F}_1 \pm i\mathcal{F}_2) \rightarrow e^{\pm i\varphi}(\mathcal{F}_1 \pm i\mathcal{F}_2)$ ,  $(\mathcal{G}_1 \pm i\mathcal{G}_2) \rightarrow e^{\pm 3i\varphi}(\mathcal{G}_1 \pm i\mathcal{G}_2)$ , thus they are spin-one and spin-three respectively. Unlike a number of previous works (e.g., [65,69]), we will take flexion to be defined by (17), rather than considering them to be a derived quantity arising in second-order lensing. The effects of shear and flexion on a circular source are depicted in Fig. 1.

#### B. Shear and flexion: Full-sky

By combining the shear and flexion measurements from a large catalog of galaxies, we can produce maps of the large-scale distortion fields binned in comoving distance,  $\chi$ . These are defined as

$$X_a(\hat{n}) = \int_0^{\chi_H} d\chi n_a(\chi) X(\chi\hat{n}, \chi), \quad X \in \{\gamma, \mathcal{F}, \mathcal{G}\}, \tag{18}$$

where  $X(\chi\hat{n}, \chi)$  is the shear or flexion at position  $\mathbf{x} = \chi\hat{n}$  and comoving distance  $\chi = \eta_0 - \eta$  (which acts as a time coordinate, with horizon  $\chi_H$ ). Here, we have averaged over a bin  $n_a(\chi)$  in distance (or redshift, via  $n_a(\chi)d\chi \equiv n_a(z)dz$ ); due to the difficulties in measuring the redshifts of lensed galaxies, these are usually broad.

In practice, computing maps of shear and flexion over large swathes of the sky is nontrivial. Unless one restricts to very small scales, it is imperative to account for the variation of the basis vectors entering the shear and flexion definitions (15) across the sky.<sup>3</sup> To this end, we rely on

<sup>3</sup>Note that this is ignored in many previous flexion treatments (though see [71] for a counterexample).

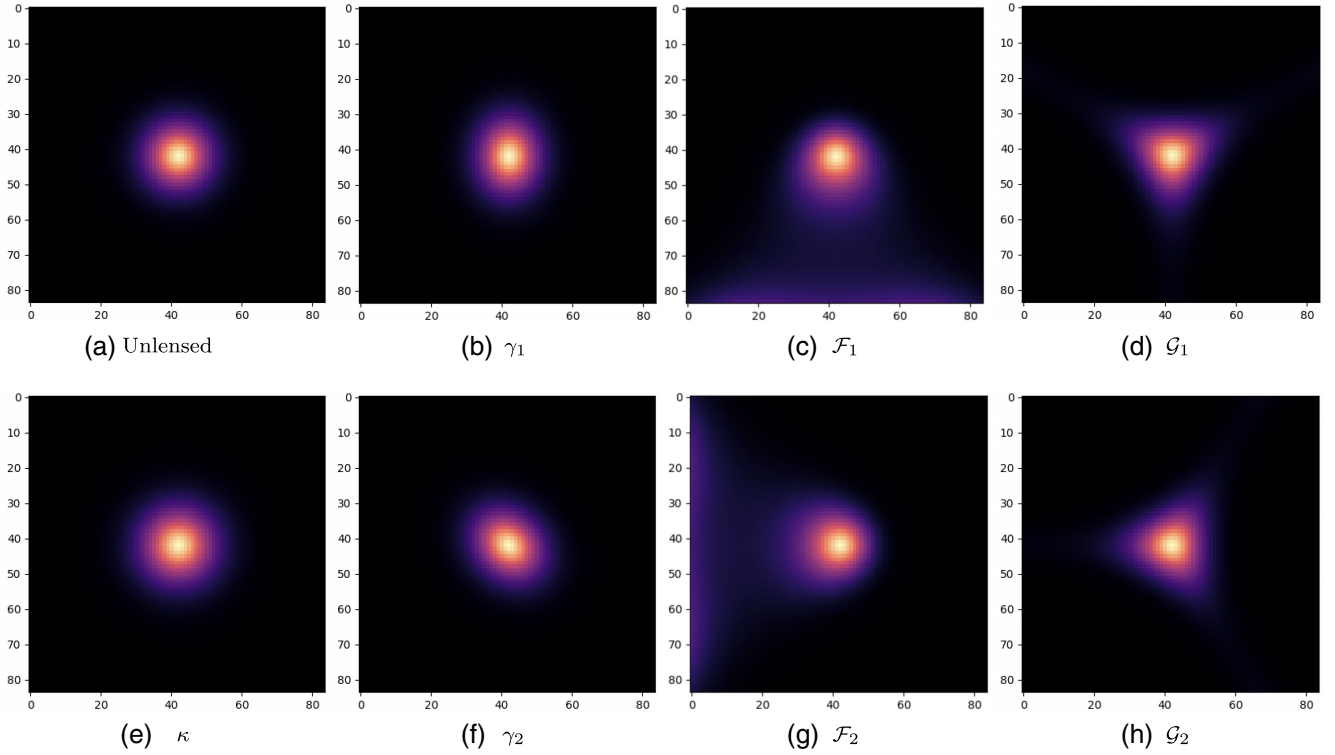


FIG. 1. Visual depiction of weak lensing distortions applied to a simulated galaxy. The unlensed galaxy in the first figure corresponds to a perfect Gaussian circle (neglecting shape noise for the purpose of visualization), and the following figures show the distortion of that galaxy with 10% convergence/shear ( $\gamma_{1,2}$  and  $\kappa$ ), 1% flexion of the first kind ( $\mathcal{F}_{1,2}$ ), and 10% flexion of the second kind ( $\mathcal{G}_{1,2}$ ). The differing spins (0, 2, 1, 3 in the four columns respectively) show different characteristic distortion shapes that can be constrained from real galaxies. Figure created using the flexion code of [65].

full-sky mathematics (the basics of which are outlined in Appendix A), first defining the basis vectors

$$\mathbf{m}_{\pm}(\hat{\mathbf{n}}) = \frac{1}{\sqrt{2}}(\hat{\mathbf{e}}_{\theta} \mp i\hat{\mathbf{e}}_{\varphi})(\hat{\mathbf{n}}) = \frac{1}{\sqrt{2}} \begin{pmatrix} \cos\theta\cos\varphi \pm i\sin\varphi \\ \cos\theta\sin\varphi \mp i\cos\varphi \\ -\sin\theta \end{pmatrix}, \quad (19)$$

(e.g., [8,84]) where we henceforth omit the dependence on  $\hat{\mathbf{n}} \equiv (\theta, \varphi)$  for clarity. These satisfy  $m_{\pm}^i m_{\pm i} = 0$ ,  $m_{\pm}^i m_{\mp i} = 1$ , and  $m_{\pm}^i \hat{n}_i = 0$ . Given some locally orthogonal vector set  $\{\hat{\mathbf{e}}_1, \hat{\mathbf{e}}_2, \hat{\mathbf{n}}\}$ , these asymptote to  $\mathbf{m}_{\pm} = (\hat{\mathbf{e}}_1 \mp i\hat{\mathbf{e}}_2)/\sqrt{2}$ , restoring the definitions of Sec. III A.

As discussed in Appendix A, any rank- $n$  tensor,  $X_{i_1 \dots i_n}(\hat{\mathbf{n}})$ , defined on the two-sphere can be written uniquely in terms of the basis vectors  $\mathbf{m}_{\pm}$  and coefficients with spin- $\pm n$ , spin- $\pm(n-2)$ , etc. As such, the (redshift-binned) image quadrupole can be written in a coordinate independent form in terms of spin- $\pm 2$  coefficients  ${}_{\pm 2}\gamma(\hat{\mathbf{n}})$  (which generalize the complex  $\gamma_1 \pm i\gamma_2$  quantities defined above):

$$\frac{1}{\zeta_2} Q_{ij}(\hat{\mathbf{n}}) = {}_{+2}\gamma(\hat{\mathbf{n}}) m_{+i} m_{+j} + {}_{-2}\gamma(\hat{\mathbf{n}}) m_{-i} m_{-j}. \quad (20)$$

Similarly, the octopole distortions can be decomposed into a spin- $\pm 1$  piece  ${}_{\pm 1}\mathcal{F}(\hat{\mathbf{n}})$  and a spin- $\pm 3$  contribution  ${}_{\pm 3}\mathcal{G}(\hat{\mathbf{n}})$ :

$$\begin{aligned} \frac{1}{\zeta_3} Q_{ijk}(\hat{\mathbf{n}}) &= -\frac{9}{8} \left[ \mathcal{F}_{ijk}(\hat{\mathbf{n}}) + \frac{1}{3} \mathcal{G}_{ijk}(\hat{\mathbf{n}}) \right], \\ \mathcal{F}_{ijk}(\hat{\mathbf{n}}) &\equiv -\frac{1}{2\sqrt{2}} [{}_{+1}\mathcal{F}(\hat{\mathbf{n}})(\eta_{ij} m_{+k} + 2 \text{ perms}) + {}_{-1}\mathcal{F}(\hat{\mathbf{n}})(\eta_{ij} m_{-k} + 2 \text{ perms})], \\ \mathcal{G}_{ijk}(\hat{\mathbf{n}}) &\equiv -\frac{1}{\sqrt{2}} [{}_{+3}\mathcal{G}(\hat{\mathbf{n}}) m_{+i} m_{+j} m_{+k} + {}_{-3}\mathcal{G}(\hat{\mathbf{n}}) m_{-i} m_{-j} m_{-k}], \end{aligned} \quad (21)$$

where  $\eta_{ij} \equiv \text{diag}(1, \sin^2 \theta)$  is the spatial metric on the two-sphere. Here,  ${}_{\pm 1}\mathcal{F}$  and  ${}_{\pm 3}\mathcal{G}$  are the full-sky generalization of the first and second flexion introduced previously. In the complex notation of [65,66],  ${}_{+1}\mathcal{F} = \mathcal{F}$ ,  ${}_{-1}\mathcal{F} = \mathcal{F}^*$ , with an analogous result for the spin- $\pm 3$  flexion.

Since the basis functions are orthogonal, (20) and (21) may be used to extract the shear and flexion directly:

$$\begin{aligned} {}_{\pm 2}\gamma(\hat{\mathbf{n}}) &= \frac{1}{\zeta_2} m_{\mp}^i m_{\mp}^j Q_{ij}(\hat{\mathbf{n}}) \rightarrow \frac{1}{2\zeta_2} [(Q_{11} - Q_{22}) \pm i(Q_{12} + Q_{21})](\hat{\mathbf{n}}) \\ {}_{\pm 1}\mathcal{F}(\hat{\mathbf{n}}) &= \frac{8\sqrt{2}}{9\zeta_3} m_{\mp}^i m_{\mp}^j m_{\pm}^k Q_{ijk}(\hat{\mathbf{n}}) \rightarrow \frac{4}{9\zeta_3} [(Q_{111} + Q_{112}) \pm i(Q_{221} + Q_{222})](\hat{\mathbf{n}}) \\ {}_{\pm 3}\mathcal{G}(\hat{\mathbf{n}}) &= \frac{8\sqrt{2}}{3\zeta_3} m_{\mp}^i m_{\mp}^j m_{\mp}^k Q_{ijk}(\hat{\mathbf{n}}) \rightarrow \frac{4}{3\zeta_3} [(Q_{111} - 3Q_{112}) \pm i(3Q_{122} - Q_{222})](\hat{\mathbf{n}}), \end{aligned} \quad (22)$$

where we have taken the local limit on the right-hand side (RHS), finding equivalence with the previous results. For the remainder of this paper, we will work only with the shear and flexion components of definite spin, i.e.,  ${}_{\pm 2}\gamma(\hat{\mathbf{n}})$ ,  ${}_{\pm 1}\mathcal{F}(\hat{\mathbf{n}})$  and  ${}_{\pm 3}\mathcal{G}(\hat{\mathbf{n}})$  as in previous work using the full-sky shear (e.g., [8,71]).

### C. Angular spectra

Much as Fourier modes are a convenient manner in which to characterize information for 3D observables, spherical harmonic coefficients provide a natural description of quantities on the two sphere (e.g., [7,8]). In general, a spin- $s$  quantity  ${}_sX(\hat{\mathbf{n}})$  can be written [cf. (A7)]

$$\begin{aligned} {}_sX(\hat{\mathbf{n}}) &= \sum_{\ell=0}^{\infty} \sum_{m=-\ell}^{\ell} {}_sX_{\ell m} Y_{\ell m}(\hat{\mathbf{n}}) \leftrightarrow {}_sX_{\ell m}(\hat{\mathbf{n}}) \\ &= \int d\hat{\mathbf{n}} {}_sX(\hat{\mathbf{n}}) [{}_sY_{\ell m}(\hat{\mathbf{n}})]^*, \end{aligned} \quad (23)$$

where  ${}_sX_{\ell m}$  are the coefficients of  ${}_sX(\hat{\mathbf{n}})$ , and  ${}_sY_{\ell m}(\hat{\mathbf{n}})$  are spin-weighted spherical harmonics, which are discussed in Appendix A. In this work, the quantities of interest are the shear, and the first and second flexion, whose harmonic coefficients are respectively  ${}_{\pm 2}\gamma_{\ell m}$ ,  ${}_{\pm 1}\mathcal{F}_{\ell m}$ , and  ${}_{\pm 3}\mathcal{G}_{\ell m}$ . These can be further decomposed into components with definite behavior under parity-transforms:

$$\begin{aligned} {}_{\pm 2}\gamma_{\ell m} &= \gamma_{\ell m}^E \pm i\gamma_{\ell m}^B, & {}_{\pm 1}\mathcal{F}_{\ell m} &= \mathcal{F}_{\ell m}^c \pm i\mathcal{F}_{\ell m}^g, \\ {}_{\pm 3}\mathcal{G}_{\ell m} &= \mathcal{G}_{\ell m}^c \pm i\mathcal{G}_{\ell m}^g, \end{aligned} \quad (24)$$

where  $E$  and  $c$  (“curl”) are parity-even, whilst  $B$  and  $g$  (“gradient”) are parity-odd.

Using the harmonic coefficients, we can form angular power spectra, which are the primary quantity of interest in photometric analyses. For two fields  $X$  and  $Y$  (e.g.,  $\gamma^E$  and  $\mathcal{F}^c$ ), this is defined by

$$C_{\ell}^{XY,ab} \equiv \langle X_{\ell m}^a Y_{\ell m}^b \rangle, \quad \hat{C}_{\ell}^{XY,ab} \equiv \frac{1}{2\ell+1} \sum_{m=-\ell}^{\ell} X_{\ell m}^a Y_{\ell m}^b \quad (25)$$

for redshift bins  $a$ ,  $b$ , where the expectation is taken over the underlying random fields. The RHS gives the standard power spectrum estimator. For a parity-conserving source,  $EE$ ,  $BB$ ,  $gg$ ,  $cc$ ,  $Eg$ , and  $Bc$  spectra can be nonzero; however  $EB$ ,  $gc$ ,  $Ec$ , and  $Bg$  spectra indicate parity-violating physics, since the overall spectrum is parity-odd.

## IV. SOURCES OF SHEAR AND FLEXION

We now ask the following question: what are the possible sources of galaxy shear and flexion, and how do these depend on scalar, vector, and tensor perturbations in the Universe? Three possibilities arise: (1) intrinsic distortions present in the true galaxy shapes induced by tidal fields, (2) extrinsic distortions from weak lensing of the galaxy photons by the intervening potentials, and (3) stochastic contributions, from observational effects and noise. Below, we consider each in turn, before discussing the corresponding power spectra in Sec. V.

### A. Intrinsic alignments

The galaxy brightness profile,  $I(\vec{\theta})$ , probes the projected shape of the galaxy, and is thus sensitive to any physical processes that source nonsphericity, such as large-scale tidal fields. Understanding the intrinsic contributions from scalar degrees-of-freedom has been the subject of a large array of works (e.g., [15–20,85–88]); comparatively less attention has been paid to higher-spin perturbations and flexion (though see [70] for an overview of the scalar sources of intrinsic galaxy flexion, and [22,23,25,85,87,89] for a detailed discussion of tensorial intrinsic alignments).

As discussed in Sec. III A, galaxy shear and flexion measure the quadrupole and octopole image moments,  $Q_{ij}$  and  $Q_{ijk}$ . These are themselves projections of the three-dimensional galaxy shape, quantified by the generalized

moment of mass tensor  $I_{i_1 \dots i_n} \propto \int dx \rho(\mathbf{x}) \Delta x_{i_1} \dots \Delta x_{i_n}$  for mass distribution  $\rho(\mathbf{x})$ :

$$\begin{aligned} Q_{ij}(\mathbf{x}, \chi) &\propto \mathcal{P}_i^i \mathcal{P}_j^j \left( I_{i'j'}(\mathbf{x}, \chi) - \frac{1}{3} \delta_{i'j'}^K \text{Tr} I_{kl}(\mathbf{x}, \chi) \right), \\ Q_{ijk}(\mathbf{x}, \chi) &\propto \mathcal{P}_i^i \mathcal{P}_j^j \mathcal{P}_k^k I_{i'j'k'}(\mathbf{x}, \chi) \end{aligned} \quad (26)$$

(e.g., [85]), where  $\mathcal{P}_{ij} \equiv \delta_{ij}^K - \hat{n}_i \hat{n}_j$  is a projection operator and  $i, j, \dots \in \{1, 2, 3\}$ . Crucially, the moment of mass tensor traces the metric perturbations, which thus leads to an intrinsic shear and flexion contribution.

In the simplest approximation, we can assume that the three-dimensional galaxy shape responds linearly to the Newtonian potential  $\Phi$ ; invoking symmetry and the equivalence principle, we find  $I_{ij}(\mathbf{x}) \propto \partial_i \partial_j \Phi(\mathbf{x})$ ,  $I_{ijk}(\mathbf{x}) \propto \partial_i \partial_j \partial_k \Phi(\mathbf{x})$  (e.g., [16]). Notably, the image quadrupole depends on the trace-free combination  $t_{ij}(\mathbf{x}) \equiv (\partial_i \partial_j - \frac{1}{3} \delta_{ij}^K \nabla^2) \Phi(\mathbf{x}, \chi)$ , thus we are assuming that  $Q_{ij}$  responds linearly to the local tidal field (e.g., [15,16,18,70,85]), i.e.,

$$\begin{aligned} \frac{1}{\zeta_2} Q_{ij}(\mathbf{x}, \chi) \Big|_{\text{int}} &\propto \mathcal{P}_i^i \mathcal{P}_j^j t_{i'j'}(\mathbf{x}, \chi), \\ \frac{1}{\zeta_3} Q_{ijk}(\mathbf{x}, \chi) \Big|_{\text{v,int}} &\propto \chi \mathcal{P}_i^i \mathcal{P}_j^j \mathcal{P}_k^k \partial_{(i} t_{j'k')}(\mathbf{x}, \chi), \end{aligned} \quad (27)$$

inserting a factor of  $\chi$  to the second equation on dimensional grounds. Using (22), we thus obtain the intrinsic contributions to shear and flexion from a scalar metric perturbation at some distance  $\chi$ :

$$\begin{aligned} \pm_2 \gamma(\mathbf{x}, \chi) \Big|_{\text{s,int}} &= b_S(\chi) [m_{\mp}^i m_{\mp}^j \partial_i \partial_j] \Phi(\mathbf{x}, \chi), \\ \pm_1 \mathcal{F}(\mathbf{x}, \chi) \Big|_{\text{s,int}} &= \left( \frac{8\sqrt{2}}{9} \chi \tilde{b}_S(\chi) \right) [m_{\mp}^i m_{\mp}^j m_{\pm}^k \partial_i \partial_j \partial_k] \Phi(\mathbf{x}, \chi), \\ \pm_3 \mathcal{G}(\mathbf{x}, \chi) \Big|_{\text{s,int}} &= \left( \frac{8\sqrt{2}}{3} \chi \tilde{b}_S(\chi) \right) [m_{\mp}^i m_{\mp}^j m_{\mp}^k \partial_i \partial_j \partial_k] \Phi(\mathbf{x}, \chi), \end{aligned} \quad (28)$$

using that  $\mathcal{P}_j^i m_{\pm}^j \equiv m_{\pm}^i$  and  $\delta_{ij}^K m_{\pm}^i m_{\pm}^j = 0$ . This introduces bias parameters  $b_S(\chi)$  and  $\tilde{b}_S(\chi)$ : these quantify the linear responses of the shear and flexion to scalar metric perturbations, and depend primarily on the formation epoch of the galaxy. Working in  $2a(\chi)/(3H_0^2 \Omega_m)$  units (such that  $\nabla^2 \Phi \sim \delta$  in the Poisson equation), each bias is expected to be  $\mathcal{O}(1)$  [70,85,86], as confirmed experimentally [17]. To form the observables, (28) must be averaged over a redshift bin, as in (18).

By a similar logic, vector and tensor metric perturbations also lead to distortions in the galaxy shape. Whilst these could be modeled using the above symmetry arguments (which imply that  $Q_{ij}$  is a projection of  $\partial_{(i} B_{j)}$  and  $h_{ij}$ ), this does not properly account for time evolution. Here, we

instead adopt the approach of [22,23], which computes the shape distortion by first estimating the induced tidal field,  $t_{ij}$ . Using Fermi normal coordinates and assuming the synchronous gauge such that  $h_{0i} = 0$ , we have [22,84]

$$t_{ij}(\mathbf{x}, \chi) = \frac{1}{2} [a^{-1} (a h'_{ij})' + h_{00,ij}] (\mathbf{x}, \chi). \quad (29)$$

For scalar perturbations [defined by (2), with time-invariant  $\Phi$ ], this recovers the results of (28) [cf., [15,17]]. For vector perturbations, the synchronous gauge implies  $h'_{ij}|_{\text{sync}} = -2B_{(i,j)}|_{\text{cN}}$  (for the previously used conformal Newtonian gauge variable  $B_i$ ), thus

$$\begin{aligned} t_{ij}(\mathbf{x}, \chi) \Big|_{\text{v}} &= -[a^{-1} (a B_{(i,j)})'] (\mathbf{x}, \chi) \\ &= -\left[ \frac{\partial}{\partial \eta} + a(\chi) H(\chi) \right] B_{(i,j)} (\mathbf{x}, \chi) \\ &\equiv -\mathcal{I}_V B_{(i,j)} (\mathbf{x}, \chi), \end{aligned} \quad (30)$$

defining a time-derivative operator  $\mathcal{I}_V$  for simplicity. Similarly, the tidal field induced by a tensor mode is given by

$$t_{ij}(\mathbf{x}, \chi) \Big|_{\text{T}} = \frac{1}{2} \left[ \frac{\partial}{\partial \eta^2} + a(\chi) H(\chi) \frac{\partial}{\partial \eta} \right] h_{ij}(\mathbf{x}, \chi) \equiv \frac{1}{2} \mathcal{I}_T h_{ij}(\mathbf{x}, \chi), \quad (31)$$

defining the  $\mathcal{I}_T$  operator. Using (27), the leading-order shear and flexion contributions from vector and tensor metric perturbations are given by [cf., [25]]

$$\begin{aligned} \pm_2 \gamma(\mathbf{x}, \chi) \Big|_{\text{v,int}} &= b_V(\chi) [m_{\mp}^i m_{\mp}^j \partial_i] \mathcal{I}_V B_j(\mathbf{x}, \chi), \\ \pm_1 \mathcal{F}(\mathbf{x}, \chi) \Big|_{\text{v,int}} &= \left( \frac{8\sqrt{2}}{9} \chi \tilde{b}_V(\chi) \right) [m_{\mp}^i m_{\mp}^j m_{\pm}^k \partial_i \partial_j] \mathcal{I}_V B_k(\mathbf{x}, \chi), \\ \pm_3 \mathcal{G}(\mathbf{x}, \chi) \Big|_{\text{v,int}} &= \left( \frac{8\sqrt{2}}{3} \chi \tilde{b}_V(\chi) \right) [m_{\mp}^i m_{\mp}^j m_{\mp}^k \partial_i \partial_j] \mathcal{I}_V B_k(\mathbf{x}, \chi), \end{aligned} \quad (32)$$

and

$$\begin{aligned} \pm_2 \gamma(\mathbf{x}, \chi) \Big|_{\text{T,int}} &= b_T(\chi) [m_{\mp}^i m_{\mp}^j] \mathcal{I}_T h_{ij}(\mathbf{x}, \chi), \\ \pm_1 \mathcal{F}(\mathbf{x}, \chi) \Big|_{\text{T,int}} &= \left( \frac{8\sqrt{2}}{9} \chi \tilde{b}_T(\chi) \right) [m_{\mp}^i m_{\mp}^j m_{\pm}^k \partial_i] \mathcal{I}_T h_{jk}(\mathbf{x}, \chi), \\ \pm_3 \mathcal{G}(\mathbf{x}, \chi) \Big|_{\text{T,int}} &= \left( \frac{8\sqrt{2}}{3} \chi \tilde{b}_T(\chi) \right) [m_{\mp}^i m_{\mp}^j m_{\mp}^k \partial_i] \mathcal{I}_T h_{jk}(\mathbf{x}, \chi). \end{aligned} \quad (33)$$

As before, the bias parameters  $b_X(\chi)$  and  $\tilde{b}_X(\chi)$  encode the responses of shear and flexion to metric perturbations (which we allow to differ between scalars, vectors, and

tensors, for full generality), and are expected to be  $\mathcal{O}(1)$  in  $2a(\chi)/(3H_0^2\Omega_m)$  units, whence we can switch between density and potential fluctuations [22,23,86], with  $b_\chi \sim 0.1$  found experimentally [17]. Given these results, coupled with the power spectra of  $\Phi$ ,  $B_i$ , and  $h_{ij}$  (7), we may compute the statistics of shear and flexion; this is detailed in Sec. V.

The above derivation makes a number of limiting assumptions. Firstly, we assume that the galaxy at some lookback time  $\eta = \eta_0 - \chi$  traces the tidal field at the same same time, rather than its full history. Secondly, we neglect dependence of the bias parameters  $b_{V,T}$  on the wavelength of vector or tensor mode. A number of works have considered a more nuanced ‘‘fossil’’ approach [23,25,89], by explicitly computing the impact of tidal fields on the second-order density field, both in theory and simulations. For primordial gravitational waves, this was found to somewhat enhance the intrinsic alignment signal, and give some scale-dependence [cf. [87], Fig. 1]. For the purposes of forecasting, we neglect these effects since (a) a uniform rescaling is fully degenerate with the unknown bias parameters if the perturbations are separable in time and space, and (b) the scale dependence is weak for tensor (and vector) modes with  $k \gtrsim 10^{-3}h \text{ Mpc}^{-1}$ . We proceed with a general warning however that the precise values of vector and tensor biases are not well understood.

## B. Weak lensing

Next, we consider extrinsic distortions to the observed galaxy shape, which arise from the gravitational deflection of photons as they travel from the source galaxy to the observer (e.g., [7,8,90]). This is a well-known source of shear, convergence, and flexion [7,65,66,69], and encodes information on all types of metric perturbation.

The effects of lensing are encoded in the transformation between unlensed and lensed coordinates,  $\theta_i$  and  $\theta'_i$ :

$$\theta'_i(\vec{\theta}) = A_{ij}\theta^j + \frac{1}{2}D_{ijk}\theta^j\theta^k + \mathcal{O}(\theta^3), \quad (34)$$

where the matrices  $A_{ij}$  and  $D_{ijk}$  are linear transformations of the scalar perturbation  $\Phi(\mathbf{x}, \chi)$  (in the weak-field limit):

$$\begin{aligned} A^{ij}(\mathbf{x}, \chi) &= \delta_K^{ij} - \partial_\theta^i \partial_\theta^j \Phi(\mathbf{x}, \chi), \\ D^{ijk}(\mathbf{x}, \chi) &= -\partial_\theta^i \partial_\theta^j \partial_\theta^k \Phi(\mathbf{x}, \chi) \end{aligned} \quad (35)$$

(e.g., [7,65,90]). This uses the projected potential  $\phi(\mathbf{x}, \chi)$  for a source at  $\mathbf{x} \equiv \chi \hat{\mathbf{n}}$  and redshift  $\chi$ :

$$\phi(\chi \hat{\mathbf{n}}, \chi) = \frac{2}{c^2} \int_0^\chi d\chi' \frac{\chi - \chi'}{\chi \chi'} \Phi(\chi' \hat{\mathbf{n}}, \chi'), \quad (36)$$

(e.g., [8]), which integrates over the distribution of matter between the source (at  $\chi' = \chi$ ) and the observer (at  $\chi' = 0$ ).

Associated with this transformation is a distortion in the galaxy image,  $I(\vec{\theta})$ , which manifests as a quadrupole moment (and beyond). From the definitions in Sec. III, this sources convergence, shear, and flexion fields of the form:

$$\begin{aligned} -A_{ij}(\mathbf{x}, \chi) &= \kappa(\mathbf{x}, \chi)\eta_{ij} + {}_{+2}\gamma(\mathbf{x}, \chi)m_{+i}m_{+j} + {}_{-2}\gamma(\mathbf{x}, \chi)m_{-i}m_{-j} \\ D_{ijk}(\mathbf{x}, \chi) &= \mathcal{F}_{ijk}(\mathbf{x}, \chi) + \mathcal{G}_{ijk}(\mathbf{x}, \chi) \end{aligned} \quad (37)$$

(e.g., [8]), where  $\mathcal{F}_{ijk}$  and  $\mathcal{G}_{ijk}$  can be written in terms of spin- $\pm 1$  and  $\pm 3$  components as in (21).<sup>4</sup> Unlike for the intrinsic contribution, there is no prefactor of  $1/3$  in front of  $\mathcal{G}_{ijk}$ , thus the spin- $\pm 3$  flexion is here enhanced relative to the spin- $\pm 1$  form. In the local limit, (37) reduces to the standard relations (e.g., [65,66]):

$$\begin{aligned} A_{ij} &= \begin{pmatrix} 1 - \kappa - \gamma_1 & -\gamma_2 \\ -\gamma_2 & 1 - \kappa + \gamma_1 \end{pmatrix}, \\ D_{ij1} &= -\frac{1}{2} \begin{pmatrix} 3\mathcal{F}_1 + \mathcal{G}_1 & \mathcal{F}_2 + \mathcal{G}_2 \\ \mathcal{F}_2 + \mathcal{G}_2 & \mathcal{F}_1 - \mathcal{G}_1 \end{pmatrix}, \\ D_{ij2} &= -\frac{1}{2} \begin{pmatrix} \mathcal{F}_2 + \mathcal{G}_2 & \mathcal{F}_1 - \mathcal{G}_1 \\ \mathcal{F}_1 - \mathcal{G}_1 & 3\mathcal{F}_2 - \mathcal{G}_2 \end{pmatrix}, \end{aligned} \quad (38)$$

where  ${}_{\pm 2}\gamma = \gamma_1 \pm \gamma_2$  etc. As in (22), orthogonality of the basis vectors allows us to derive expressions for the shear and flexion in terms of  $\phi$ :

$$\begin{aligned} {}_{\pm 2}\gamma(\chi \hat{\mathbf{n}}, \chi)|_{S,\text{ext}} &= [m_{\mp i}m_{\mp j}\partial_\theta^i\partial_\theta^j]\phi(\chi \hat{\mathbf{n}}, \chi), \\ {}_{\pm 1}\mathcal{F}(\chi \hat{\mathbf{n}}, \chi)|_{S,\text{ext}} &= \sqrt{2}[m_{\mp i}m_{\mp j}m_{\pm k}\partial_\theta^i\partial_\theta^j\partial_\theta^k]\phi(\chi \hat{\mathbf{n}}, \chi), \\ {}_{\pm 3}\mathcal{G}(\chi \hat{\mathbf{n}}, \chi)|_{S,\text{ext}} &= \sqrt{2}[m_{\mp i}m_{\mp j}m_{\mp k}\partial_\theta^i\partial_\theta^j\partial_\theta^k]\phi(\chi \hat{\mathbf{n}}, \chi). \end{aligned} \quad (39)$$

Alternatively, shear and flexion can be written in terms of ‘‘spin-derivatives,’’ themselves defined in Appendix A. In this form:

$$\begin{aligned} {}_{+2}\gamma(\chi \hat{\mathbf{n}}, \chi)|_{S,\text{ext}} &= \frac{1}{2}\partial\bar{\partial}\phi(\chi \hat{\mathbf{n}}, \chi), \\ {}_{+1}\mathcal{F}(\chi \hat{\mathbf{n}}, \chi)|_{S,\text{ext}} &= -\frac{1}{6}[\partial\bar{\partial}\bar{\partial} + \bar{\partial}\bar{\partial}\bar{\partial} + \bar{\partial}\bar{\partial}\partial]\phi(\chi \hat{\mathbf{n}}, \chi) \\ {}_{+3}\mathcal{G}(\chi \hat{\mathbf{n}}, \chi)|_{S,\text{ext}} &= -\frac{1}{2}\bar{\partial}\bar{\partial}\bar{\partial}\phi(\chi \hat{\mathbf{n}}, \chi) \end{aligned} \quad (40)$$

(e.g., [8]), where  $\bar{\partial}$  ( $\partial$ ) raises (lowers) the spin by one, and components with negative spins are obtained by interchanging  $\bar{\partial}$  and  $\partial$ . This allows for convenient computation of the statistics of shear and flexion from those of  $\phi$ .

Vector and tensor perturbations provide an additional source of photon deflections, and thus contributions to shear and flexion. To obtain their form, we use the general gauge-invariant results of [[84], Eq. 64] (see also [21]), finding:

<sup>4</sup>We will ignore convergence contributions in this work since they are largely determined by shear (though see also [91]).

$$\begin{aligned}
{}_{\pm 2}\gamma(\chi\hat{\mathbf{n}},\chi)|_{S,\text{ext}} &= 2 \int_0^\chi d\chi' \frac{\chi'}{\chi} (\chi - \chi') m_{\mp}^i m_{\mp}^j \partial_i \partial_j \Phi(\chi' \hat{\mathbf{n}}, \chi'), \\
{}_{\pm 2}\gamma(\chi\hat{\mathbf{n}},\chi)|_{V,\text{ext}} &= - \int_0^\chi d\chi' \left[ \left(1 - 2\frac{\chi'}{\chi}\right) m_{\mp}^k \partial_{\pm} B_k + \frac{\chi'}{\chi} (\chi - \chi') (\hat{n}^k m_{\mp}^i m_{\mp}^j \partial_i \partial_j B_k) \right] (\chi' \hat{\mathbf{n}}, \chi'), \\
{}_{\pm 2}\gamma(\chi\hat{\mathbf{n}},\chi)|_{T,\text{ext}} &= -\frac{1}{2} h_{\pm}(\chi\hat{\mathbf{n}},\chi) - \frac{1}{2} h_{\pm}(\mathbf{0},0) \\
&\quad - \int_0^\chi d\chi' \left[ \left(1 - 2\frac{\chi'}{\chi}\right) [(\partial_{\pm} h_{lk}) m_{\mp}^l \hat{n}^k] - \frac{1}{\chi} h_{\pm} + \frac{\chi'}{2\chi} (\chi - \chi') m_{\mp}^i m_{\mp}^j (\partial_i \partial_j h_{kl}) \hat{n}^k \hat{n}^l \right] (\chi' \hat{\mathbf{n}}, \chi'), \quad (41)
\end{aligned}$$

where  $h_{ij}(\mathbf{0},0)$  is the tensor perturbation evaluated at the observers position,  $\partial_{\pm} \equiv m_{\mp}^i \partial_i$ , and  $h_{\pm} \equiv m_{\mp}^i m_{\mp}^j h_{ij}$ . Noting that  $\partial_{\theta}^i = \chi^{-1} \mathcal{P}_j^i \partial_j$ , it is straightforward to show the scalar piece equals that of (39). For the vector piece (which is equivalent to that of [24]), we have two contributions, depending on the first and second derivatives of  $B$  respectively; in practice, the second term is expected to dominate on all but the largest scales. The tensor spectrum contains unintegrated terms corresponding to the field at the source and observer positions; the former contributes analogously to the intrinsic piece discussed in Sec. IV A, and can be absorbed by redefining  $\mathcal{I}_T h_{ij} \rightarrow [\mathcal{I}_T - 1/(2b_T(\chi))] h_{ij}$ . The latter piece contributes only to the  $\ell = 2$  modes [22,84], and acts to remove the  $k \rightarrow 0$  limit.

The approach of [84] may be further extended to compute the lensing contribution to the flexion parameters  $\mathcal{F}$  and  $\mathcal{G}$  from vector and tensor modes. However, this is nontrivial, and, foreshadowing the conclusions of Sec. VI, unlikely to be of significant practical use. For our purposes, we will make the following assumption for vector and tensor sources:

$$\begin{aligned}
{}_{+1}\mathcal{F}(\chi\hat{\mathbf{n}},\chi)|_{\text{ext}} &\approx -\bar{\delta}_{+2}\gamma(\chi\hat{\mathbf{n}},\chi)|_{\text{ext}}, \\
{}_{+3}\mathcal{G}(\chi\hat{\mathbf{n}},\chi)|_{\text{ext}} &\approx -\bar{\delta}_{+2}\gamma(\chi\hat{\mathbf{n}},\chi)|_{\text{ext}}, \\
{}_{-1}\mathcal{F}(\chi\hat{\mathbf{n}},\chi)|_{\text{ext}} &\approx -\bar{\delta}_{-2}\gamma(\chi\hat{\mathbf{n}},\chi)|_{\text{ext}}, \\
{}_{-3}\mathcal{G}(\chi\hat{\mathbf{n}},\chi)|_{\text{ext}} &\approx -\bar{\delta}_{-2}\gamma(\chi\hat{\mathbf{n}},\chi)|_{\text{ext}}. \quad (42)
\end{aligned}$$

This is justified by noting that the flexion lensing tensor  $D^{ijk} = \partial_{\theta}^i A^{jk}$  contains one additional spin-derivative compared to  $A^{jk}$  (since  $m_{-i} \partial_{\theta}^i = -\bar{\delta}$  and  $m_{+i} \partial_{\theta}^i = -\bar{\delta}$  locally). On small scales,  $\bar{\delta}$  and  $\delta$  permute, thus this recovers the scalar results of (40) (e.g., [65,66]). In practice, the contribution of flexion is strongly subdominant outside the small-scale limit, thus this approximation is generally appropriate.

### C. Other sources

The last major source of shear and flexion is stochasticity due to both experimental noise and the intrinsic variation in

galaxy shapes (e.g., [1]). Here, we assume that the local measurement of a given observable,  $X \in \{\gamma, \mathcal{F}, \mathcal{G}\}$ , follows a Gaussian distribution with variance  $\sigma_X^2$ , and (ignoring other sources) zero mean, i.e.,

$$\hat{X}_i \sim \mathcal{N}\left(0, \frac{\sigma_X^2}{2}\right), \quad i \in \{1, 2\}, \quad (43)$$

for the component projected onto the  $\hat{\mathbf{e}}_i$  axis. We will further assert that the noise is uncorrelated (such that each galaxy is independent), and that the variances are independent of redshift and position. This yields a Poissonian distribution, with a simple power spectrum (cf. Sec. III C). Typical values for the noise amplitudes are  $\sigma_{\gamma} = 0.4$  [86], and  $\sigma_{\mathcal{F}} = \sigma_{\mathcal{G}}/3 = 0.009 \text{ sr}^{-1}$  [69]; the additional factor of three in the second flexion arises from its definition in (21).

Additional contributions to shear and flexion arise from higher-order effects, neglected in the above sections. Under our previous assumption, conventional physics generates only parity-conserving modes ( $\gamma^E, \mathcal{F}^g, \mathcal{G}^g$ ), thus any robust detection of the parity-breaking modes ( $\gamma^B, \mathcal{F}^c, \mathcal{G}^c$ ) would imply evidence for new phenomena. In praxis, second-order effects can generate  $B$ - and  $c$ -modes even from scalar sources, and thus yield correlators such as  $\langle \gamma^B \gamma^{B*} \rangle$ , which requires new physics. For example, the intrinsic alignment of galaxies contains a term  $\propto t_{ij} \delta$  (for matter overdensity  $\delta$ ) due to the nonuniform distribution of source galaxies; as shown in [15,25], this generates both shear  $E$  and  $B$  components, whose spectra involve the convolution of two  $P_{\Phi}$  spectra (via the Poisson equation). Similarly, post-Born effects in weak lensing lead to a shear  $B$ -mode signal [92], with another generated from the relation between shear and ‘‘reduced shear,’’  $g \equiv \gamma/(1 - \kappa)$  [22]. In the forecasts of Sec. VI, we will consider contributions of these phenomena to the  $E$ - and  $g$ -mode spectra (since they are heavily subdominant), but add a rough estimate of their size in the  $B$ -mode spectra, following previous works. Importantly, such effects cannot contribute to the parity-odd correlators such as  $EB$ , since their underlying physics is parity-conserving. Ignoring systematic contamination,

this makes  $EB$ -spectra a bountiful place in which to search for new physics.

## V. POWER SPECTRA

Armed with the statistics of scalar, vector, and tensor perturbations and their relation to shear and flexion, we may now proceed to compute the observed angular power spectra,  $C_\ell^{XY}$ . We will first compute the general full-sky

form for both intrinsic and extrinsic sourcing, before considering the flat-sky simplifications in Sec. VB.

### A. Full-sky spectra

In the weak-field regime, the observable quantities  $\gamma^{E,B}$ ,  $\mathcal{F}^{g,c}$ , and  $\mathcal{G}^{g,c}$  are linear transformations of the underlying metric perturbations (Sec. III). As such, the power spectra,  $C_\ell^{XY}$ , depend on two copies of the perturbation in question and can be written in the general form

$$\begin{aligned} C_\ell^{XY}(\chi, \chi')|_S &= \frac{2}{\pi} \int_0^\infty k^2 dk F_\ell^{X,S}(k, \chi) F_\ell^{Y,S*}(k, \chi') P_\Phi(k, \chi, \chi') \\ C_\ell^{XY}(\chi, \chi')|_V &= \frac{2}{\pi} \int_0^\infty k^2 dk F_\ell^{X,V}(k, \chi) F_\ell^{Y,V*}(k, \chi') [P_{B_+}(k, \chi, \chi') \pm P_{B_-}(k, \chi, \chi')] \\ C_\ell^{XY}(\chi, \chi')|_T &= \frac{2}{\pi} \int_0^\infty k^2 dk F_\ell^{X,T}(k, \chi) F_\ell^{Y,T*}(k, \chi') [P_{h_+}(k, \chi, \chi') \pm P_{h_-}(k, \chi, \chi')], \end{aligned} \quad (44)$$

where the transfer function  $F_\ell^{X,P}$  encodes the (local) response of the field  $X$  to the perturbation  $P \in \{S, V, T\}$ , and the second and third lines have a negative sign only for parity-odd spectra. In practice, the observables are binned in redshift via (18), which modifies the kernels

$$F_\ell^{X,S}(k, \chi) \rightarrow F_{\ell,a}^X(k) \equiv \int_0^{\chi_H} d\chi n_a(\chi) F_\ell^{X,S}(k, \chi) \quad (45)$$

and  $C_\ell^{XY}(\chi, \chi') \rightarrow C_{\ell,ab}^{XY}$  (absorbing the redshift-dependent parts of  $P_\Phi, P_B, P_h$  into the transfer functions). In the below, we will present the relevant transfer functions, which fully specify the observable power spectra.

#### 1. Intrinsic contributions

As shown in [84], the angular power spectrum of a general spin- $\pm s$  quantity  ${}_{\pm s}\mathcal{W}(\chi\hat{n}, \chi)$  (with  $s > 0$ ), can be obtained as follows:

- (1) Compute the contributions to  ${}_{\pm s}\mathcal{W}(\chi\hat{n}, \chi)$  arising from a single Fourier mode parallel to the  $\hat{z}$  axis, i.e.,  $\mathbf{k} = k\hat{z}$ , and a single helicity state  $\lambda$ .
- (2) Apply spin-raising and spin-lowering operators (see Appendix A) to  ${}_{\pm s}\mathcal{W}(\chi\hat{n}, \chi; k\hat{z}, \lambda)$  to obtain

$$\begin{aligned} F_\ell^{\gamma^E,P}(k, \chi)|_{\text{int}} &= \sqrt{\frac{(\ell-2)!(\ell+s_P)! b_P(\chi)}{(\ell+2)!(\ell-s_P)! 2\chi^2}} \left(\frac{\chi}{\sqrt{2}}\right)^{s_P} \text{Re}[\hat{Q}_{\gamma,P}^{(+1)}(x)] \frac{j_\ell(x)}{x^{s_P}} \mathcal{I}_P(\chi) \\ F_\ell^{\gamma^B,P}(k, \chi)|_{\text{int}} &= \sqrt{\frac{(\ell-2)!(\ell+s_P)! b_P(\chi)}{(\ell+2)!(\ell-s_P)! 2\chi^2}} \left(\frac{\chi}{\sqrt{2}}\right)^{s_P} \text{Im}[\hat{Q}_{\gamma,P}^{(+1)}(x)] \frac{j_\ell(x)}{x^{s_P}} \mathcal{I}_P(\chi), \end{aligned} \quad (46)$$

where  $P \in \{S, V, T\}$  labels the source-type, with corresponding source spin  $s_P = \{0, 1, 2\}$ . This involves two sets of operators: (a) the time-derivative operators  $\mathcal{I}_P$  of Sec. IVA (with  $\mathcal{I}_S(\chi) = 1$ ), acting on the source power

the spin-zero quantities  $\bar{\delta}_{+s}^s \mathcal{W}(\chi\hat{n}, \chi; k\hat{z}, \lambda)$  and  $\bar{\delta}_{-s}^s \mathcal{W}(\chi\hat{n}, \chi; k\hat{z}, \lambda)$ .

- (3) Extract the spherical harmonic coefficients,  ${}_{\pm s}\mathcal{W}_{\ell m}(\chi; k\hat{z}, \lambda)$ , by integrating the scalars against  $Y_{\ell m}^*(\hat{n})$  (A12). These may be split into  $E$  and  $B$  (or  $g$  and  $c$ ) contributions, as in Sec. III C.
- (4) Compute the angular power spectra by taking the expectation of two  $\mathcal{W}_{\ell m}^X(\chi; k\hat{z}, \lambda)$  functions, integrating over Fourier modes  $\mathbf{k}$  and averaging over  $m$ . Via isotropy, this gives the full power spectrum from all  $\mathbf{k}$  modes, not just  $\mathbf{k} = k\hat{z}$ , and allows extraction of the associated transfer functions via (44).

In Appendix C, we utilize this scheme to derive the shear and flexion power spectra sourced by intrinsic vector alignments (a novel feature of this work). Since the computations for scalars and tensors are analogous (and the shear results can be found in previous work, e.g., [22,85] for scalars, though with less attention paid to parity-breaking contributions), we present only the final expressions here. Before redshift integration, the shear kernels are given by (dropping factors of  $i^\ell$ )

spectrum; and (b) the spatial  $\hat{Q}_{\gamma,P}(x)$  operators acting on the spherical Bessel functions,  $j_\ell(x)$ , with  $x = k\chi$ . These are low-order polynomials in  $x$  and  $\partial_x$ , and their form is given explicitly in (E1) of Appendix E.

A similar calculation yields the flexion kernels:

$$\begin{aligned}
F_{\ell}^{\mathcal{F}^{\mathcal{F},P}}(k, \chi)|_{\text{int}} &= \sqrt{\frac{(\ell-1)!(\ell+s_P)!}{(\ell+1)!(\ell-s_P)!}} \frac{4\tilde{b}_P(\chi)}{27\chi^2} \left(\frac{\chi}{\sqrt{2}}\right)^{s_P} \text{Re}[\hat{Q}_{\mathcal{F},P}^{(+1)}(x)] \frac{j_{\ell}(x)}{x^{s_P}} \mathcal{I}_P(\chi) \\
F_{\ell}^{\mathcal{F}^{\mathcal{C},P}}(k, \chi)|_{\text{int}} &= -\sqrt{\frac{(\ell-1)!(\ell+s_P)!}{(\ell+1)!(\ell-s_P)!}} \frac{4\tilde{b}_P(\chi)}{27\chi^2} \left(\frac{\chi}{\sqrt{2}}\right)^{s_P} \text{Im}[\hat{Q}_{\mathcal{F},P}^{(+1)}(x)] \frac{j_{\ell}(x)}{x^{s_P}} \mathcal{I}_P(\chi) \\
F_{\ell}^{\mathcal{G}^{\mathcal{F},P}}(k, \chi)|_{\text{int}} &= \sqrt{\frac{(\ell-3)!(\ell+s_P)!}{(\ell+3)!(\ell-s_P)!}} \frac{4\tilde{b}_P(\chi)}{3\chi^2} \left(\frac{\chi}{\sqrt{2}}\right)^{s_P} \text{Re}[\hat{Q}_{\mathcal{G},P}^{(+1)}(x)] \frac{j_{\ell}(x)}{x^{s_P}} \mathcal{I}_P(\chi) \\
F_{\ell}^{\mathcal{G}^{\mathcal{C},P}}(k, \chi)|_{\text{int}} &= -\sqrt{\frac{(\ell-3)!(\ell+s_P)!}{(\ell+3)!(\ell-s_P)!}} \frac{4\tilde{b}_P(\chi)}{3\chi^2} \left(\frac{\chi}{\sqrt{2}}\right)^{s_P} \text{Im}[\hat{Q}_{\mathcal{G},P}^{(+1)}(x)] \frac{j_{\ell}(x)}{x^{s_P}} \mathcal{I}_P(\chi); \tag{47}
\end{aligned}$$

these depend on a new set of derivative operators  $\hat{Q}_{\mathcal{F},P}$  and  $\hat{Q}_{\mathcal{G},P}$  given in (E2) and (E3) respectively. Each of these kernels can be binned in redshift via (45).

Notably, the above scalar operators  $\hat{Q}_{X,S}(x)$  are explicitly real, thus the scalar  $B$ - and  $c$ -mode transfer functions vanish. This is as expected; a scalar contains insufficient degrees-of-freedom to generate parity-breaking distortions. As such, if one is interested only in scalar physics (which is usually the case), we need analyze only  $E$  and  $g$  mode spectra. In contrast, vector and tensor modes generically source both  $E/g$  and  $B/c$  distortions, making the latter observable a smoking gun for new physics (once noise and higher-order effects are taken into account). Furthermore,

we note that the vector and tensor spectra entering (44) involve either the sum or the difference of the two helicity spectra; this enters in the  $EB$ ,  $gc$ ,  $Ec$ , and  $Bg$  correlators, and implies that such spectra provide access to the parity-violating physical sector (e.g., [25]).

## 2. Extrinsic contributions

For scalar perturbations, computation of the weak lensing power spectrum is straightforward [8]. First, we write the definition of shear and flexion in terms of the lensing potential  $\phi$  (40), expanding the latter in spherical harmonics:

$$\begin{aligned}
+2\gamma(\chi\hat{\mathbf{n}}, \chi)|_{S,\text{ext}} &= \frac{1}{2} \sum_{\ell m} \phi_{\ell m}(\chi) \partial\bar{\partial} Y_{\ell m}(\hat{\mathbf{n}}), \\
+1\mathcal{F}(\chi\hat{\mathbf{n}}, \chi)|_{S,\text{ext}} &= -\frac{1}{6} \sum_{\ell m} \phi_{\ell m}(\chi) [\partial\bar{\partial}\bar{\partial} + \bar{\partial}\partial\bar{\partial} + \bar{\partial}\bar{\partial}\partial] Y_{\ell m}(\hat{\mathbf{n}}), \\
+3\mathcal{G}(\chi\hat{\mathbf{n}}, \chi)|_{S,\text{ext}} &= -\frac{1}{2} \sum_{\ell m} \phi_{\ell m}(\chi) \partial\bar{\partial}\partial Y_{\ell m}(\hat{\mathbf{n}}). \tag{48}
\end{aligned}$$

Using the spin-derivative relations given in (A8), this can be rewritten in terms of spin-weighted spherical harmonics, allowing the relevant  $E$  and  $B$  mode coefficients to be extracted via orthogonality (A9):

$$\begin{aligned}
\gamma_{\ell m}^E(\chi)|_{S,\text{ext}} &= \frac{1}{2} \sqrt{\frac{(\ell+2)!}{(\ell-2)!}} \phi_{\ell m}(\chi), \\
i\mathcal{F}_{\ell m}^g(\chi)|_{S,\text{ext}} &= \frac{1}{6} \sum_{\ell m} \phi_{\ell m}(\chi) \sqrt{\frac{(\ell+1)!}{(\ell-1)!}} [(\ell-1)(\ell+2) + 2\ell(\ell+1)], \\
i\mathcal{G}_{\ell m}^g(\chi)|_{S,\text{ext}} &= \frac{1}{2} \sqrt{\frac{(\ell+3)!}{(\ell-3)!}} \phi_{\ell m}(\chi). \tag{49}
\end{aligned}$$

As in Sec. VA 1, scalar physics sources only  $E$  and  $g$  modes at leading order. To form power spectra we proceed to expand the scalar perturbation in Fourier space and evaluate its two-point correlator yielding:

$$\phi_{\ell m}(\chi) = \frac{2}{c^2} \int_0^{\chi} d\chi' \frac{\chi - \chi'}{\chi\chi'} \int d\hat{\mathbf{n}} \Phi(\chi'\hat{\mathbf{n}}, \chi') Y_{\ell m}^*(\hat{\mathbf{n}}) = \frac{2}{c^2} \int_0^{\chi} d\chi' \frac{\chi - \chi'}{\chi\chi'} \int_{\mathbf{k}} 4\pi i^{\ell} j_{\ell}(k\chi') \Phi(\mathbf{k}, \chi') Y_{\ell m}^*(\hat{\mathbf{k}}), \tag{50}$$

using (36) (e.g., [8]). Integrating over redshift, we find the extrinsic scalar transfer functions:

$$\begin{aligned}
F_{\ell,a}^{\gamma^E,S}(k)|_{\text{ext}} &= \frac{1}{c^2} \sqrt{\frac{(\ell+2)!}{(\ell-2)!}} \int_0^{\chi_H} \frac{d\chi}{\chi} q_a(\chi) j_\ell(k\chi) \\
F_{\ell}^{\mathcal{F}^g,S}(k,\chi)|_{\text{ext}} &= \frac{1}{3c^2} \sqrt{\frac{(\ell+1)!}{(\ell-1)!}} [(\ell-1)(\ell+2) + 2\ell(\ell+1)] \int_0^{\chi_H} \frac{d\chi}{\chi} q_a(\chi) j_\ell(k\chi) \\
F_{\ell}^{\mathcal{G}^g,S}(k,\chi)|_{\text{ext}} &= \frac{1}{c^2} \sqrt{\frac{(\ell+3)!}{(\ell-3)!}} \int_0^{\chi_H} \frac{d\chi}{\chi} q_a(\chi) j_\ell(k\chi),
\end{aligned} \tag{51}$$

where  $q_a(\chi) \equiv \int_{\chi'}^{\chi_H} d\chi' n_a(\chi') (\chi' - \chi) / \chi'$  is the lensing efficiency. We note that any redshift-dependent contribution to the power spectrum (i.e., the potential growth factor) should be included in the  $\chi$  integrals. Finally, we note that the full scalar transfer functions are the sum of the intrinsic and extrinsic contributions (which are nontrivially correlated).

The power spectra arising from vector and tensor lensing can be computed analogously to the intrinsic contributions (Sec. VA 1); this is presented in Appendix D, with the tensor case following [22] (see also [23,84,85]). The main result is the following set of shear transfer functions

$$\begin{aligned}
F_{\ell,a}^{\gamma^E,V}(k)|_{\text{ext}} &= \frac{1}{2\sqrt{2}} \sqrt{\frac{(\ell-2)! (\ell+1)!}{(\ell+2)! (\ell-1)!}} \int_0^{\chi_H} \frac{d\chi}{\chi} (m_a(\chi) \text{Re}[\hat{Q}_{\gamma,V,1}^{(+)}(x)] + (m_a(\chi) - q_a(\chi)) \text{Re}[\hat{Q}_{\gamma,V,2}^{(+)}(x)]) \frac{j_\ell(x)}{x} \\
F_{\ell,a}^{\gamma^B,V}(k)|_{\text{ext}} &= \frac{1}{2\sqrt{2}} \sqrt{\frac{(\ell-2)! (\ell+1)!}{(\ell+2)! (\ell-1)!}} \int_0^{\chi_H} \frac{d\chi}{\chi} m_a(\chi) \text{Im}[\hat{Q}_{\gamma,V,1}^{(+)}(x)] \frac{j_\ell(x)}{x} \\
F_{\ell,a}^{\gamma^E,T}(k)|_{\text{ext}} &= \frac{1}{4} \int_0^{\chi_H} \frac{d\chi}{\chi} (m_a(\chi) \text{Re}[\hat{Q}_{\gamma,T,1}^{(+)}(x)] + (m_a(\chi) - q_a(\chi)) \text{Re}[\hat{Q}_{\gamma,T,2}^{(+)}(x)]) \frac{j_\ell(x)}{x^2} \\
F_{\ell,a}^{\gamma^B,T}(k)|_{\text{ext}} &= \frac{1}{4} \int_0^{\chi_H} \frac{d\chi}{\chi} m_a(\chi) \text{Im}[\hat{Q}_{\gamma,T,1}^{(+)}(x)] \frac{j_\ell(x)}{x^2},
\end{aligned} \tag{52}$$

defining the redshift-integrated kernel  $m_a(\chi) \equiv \int_{\chi'}^{\chi_H} d\chi' n_a(\chi')$ . This depends on the  $\hat{Q}$  derivative operators whose forms are given in (E4). As before, the vector and tensor modes source both  $E$  and  $B$  mode contributions, and, if the underlying physics is parity-violating, leads to an  $EB$  spectrum.

Under the approximation (42), we may compute the flexion correlators directly from those for the shear. In particular, expanding  $\pm_2\gamma$  in spin-weighted spherical harmonics and using relation (A10) leads to:

$$\begin{aligned}
iF_{\ell,a}^{\mathcal{F}^g,V/T}(k)|_{\text{ext}} &= \sqrt{\frac{(\ell+2)! (\ell-1)!}{(\ell-2)! (\ell+1)!}} F_{\ell,a}^{\gamma^E,V/T}(k)|_{\text{ext}}, & iF_{\ell,a}^{\mathcal{F}^c,V/T}(k)|_{\text{ext}} &= -\sqrt{\frac{(\ell+2)! (\ell-1)!}{(\ell-2)! (\ell+1)!}} F_{\ell,a}^{\gamma^B,V/T}(k)|_{\text{ext}} \\
iF_{\ell,a}^{\mathcal{G}^g,V/T}(k)|_{\text{ext}} &= -\sqrt{\frac{(\ell+3)! (\ell-2)!}{(\ell-3)! (\ell+2)!}} F_{\ell,a}^{\gamma^E,V/T}(k)|_{\text{ext}}, & iF_{\ell,a}^{\mathcal{G}^c,V/T}(k)|_{\text{ext}} &= \sqrt{\frac{(\ell+3)! (\ell-2)!}{(\ell-3)! (\ell+2)!}} F_{\ell,a}^{\gamma^B,V/T}(k)|_{\text{ext}}.
\end{aligned} \tag{53}$$

The flexion power spectra thus take the forms of (52), but with the additional  $\ell$ -dependent prefactors given above, which asymptote to  $\pm\ell$  in the large- $\ell$  limit.

### 3. Other contributions

As discussed in Sec. IV C, stochastic contributions to shear and flexion are modeled as a random fluctuations in each of two orthogonal directions (e.g., [7]). Averaging over sources within some bin  $a$ , the contribution to the spin- $\pm s$  piece in harmonic space is

$$\pm_s \hat{X}_{a,\ell m} = \int d\chi n_a(\chi) \int d\hat{\mathbf{n}}_{\pm s} Y_{\ell m}^*(\hat{\mathbf{n}}) [\hat{X}_1 \pm i\hat{X}_2](\chi \hat{\mathbf{n}}, \chi), \tag{54}$$

where the left-hand side can be decomposed into  $E$  and  $B$  (or  $g$  and  $c$ ) modes, both of which are nonvanishing. Assuming each galaxy to be uncorrelated implies that  $\langle \hat{X}_i(\mathbf{x}) \hat{X}_i^*(\mathbf{x}') \rangle = \sigma_\chi^2 \delta_D(\mathbf{x} - \mathbf{x}')$ ; after imposing spin-weighted spherical harmonic orthonormality (A9), this leads to the shear spectra

$$\begin{aligned} C_{\ell}^{\gamma^E \gamma^E, ab} \Big|_{\text{noise}} &= C_{\ell}^{\gamma^B \gamma^B, ab} \Big|_{\text{noise}} \\ &= \int_0^{\chi_H} d\chi n_a(\chi) n_b(\chi) \sigma_{\gamma}^2 \approx \delta_{ab}^K \frac{\sigma_{\gamma}^2}{\bar{n}_a}, \end{aligned} \quad (55)$$

with analogous forms for flexion. The RHS is obtained in the limit of nonoverlapping bins containing  $\bar{n}_a$  discrete sources per unit steradian. As expected, the Poisson noise is scale-independent, and contributes only to autospectra.

Higher-order contributions to the  $B$  and  $g$  modes are more difficult to compute since the underlying integrals are convolutional. [92,93] present a careful treatment of second-order lensing effects; here, we use a rough estimate of their magnitude only, since our focus is on non- $\Lambda$ CDM physics. This is obtained by assuming that the spectra are dominated by reduced shear contributions (i.e., those  $\propto \kappa \gamma_{ij}$ ), which lead to the approximate form  $C_{\ell}^{\gamma^B \gamma^B} \Big|_{S^2, \text{ext}} \approx 10^{-3} \times (1+q)^2 C_{\ell}^{\gamma^E \gamma^E} \Big|_{S, \text{ext}}$ , where  $q \approx 1$  is the lensing bias (cf. Fig. 7 of [22]). We assume a similar form for the flexion  $c$ -mode spectra;  $C_{\ell}^{\mathcal{F}^c \mathcal{F}^c} \Big|_{S^2, \text{ext}} \approx 10^{-3} \times (1+q)^2 C_{\ell}^{\mathcal{F}^g \mathcal{F}^g} \Big|_{S, \text{ext}}$ , and similarly for  $\mathcal{G}$ .

## B. Flat-sky limits

The results presented in Sec. VA give the complete descriptions of the angular power spectra of shear and flexion on all scales; however, they are expensive to

implement, and difficult to interpret. At large  $\ell$ , one can make use of the Limber approximation, which states [94] (see, e.g., [95–97] for associated works):

$$j_{\ell}(x) \approx \sqrt{\frac{\pi}{2\nu}} \delta_D(x - \nu), \quad \ell \gg 1, \quad (56)$$

where  $\nu \equiv \ell + 1/2$ . This can be used to remove the Bessel function integrals present in each transfer function, allowing the full spectrum to be computed via a single integral.<sup>5</sup> Below, we discuss the limiting forms for both the intrinsic and extrinsic spectra, paying close attention to their scale dependence.

### 1. Intrinsic contributions

In the large- $\ell$  limit, the scalar intrinsic alignment kernels (46) and (47) have the limiting forms:

$$\begin{aligned} F_{\ell}^{\gamma^E, S}(k, \chi) \Big|_{\text{int}} &\approx \ell^2 \frac{b_S(\chi)}{2\chi^2} j_{\ell}(x), \\ F_{\ell}^{\mathcal{F}^g, S}(k, \chi) \Big|_{\text{int}} &\approx -\frac{1}{3} F_{\ell}^{\mathcal{G}^g, S}(k, \chi) \Big|_{\text{int}} \approx \ell^3 \frac{4\tilde{b}_S(\chi)}{9\chi^2} j_{\ell}(x), \end{aligned} \quad (57)$$

using the small-scale limit of the  $\hat{Q}_{\chi, S}^{(+1)}$  operators given in Appendix E. Integrating over redshift and using (56) leads to the simplified forms:

$$\begin{aligned} F_{\ell}^{\gamma^E, S, a}(k) \Big|_{\text{int}} &= \frac{k}{2\nu^{1/2}} \sqrt{\frac{\pi}{2\nu}} n_a(\nu/k) b_S(\nu/k), \\ F_{\ell}^{\mathcal{F}^g, S, a}(k) \Big|_{\text{int}} &\approx -\frac{1}{3} F_{\ell}^{\mathcal{G}^g, S, a}(k) \Big|_{\text{int}} \approx \frac{4k\nu}{9} \sqrt{\frac{\pi}{2\nu}} n_a(\nu/k) \tilde{b}_S(\nu/k), \end{aligned} \quad (58)$$

where we omit the  $\chi$ -dependent part of the power spectrum for clarity. The utility of such expressions is clear if we consider the power spectra themselves, for example:

$$\begin{aligned} C_{\ell}^{\gamma^E \gamma^E, ab} \Big|_{S, \text{int}} &\approx \frac{\nu^4}{4} \int_0^{\infty} \frac{d\chi}{\chi^6} n_a(\chi) n_b(\chi) b_S^2(\chi) P_{\Phi}(\nu/\chi, \chi, \chi) \\ C_{\ell}^{\mathcal{F}^g \mathcal{F}^g, ab} \Big|_{S, \text{int}} &\approx \frac{1}{9} C_{\ell}^{\mathcal{G}^g \mathcal{G}^g, ab} \Big|_{S, \text{int}} \approx \frac{16\nu^6}{81} \int \frac{d\chi}{\chi^6} n_a(\chi) n_b(\chi) \tilde{b}_S^2(\chi) P_{\Phi}(\nu/\chi, \chi, \chi) \end{aligned} \quad (59)$$

[95,98]; this can now be computed as a single redshift integral, which is highly accurate for  $\ell \gtrsim 100$ . Notably, the spectra are diagonal in redshift if bins  $a$  and  $b$  do not overlap.

The limiting forms for vector and tensor sources are a little more complex. Using the results of Appendix E, the limiting forms of the vector unbinned kernels are given by

<sup>5</sup>This assumption is not always appropriate: primordially sourced tensors evolve under an oscillatory transfer function  $T_T \propto j_1(k\eta)/(k\eta)$ , thus the integrals in question contain two Bessel functions, and are thus not well approximated by (56).

$$\begin{aligned}
F_\ell^{\gamma^E, V}(k, \chi) \Big|_{\text{int}} &\approx \ell \frac{b_V(\chi)}{2\sqrt{2}\chi} j'_\ell(x) \mathcal{I}_V(\chi), & F_\ell^{\gamma^B, V}(k, \chi) \Big|_{\text{int}} &\approx \ell \frac{b_V(\chi)}{2\sqrt{2}\chi} j_\ell(x) \mathcal{I}_V(\chi), \\
F_\ell^{\mathcal{F}^q, V}(k, \chi) \Big|_{\text{int}} &\approx -\frac{1}{3} F_\ell^{\mathcal{G}^q, V}(k, \chi) \Big|_{\text{int}} \approx \ell^2 \frac{2\sqrt{2}\tilde{b}_V(\chi)}{9\chi} j'_\ell(x) \mathcal{I}_V(\chi), \\
F_\ell^{\mathcal{F}^c, V}(k, \chi) \Big|_{\text{int}} &\approx -\frac{1}{9} F_\ell^{\mathcal{G}^c, V}(k, \chi) \Big|_{\text{int}} \approx -\ell^2 \frac{2\sqrt{2}\tilde{b}_V(\chi)}{27\chi} j_\ell(x) \mathcal{I}_V(\chi).
\end{aligned} \tag{60}$$

Notably, the  $B$ - and  $c$ -modes are proportional to  $j_\ell(x)$ , whilst the  $E$  and  $g$ -modes depend on the Bessel function derivatives  $j'_\ell(x)$ , and are thus suppressed. This occurs due to projection: the 3D vector field is parity-odd, but can induce a small parity-even component when projected onto the two-sphere [cf. [99]].

Integrals involving Bessel function derivatives are harder to simplify using the Limber approximation (though see Appendix E of [25] for a number of useful simplifications).<sup>6</sup> Instead, one can obtain the redshift-binned kernels using integration-by-parts, for example:

$$\begin{aligned}
F_\ell^{\gamma^E, V, a}(k) \Big|_{\text{int}} &\approx \ell \int_{\chi_1}^{\chi_2} d\chi n_a(\chi) \frac{b_V(\chi)}{2\sqrt{2}\chi} j'_\ell(x) = \left[ n_a(\chi) \frac{b_V(\chi)}{2\sqrt{2}k\chi} j_\ell(x) \right]_{\chi_1}^{\chi_2} - \int_{\chi_1}^{\chi_2} d\chi \partial_\chi \left[ n_a(\chi) \frac{b_V(\chi)}{2\sqrt{2}k\chi} \right] j_\ell(x), \\
&\approx \left[ n_a(\chi) \frac{b_V(\chi)}{2\sqrt{2}k\chi} j_\ell(x) \right]_{\chi_1}^{\chi_2} - \sqrt{\frac{\pi}{2\nu}} \partial_\chi \left[ n_a(\chi) \frac{b_V(\chi)}{2\sqrt{2}k^2\chi} \right]_{\chi=\nu/k},
\end{aligned} \tag{61}$$

assuming the redshift bin to have finite support over  $[\chi_1, \chi_2]$ , and inserting (56) in the second expression.<sup>7</sup> If the number density distribution falls smoothly to zero at the boundaries, then the first term is negligible; however, it can be important in the case of (largely unphysical) sharp bin boundaries. Using these relations, one can derive the flat-sky limits of power spectra, for example, the auto-spectra of  $B$ - and  $c$ -modes:

$$\begin{aligned}
C_\ell^{\gamma^B, \gamma^B, ab} \Big|_{V, \text{int}} &\approx \frac{\nu^2}{8} \int_0^\infty \frac{d\chi}{\chi^4} n_a(\chi) n_b(\chi) b_V^2(\chi) [P_{\mathcal{I}_V B_+}(\nu/\chi, \chi, \chi) + P_{\mathcal{I}_V B_-}(\nu/\chi, \chi, \chi)] \\
C_\ell^{\mathcal{F}^c, \mathcal{F}^c, ab} \Big|_{V, \text{int}} &\approx \frac{1}{81} C_\ell^{\mathcal{G}^c, \mathcal{G}^c, ab} \Big|_{V, \text{int}} \approx \left( \frac{2\sqrt{2}\nu^2}{27} \right)^2 \int_0^\infty \frac{d\chi}{\chi^4} n_a(\chi) n_b(\chi) \tilde{b}_V^2(\chi) [P_{\mathcal{I}_V B_+}(\nu/\chi, \chi, \chi) + P_{\mathcal{I}_V B_-}(\nu/\chi, \chi, \chi)],
\end{aligned} \tag{62}$$

absorbing the  $\mathcal{I}_V$  operators into the power spectrum.

The flat-sky limits of tensor correlators can be derived similarly. The unbinned kernels can be written:

$$F_\ell^{\gamma^E, T}(k, \chi) \Big|_{\text{int}} \approx \left( \frac{\ell^2}{x^2} - 2 \right) \frac{b_T(\chi)}{4} j_\ell(x) \mathcal{I}_T(\chi), \quad F_\ell^{\gamma^B, T}(k, \chi) \Big|_{\text{int}} \approx \frac{b_T(\chi)}{2} j'_\ell(x) \mathcal{I}_T(\chi), \tag{63}$$

$$\begin{aligned}
F_\ell^{\mathcal{F}^q, T}(k, \chi) \Big|_{\text{int}} &\approx \ell \left( 3 \frac{\ell^2}{x^2} - 2 \right) \frac{2\tilde{b}_T(\chi)}{27} j_\ell(x) \mathcal{I}_T(\chi), & F_\ell^{\mathcal{G}^q, T}(k, \chi) \Big|_{\text{int}} &\approx -\ell \left( \frac{\ell^2}{x^2} - 2 \right) \frac{2\tilde{b}_T(\chi)}{3} j_\ell(x) \mathcal{I}_T(\chi), \\
F_\ell^{\mathcal{F}^c, T}(k, \chi) \Big|_{\text{int}} &\approx -\frac{1}{9} F_\ell^{\mathcal{G}^c, T}(k, \chi) \Big|_{\text{int}} \approx -\ell \frac{4\tilde{b}_T(\chi)}{27} j'_\ell(x) \mathcal{I}_T(\chi).
\end{aligned} \tag{64}$$

We find the opposite conclusion to the vector case: the  $B$ - and  $c$ -modes are derivative suppressed compared to the  $E$ - and  $g$ -modes [99]. Their binned forms can be obtained using integration by parts, as in (61). The unsuppressed flat-sky auto-power spectra take the form:

$$\begin{aligned}
C_\ell^{\gamma^E, \gamma^E, ab} \Big|_{T, \text{int}} &\approx \frac{1}{16} \int_0^\infty \frac{d\chi}{\chi^2} n_a(\chi) n_b(\chi) b_T^2(\chi) [P_{\mathcal{I}_T h_+}(\nu/\chi, \chi, \chi) + P_{\mathcal{I}_T h_-}(\nu/\chi, \chi, \chi)] \\
C_\ell^{\mathcal{F}^q, \mathcal{F}^q, ab} \Big|_{T, \text{int}} &\approx \frac{1}{81} C_\ell^{\mathcal{G}^q, \mathcal{G}^q, ab} \Big|_{T, \text{int}} \approx \left( \frac{2\ell}{9} \right)^2 \int_0^\infty \frac{d\chi}{\chi^2} n_a(\chi) n_b(\chi) \tilde{b}_T^2(\chi) [P_{\mathcal{I}_T h_+}(\nu/\chi, \chi, \chi) + P_{\mathcal{I}_T h_-}(\nu/\chi, \chi, \chi)].
\end{aligned} \tag{65}$$

<sup>6</sup>Whilst one can rewrite  $j'_\ell(x)$  as the difference between two spherical Bessel functions then apply the Limber approximation, this is numerically unstable.

<sup>7</sup>For clarity, we have dropped the  $\chi$  dependence arising from  $\mathcal{I}_V(\chi)\mathcal{I}_V(\chi')P_{B_\pm}(k, \chi, \chi')$ . In practice, this can be included by enforcing a separable correlator via  $P_X(k, \chi, \chi') \approx \sqrt{P_X(k, \chi, \chi)P_X(k, \chi', \chi')}$  for  $X \in \{\Phi, B_\pm, h_\pm\}$ .

The utility of the above simplifications is twofold: firstly, they allow for efficient computation of the high- $\ell$  spectra (which would otherwise require a dense three-dimensional numerical integration grid), and secondly, one can easily assess the  $\ell$ -scalings of the correlators. These are given explicitly in Table I for each intrinsic autospectrum sourced by scalar, vector, and tensor physics. This clearly demonstrates three points, noted above:

- (1) All flexion spectra are suppressed by  $\ell^2$  with respect to shear, and thus contribute significantly only on small scales.
- (2) Scalar perturbations generate only  $E$ - and  $g$ -modes at leading-order, whilst vectors and tensors generate also  $B$ - and  $c$ -modes.
- (3) Intrinsic vector  $E$ - and  $g$ -mode spectra are derivative-suppressed compared to  $B$ - and  $c$ -modes; the reverse is true for tensors.

The first property implies that flexion will be useful only on small scales, matching previous conclusions (e.g. [65]). From the third, we conclude that the often-ignored  $B$ - and  $c$ -mode spectra are an excellent place in which to search for vector perturbations; in contrast, tensors require  $E$ - and  $g$ -modes, which contain large contributions from scalar physics, thus hampering their detectability. If the sources are parity-violating, the cross-spectra (particularly  $EB$ ) can be of significant use, though the projection effects partially suppress such signals [25,99].

## 2. Extrinsic contributions

The large- $\ell$  limit of scalar lensing spectra is straightforward. From (50), the scalar transfer functions have the asymptotic form

$$F_{\ell,a}^{\gamma^E,S}(k) \Big|_{\text{ext}} \approx \frac{1}{\ell} F_{\ell}^{\mathcal{F}^g,S}(k,\chi) \Big|_{\text{ext}} \approx \frac{1}{\ell} F_{\ell}^{\mathcal{G}^g,S}(k,\chi) \Big|_{\text{ext}} \approx \frac{\ell^2}{c^2} \int_0^{\chi_H} \frac{d\chi}{\chi} q_a(\chi) j_{\ell}(k\chi), \quad (66)$$

leading to autospectra of the form

$$C_{\ell}^{\gamma^E,\gamma^E,ab} \approx \frac{\nu^4}{c^4} \int_0^{\infty} \frac{d\chi}{\chi^4} q_a(\chi) q_b(\chi) P_{\Phi}(\nu/\chi, \chi, \chi) \quad (67)$$

TABLE I. Approximate scalings of the intrinsic alignment and lensing power spectra in the large- $\ell$  limit, as derived from Sec. VB. In each case, we give the  $\ell$ -dependence of  $C_{\ell}^{XX}/C_{\ell}^{\gamma^E,\gamma^E}$ , considering both shear and flexion, and scalar, vector, and tensor physics. We display results only for the first flexion, noting that  $\mathcal{F}$  and  $\mathcal{G}$  have the same scalings at large- $\ell$ . The scalings of cross-spectra may be found by taking the harmonic mean of autospectra scalings, i.e., the  $C_{\ell}^{\gamma^B,\mathcal{F}^c}$  scaling for vector intrinsic alignments is  $\sqrt{\ell^2 \times \ell^4} = \ell^3$  that of  $C_{\ell}^{\gamma^E,\gamma^E}$ . Note that the amplitudes of intrinsic vector  $E/g$ -modes and tensor intrinsic  $B/c$ -modes are suppressed due to the presence of Bessel function derivatives.

Intrinsic	$\gamma^E\gamma^E$	$\gamma^B\gamma^B$	$\mathcal{F}^g\mathcal{F}^g$	$\mathcal{F}^c\mathcal{F}^c$
Scalar	1	0	$\ell^2$	0
Vector	1	$\ell^2$	$\ell^2$	$\ell^4$
Tensor	1	$\ell^{-2}$	$\ell^2$	$\ell^0$
Extrinsic	$\gamma^E\gamma^E$	$\gamma^B\gamma^B$	$\mathcal{F}^g\mathcal{F}^g$	$\mathcal{F}^c\mathcal{F}^c$
Scalar	1	0	$\ell^2$	0
Vector	1	$\ell^{-2}$	$\ell^2$	$\ell^0$
Tensor	1	$\ell^{-2}$	$\ell^2$	$\ell^0$

(e.g., [95]), invoking the Limber approximation (56). Unlike the intrinsic spectra, this is not diagonal in redshift.

For the vector and tensor kernels, computation proceeds analogously to Sec. VB 1. From (52), and using the limiting forms of the  $\hat{Q}$  operators given in Appendix E, we find

$$F_{\ell,a}^{\gamma^E,V}(k) \Big|_{\text{ext}} \approx -\frac{\ell^3}{2\sqrt{2}} \int_0^{\chi_H} \frac{d\chi}{\chi} q_a(\chi) \frac{j_{\ell}(x)}{x},$$

$$F_{\ell,a}^{\gamma^B,V}(k) \Big|_{\text{ext}} \approx \frac{\ell}{2\sqrt{2}} \int_0^{\chi_H} \frac{d\chi}{\chi} m_a(\chi) j_{\ell}(x)$$

$$F_{\ell,a}^{\gamma^E,T}(k) \Big|_{\text{ext}} \approx -\frac{\ell^4}{8} \int_0^{\chi_H} \frac{d\chi}{\chi} q_a(\chi) \frac{j_{\ell}(x)}{x^2},$$

$$F_{\ell,a}^{\gamma^B,T}(k) \Big|_{\text{ext}} \approx \frac{\ell^2}{4} \int_0^{\chi_H} \frac{d\chi}{\chi} m_a(\chi) \frac{j_{\ell}(x)}{x}. \quad (68)$$

This leads to power spectra of the form

$$C_{\ell}^{\gamma^E,\gamma^E,ab} \Big|_{V,\text{ext}} \approx \frac{\nu^4}{8} \int_0^{\infty} \frac{d\chi}{\chi^4} q_a(\chi) q_b(\chi) [P_{B_+}(\nu/\chi, \chi, \chi) + P_{B_-}(\nu/\chi, \chi, \chi)]$$

$$C_{\ell}^{\gamma^B,\gamma^B,ab} \Big|_{V,\text{ext}} \approx \frac{\nu^2}{8} \int_0^{\infty} \frac{d\chi}{\chi^4} m_a(\chi) m_b(\chi) [P_{B_+}(\nu/\chi, \chi, \chi) + P_{B_-}(\nu/\chi, \chi, \chi)]$$

$$C_{\ell}^{\gamma^E,\gamma^E,ab} \Big|_{T,\text{ext}} \approx \frac{\nu^4}{64} \int_0^{\infty} \frac{d\chi}{\chi^4} q_a(\chi) q_b(\chi) [P_{h_+}(\nu/\chi, \chi, \chi) + P_{h_-}(\nu/\chi, \chi, \chi)]$$

$$C_{\ell}^{\gamma^B,\gamma^B,ab} \Big|_{T,\text{ext}} \approx \frac{\nu^2}{16} \int_0^{\infty} \frac{d\chi}{\chi^4} m_a(\chi) m_b(\chi) [P_{h_+}(\nu/\chi, \chi, \chi) + P_{h_-}(\nu/\chi, \chi, \chi)], \quad (69)$$

under the Limber approximation. For the flexion spectra, we employ the simplifying *ansatz* of (53), which implies

$$\begin{aligned} iF_{\ell,a}^{\mathcal{F}^{g,V/T}}(k)\Big|_{\text{ext}} &\approx -iF_{\ell,a}^{\mathcal{G}^{g,V/T}}(k)\Big|_{\text{ext}} \approx \ell \times F_{\ell,a}^{\gamma^E,V/T}(k)\Big|_{\text{ext}}, \\ iF_{\ell,a}^{\mathcal{F}^{c,V/T}}(k)\Big|_{\text{ext}} &\approx -iF_{\ell,a}^{\mathcal{G}^{c,V/T}}(k)\Big|_{\text{ext}} \approx -\ell \times F_{\ell,a}^{\gamma^B,V/T}(k)\Big|_{\text{ext}}, \end{aligned} \quad (70)$$

allowing simple computation of the flexion spectra (e.g., [65,66]).

A summary of the extrinsic autospectrum scalings is given in Table I, alongside the intrinsic results. As before, the flexion spectra are suppressed by  $\ell^2$  compared to the shear spectra, and the tensor  $B$ - and  $c$ -modes are suppressed compared to the  $E$ - and  $g$ -modes, though there are no Bessel function derivatives in this case. Here, we find the opposite scalings of vector modes (with  $E$ - and  $c$ -modes enhanced on large scales rather than  $B$ - and  $g$ -modes). This can be rationalized by looking at how vector modes impact intrinsic and extrinsic shear, (32) and (41). In the former case, we have dependence only through the projected derivatives  $\partial_{\pm}B_{\pm}$ , whilst the latter also contains a term involving  $\partial_{\pm}\partial_{\pm}B_{\parallel}$  (proportional to  $q(\chi)$ ) for  $B_{\parallel} \equiv B_i\hat{n}^i$ , which dominates in the large- $\ell$  regime. Since this is a radial projection instead of an angular projection,  $E$ - and  $B$ -modes are interchanged, leading to the different scalings.

## VI. NUMERICAL RESULTS

Having discussed the physical sources of galaxy shape distortions and their associated power spectra, we now proceed to perform a numerical study of new physics in shear and flexion. To this end, we will consider two beyond- $\Lambda$ CDM physics models, described in Sec. II: (1) nonstandard inflation, with independent primordial sourcing of vector and tensor degrees of freedom; and (2) a late-Universe network of cosmic strings, which jointly sources vector and tensor modes. By combining the power spectra of the metric fluctuations with the above results, we can consider the heuristic forms of the generated shear and flexion spectra, and forecast the possible constraints on the model amplitudes.

### A. Setup

*a. Perturbations* As discussed in Sec. II B 1, we model primordial power spectra using power laws, relative to a fiducial scale  $k_0 = 0.002 \text{ Mpc}^{-1}$  (e.g., [36]). Here, we assume a tensor exponent  $n_T = -r_T/8$  (motivated by simple inflationary models), with an independent

scale-invariant vector exponent,  $n_V = 1$ .<sup>8</sup> For plotting, we will assume the fiducial values  $r_T = r_V = 1$ , with the vector transfer functions normalized to their values at the last scattering surface (noting the strong decay as  $a^{-2}(z)$ ). To test constraints on parity-violating physics, we will allow for maximum fiducial chirality  $\epsilon_{V,T} = 1$ , noting that the set of spectra sourced by parity-odd and parity-even physics are disjoint at leading order.

The power spectra of the cosmic shear metric perturbations is modeled as described in Sec. II B 2 (using the results derived in Appendix B), using the fiducial parameter values given therein, with a baseline (squared) string tension  $(G\mu)^2 = 10^{-16}$  and an intercommuting probability of  $P = 10^{-3}$ , which sets the amplitude of both vector and tensor contributions (e.g., [24]). In the standard string model, only parity-even correlators are sourced; here, we will allow for parity-breaking contributions via a global chirality parameter  $\epsilon = 1$ , analogous to the primordial case. Finally, the intrinsic alignment spectra require the time-differentiated vector and tensor spectra: following a similar derivation to that given in Appendix B, the equal-time correlators can be shown to equal

$$\begin{aligned} P_{\mathcal{I}_V B_{\pm}}(k, \eta, \eta) &= \left\{ (3aH)^2 + \frac{1}{3}k^2 v_{\text{rms}}^2 \right\} P_{B_{\pm}}(k, \eta, \eta), \\ P_{\mathcal{I}_T h_{\pm}}(k, \eta, \eta) &= \left\{ [6(aH)^2 + 2\partial_{\eta}(aH)]^2 + \frac{1}{3}(5aH)^2 k^2 v_{\text{rms}}^2 \right. \\ &\quad \left. + \frac{2}{9}k^4 v_{\text{rms}}^4 \right\} P_{h_{\pm}}(k, \eta, \eta) \end{aligned} \quad (71)$$

assuming time independence for  $v_{\text{rms}}^2$  and the comoving string density.

*b. Experimental parameters* To compute the shear and flexion power spectra we must also specify the number-density of source galaxies and their noise properties. Following [70], we will assume a projected galaxy density of  $40 \text{ arcmin}^{-2}$ , with the normalized distribution

$$n(z) \propto \left(\frac{z}{z_0}\right)^{\alpha} e^{-(z/z_0)^{\beta}}, \quad (72)$$

where  $\alpha = 2$ ,  $\beta = 3/2$ , and  $z_0 = 0.64$ , as relevant for a *Euclid*-like survey [100]. This is split into three equally populated bins, each following a smooth (overlapping) distribution. We will assume a sky fraction of  $f_{\text{sky}} = 0.3636$ , as relevant for *Euclid* [101].

<sup>8</sup>Strictly, it is inconsistent to simultaneously assume *almost* scale-invariant tensors ( $n_T = -r_T/8$ ) and *exactly* scale-invariant vectors ( $n_V = 1$ ), if sourced by a common inflationary origin. Here, we consider the two perturbations separately, and note that small deviations of either from scale-invariance will have very minor impact on our constraints.

To model the intrinsic contributions, we require the shear and flexion alignment biases,  $b_X(\chi)$  and  $\tilde{b}_X(\chi)$ . Due to hydrodynamic effects, these are difficult to predict from theory or simulations, even for the scalar case. Here, we follow [85], and fix the scalar shear bias to  $b_S(\chi) = b_1^I(\chi) \frac{2\alpha(\chi)}{3H_0^2\Omega_{m0}}$ , with  $b_1^I(\chi) = -0.1\Omega_{m0}D(0)/D(\chi)$ , consistent with [17]. Assuming all components to impact the shear only through the tidal tensor yields the relations  $b_T = b_S/2$ ,  $b_V = -b_S$ , reinserting the previously dropped constants of proportionality [cf., [22]]. We additionally assume the same bias for shear and flexion, i.e.,  $b_X = \tilde{b}_X$ , motivated by the analytic results of [[70], Eq. 18].

*c. Numerical setup* We numerically compute angular power spectra for all auto- and cross-spectra of shear and spin- $\pm 1$  flexion for  $39\ell$ -bins in the range [2, 2000], using linear spacing for  $\ell \leq 10$  and logarithmic else. We ignore the spin- $\pm 3$  flexion for clarity, noting that this will not change our overall conclusions. Spectra are computed in Python using numerical quadrature, with the Limber approximation (Sec. V B) used for  $\ell > 100$  (except for pathological situations, such as primordially sourced tensors). Throughout, we assume the fiducial cosmology  $\{h = 0.7, A_s = 1.95 \times 10^{-9}, n_s = 0.96, \Omega_b = 0.049, \Omega_m = 0.3\}$ , and evaluate scalar spectra using the ‘‘halofit’’ formalism to approximate nonlinear effects [102].

## B. Power spectra

Under null assumptions (i.e., without vector and tensor modes), the following spectra are sourced at leading order:

$$\begin{aligned} C_\ell^{\gamma^E\gamma^E}, C_\ell^{\mathcal{F}^g\mathcal{F}^g}, C_\ell^{\gamma^E\mathcal{F}^g} & \quad (\text{from scalars}) \\ C_\ell^{\gamma^E\gamma^E}, C_\ell^{\mathcal{F}^g\mathcal{F}^g}, C_\ell^{\gamma^B\gamma^B}, C_\ell^{\mathcal{F}^c\mathcal{F}^c} & \quad (\text{from noise}). \end{aligned} \quad (73)$$

For noise and intrinsic-only contributions, only autospectra  $a = b$  are sourced (for redshift bins  $a, b$ , in the large- $\ell$  limit), whilst lensing sources also  $a \neq b$  bin pairs and cross-correlations with intrinsic effects. At second order, scalars also source contributions to  $C_\ell^{\gamma^B\gamma^B}$ ,  $C_\ell^{\mathcal{F}^c\mathcal{F}^c}$ , and  $C_\ell^{\gamma^E\mathcal{F}^c}$ , which are modeled as discussed in Sec. VA 3. In the presence of vector or tensor perturbations, we source the following spectra:

$$\begin{aligned} C_\ell^{\gamma^E\gamma^E}, C_\ell^{\gamma^B\gamma^B}, C_\ell^{\mathcal{F}^g\mathcal{F}^g}, C_\ell^{\mathcal{F}^c\mathcal{F}^c}, C_\ell^{\gamma^E\mathcal{F}^g}, C_\ell^{\gamma^B\mathcal{F}^c} & \quad (\text{parity-conserving}) \\ C_\ell^{\gamma^E\gamma^B}, C_\ell^{\mathcal{F}^g\mathcal{F}^c}, C_\ell^{\gamma^E\mathcal{F}^c}, C_\ell^{\gamma^B\mathcal{F}^g} & \quad (\text{parity-breaking}), \end{aligned} \quad (74)$$

depending on the parity-properties of the underlying metric correlators.

*a. Inflationary perturbations* In Fig. 2, we plot the primordially-sourced vector and tensor correlators of shear and flexion, alongside the fiducial power spectra arising from scalar physics and noise. Notably, detecting such spectra will be challenging. Whilst we forecast a very

strong shear  $E$ -mode signal (principally arising from lensing), the only other scalar cross-spectrum with a realistic hope of being detected is that between  $\gamma^E$  and  $\mathcal{F}^g$  (or between  $\gamma^E$  and  $\mathcal{G}^g$ ), which requires a large  $\ell_{\max}$  [cf. [67,68,70]]. As previously noted, the parity-odd scalar modes are strongly suppressed compared to the parity-even forms, and do not contribute to parity-violating cross-spectra.

Spectra sourced by primordial vector perturbations show a strong scale dependence, with largest contributions seen on smallest scales. In this scenario, the correlators are dominated by weak lensing contributions, and, as predicted in Table I,  $E$ -modes exhibit steeper scalings with  $\ell$  than  $B$ -modes. If one considers the intrinsic contributions alone, the opposite is true, matching Sec. V B, and analogous conclusions can be drawn for flexion (though at much lower signal-to-noise). In our fiducial parametrization, we find extremely small amplitudes for the vector spectra; we will discuss the resulting constraints on  $r_V$  and  $\epsilon_V r_V$  in Sec. VI C.

The primordial tensor contributions are very different from those of vectors. As in [22], the spectra peak on ultralarge scales but quickly decay away to small values (whose inference is complicated by numerical error intrinsic to the Bessel function integrals). In this case, the intrinsic alignment  $E$ -mode contribution dominates at large scales, but much of this power is canceled by an analogous extrinsic contribution due to the equivalence principle. The gravitational waves contribute nontrivially to an array of correlators with different  $\ell$ -dependencies; however, their power is always small, even at the fiducial amplitude  $r_T = 1$ . As shown in [22] and discussed below, the signal can be boosted somewhat by using a higher-redshift galaxy sample.

*b. Cosmic strings* Figure 3 shows the analogous results for the cosmic string power spectrum, which are much more promising. With the fiducial string tension of  $G\mu = 10^{-8}$ , vector contributions to galaxy shapes are significant, and are usually larger than the scalar pieces, particularly for low- $\ell$   $B$ -modes and high- $\ell$   $E$ -modes. Many of spectra are dominated by lensing contributions [cf., [24]], though intrinsic alignment contributions are found to be important for  $B$ -modes, and the cross-correlation of lensing and intrinsic effects dominates in the  $\gamma^E - \gamma^B$  spectrum. Flexion spectra are also of interest, with a clear signal appearing in the  $\gamma^E - \mathcal{F}^g$  correlator for  $\ell \gtrsim 100$ . The parity-odd signal may also be detectable through the  $\gamma^E - \gamma^B$  cross-spectrum though we note that this is not sourced in the standard string paradigm.

The tensorial contributions induced by cosmic strings are heavily suppressed compared to the vector pieces, with correlators one-to-two orders of magnitude smaller. The overall scalings with  $\ell$  also differ slightly from vectors, due to differing absolute importance of intrinsic and extrinsic contributions (cf. Table I). For the string scenario, we

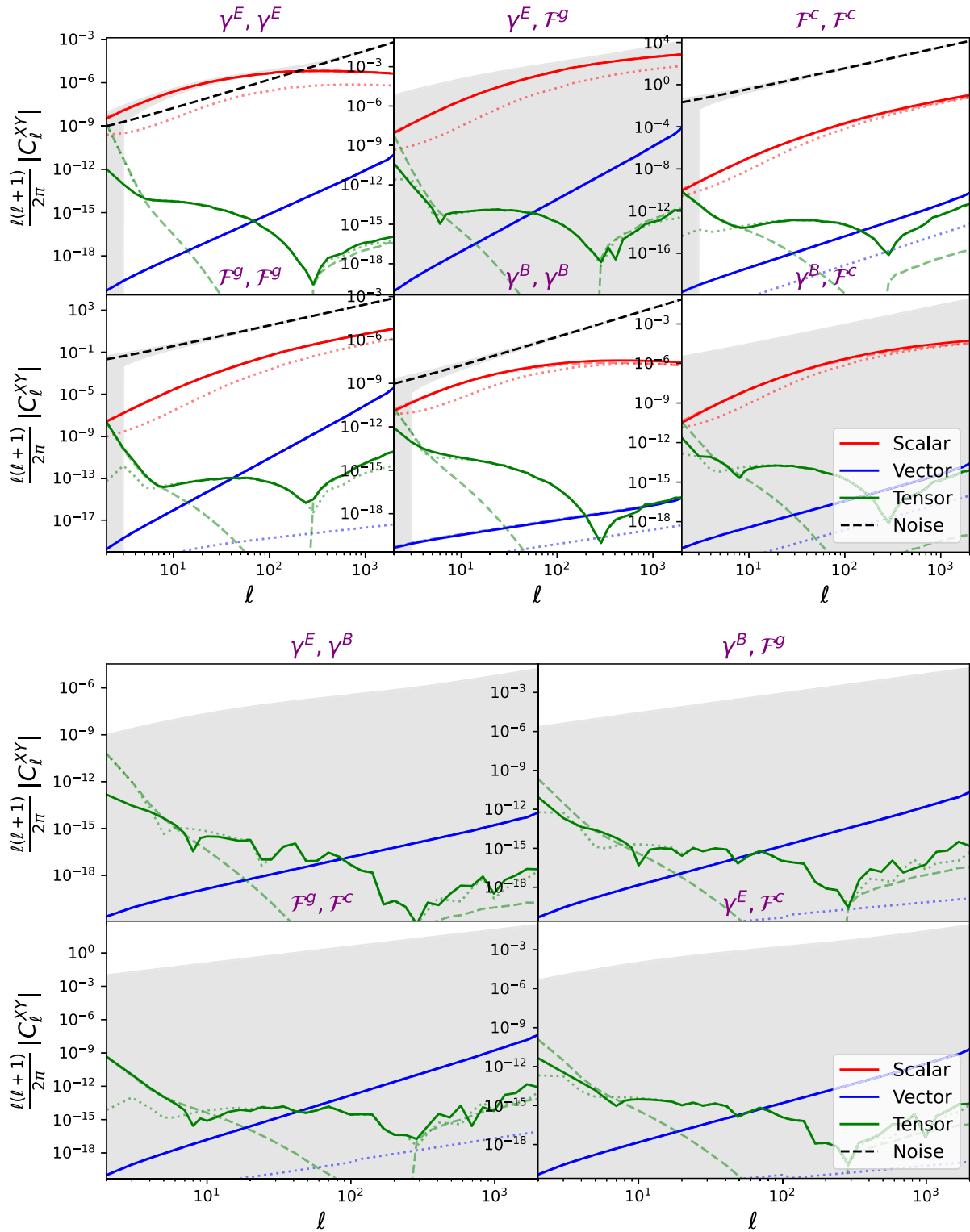


FIG. 2. Shear and flexion spectra sourced by scalar physics as well as primordial-generated vector and tensor modes. Each panel shows a separate cross-spectrum, as marked in the title, and the two plots show parity-conserving (top) and parity-breaking (bottom) correlators. The gray bands indicate  $1\sigma$  errorbars, with dashed (dotted) lines showing spectra containing only lensing (intrinsic alignment) contributions. The experimental setup is as described in Sec. VIA for a *Euclid*-like experiment, and we plot only results from the central redshift bin with  $\bar{z} \approx 0.95$ . The fiducial spectra have amplitudes  $r_T = 1$  for tensors, and  $r_V = 1$  for vectors, with the latter spectra defined relative to the surface of last scattering. For parity-violating correlators, we assume a chirality parameter  $\epsilon_{V,T} = 1$ . Gravitational wave contributions (green) are difficult to detect except on ultralarge scales in shear. Vector modes of this type contribute significantly only on small scales, though this depends on the primordial tilt. The scatter in the tensor curves is not physical; this arises from numerical inaccuracies in the oscillatory integrals.

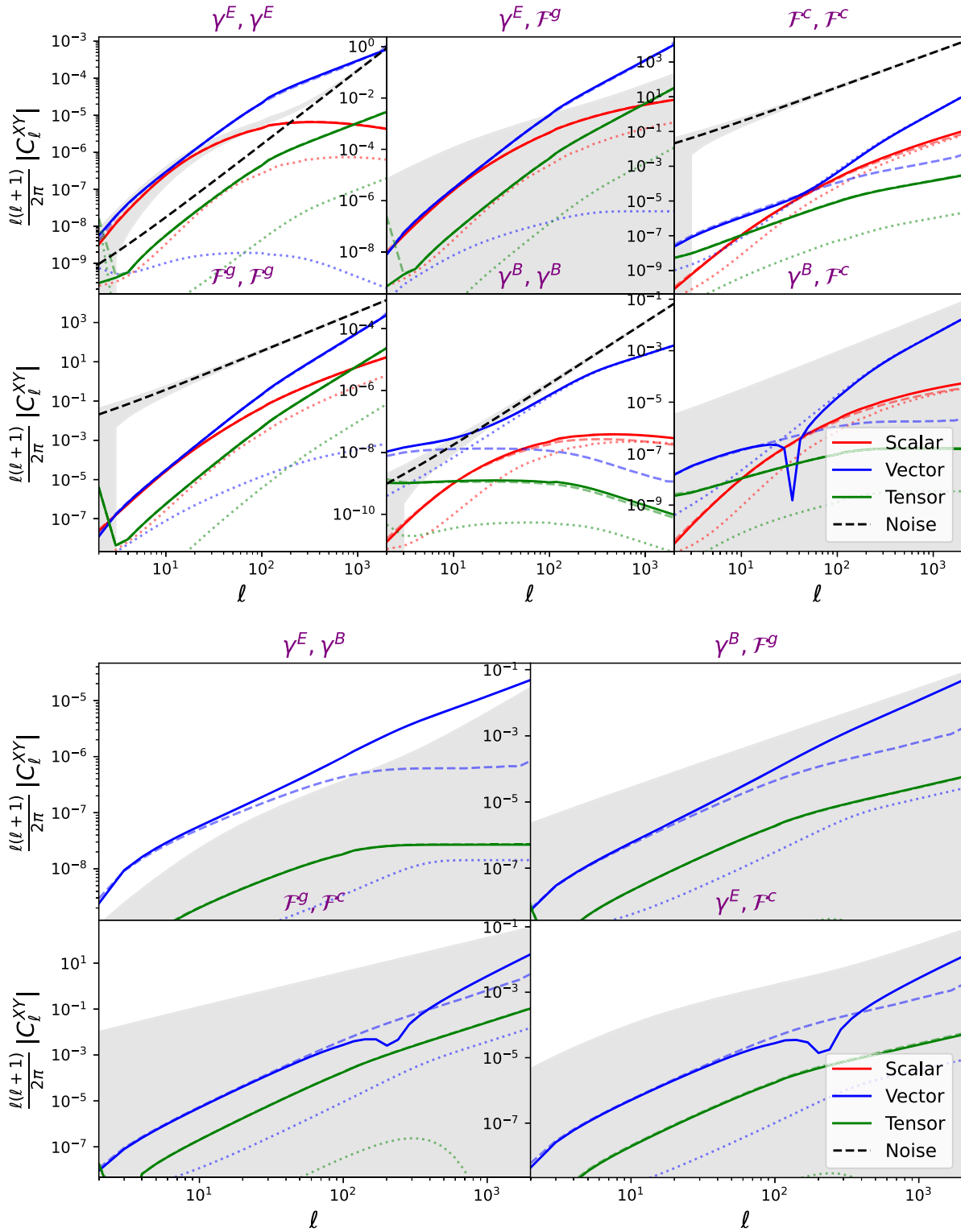


FIG. 3. As Fig. 2, but for a late-time network of cosmic strings, which sources both vector and tensor correlators. Here, we set the fiducial string tension to  $G\mu = 10^{-8}$ , and optionally allow for parity-odd contributions with chirality  $\epsilon = 1$ . For this choice of amplitude, we find large contributions from vector lensing modes, particularly in shear  $E$ - and  $B$ -mode correlators on small scales.

TABLE II. Constraints on the amplitudes of primordial and string-induced vector and tensor modes, obtained from Fisher forecasts appropriate for a *Euclid*-like survey, measuring shear and flexion for  $\ell \in [2, 2000]$ . In each case, we give the  $1\sigma$  constraint on the model amplitude ( $r_X$  for primordial sources,  $(G\mu)^2$  for strings), quoting primordial vector results relative to the amplitude at last scattering. Parity-odd constraints assume maximal chirality ( $\epsilon = 1$ ), and we additionally separate vector and tensor contributions to  $(G\mu)^2$ . In general, we find that the addition of flexion somewhat improves constraining power for spectra contributing at high- $\ell$ , and parity-odd spectra are less constraining than parity-even spectra. The constraints on primordial tensors (i.e., gravitational waves) are generally weak, whilst those on strings are relatively tight. The  $\ell$ -dependence of these constraints is explored in Figs. 4 and 5.

Observable	Parity	$\sigma[r_V]$	$\sigma[r_T]$	$\sigma_V[(G\mu)^2]$	$\sigma_T[(G\mu)^2]$
Shear	Even	$4.5 \times 10^4$	260	$2.2 \times 10^{-20}$	$1.2 \times 10^{-19}$
Shear	Odd	$2.6 \times 10^7$	600	$1.1 \times 10^{-19}$	$5.0 \times 10^{-17}$
Shear & flexion	Even	$3.9 \times 10^4$	260	$2.0 \times 10^{-20}$	$1.1 \times 10^{-19}$
Shear & flexion	Odd	$2.3 \times 10^7$	600	$1.0 \times 10^{-19}$	$5.0 \times 10^{-17}$

conclude that the vector contributions will dominate the constraining power on the model amplitude; however, this statement is strongly model-dependent.

### C. Fisher forecasts

We now elucidate the constraining power of shear and flexion on the physical models themselves. For this, we utilize a Fisher forecast (e.g., [103]), computing the optimal constraints on some set of parameters  $\{p_\alpha\}$ , via  $\sigma^2(p_\alpha) \geq F_{\alpha\alpha}^{-1}$ , for Fisher matrix

$$F_{\alpha\beta} \equiv \sum_{\ell} \frac{\partial \mathbf{D}_{\ell}}{\partial p_{\alpha}} \mathbb{C}_{\ell}^{-1} \frac{\partial \mathbf{D}_{\ell}}{\partial p_{\beta}}. \quad (75)$$

This depends on a data-vector,  $\mathbf{D}_{\ell}$ , and covariance  $\mathbb{C}_{\ell}$ , where the former contains all independent auto- and cross-spectra. Using three tomographic bins, we find a total of 42 (12) parity-even and 36 (9) parity-odd spectra when flexion is (is not) included. Assuming Gaussian statistics, the covariance between any pair of spectra is given by:

$$\begin{aligned} \text{Cov}(C_{\ell}^{XY,ab}, C_{\ell'}^{ZW,cd}) \\ = \frac{2\delta_{\ell\ell'}^K}{(2\ell+1)f_{\text{sky}}} [C_{\ell}^{XZ,ac} C_{\ell'}^{YW,bd} + C_{\ell}^{XW,ad} C_{\ell'}^{YZ,bc}], \end{aligned} \quad (76)$$

which is diagonal in  $\ell$ . Under null hypotheses, the spectra on the RHS contain only signals from scalar perturbations and stochasticity; furthermore, parity-odd and parity-even spectra are uncorrelated, thus we may compute their contributions to parameter constraints separately.

Table II lists the forecasted constraints on the model amplitudes of the two sources of vector and tensor physics discussed above: the vector/tensor-to-scalar amplitude  $r_X$ , and the squared string tension parameter  $(G\mu)^2$ . We consider constraints from both parity-even and parity-odd correlators, and optionally include the flexion auto- and cross-spectra. To ascertain the scale-dependence of the constraints, we plot the derivatives of the Fisher matrix with

$\ell$  in Figs. 4 and 5; this additionally shows whether the intrinsic or lensing contributions are dominant.

*a. Inflationary perturbations* Considering first the primordial sources, we find that the  $1\sigma$  constraints on  $r_V$  are weak, with the tightest bound of  $\sigma(r_V) = \mathcal{O}(10^4)$ . This constraint is dominated by the smallest scales and lensing, matching the conclusions drawn from Fig. 2; the former property implies that flexion can (and does) add significant information, tightening the bounds by some 10–20% at  $\ell \leq 2000$ . Noting that the amplitude parameter has been normalized relative to the CMB, the implication of this study is that galaxy shapes are highly unlikely to yield useful constraints on primordially sourced vector modes. This occurs due to the  $a^{-2}(z)$  transfer function intrinsic to vectorial physics.

The constraints on  $r_T$  are considerably tighter than those on  $r_V$ , yet still unlikely to be competitive in the near future. Here, we find  $\sigma(r_T) \approx 260$  from a *Euclid*-like experiment, which is dominated by the lowest  $\ell$ -modes, and highly sensitive to the sample redshift; restricting to the first redshift bin reduces the constraining power by roughly a factor of ten, matching the conclusions of [22]. Furthermore, intrinsic alignments dominate the information content; this matches the results of [[22], Fig. 6], and imparts significant model dependence since the intrinsic alignment biases are not well known. The situation is similar for parity-odd tensor modes, with a somewhat weaker bound of  $\sigma(\epsilon_T r_T) \approx 600$ ; such modes are less commonly constrained in other probes, though our bound is still unlikely to be competitive [cf., [25]]. In this scenario, the addition of flexion does not improve the constraints due to the strong scale dependence.

*b. Cosmic strings* Turning to the cosmic string constraints, we find  $1\sigma$  bounds on the squared string tension  $(G\mu)^2$  of  $\mathcal{O}(10^{-20})$  from parity-even correlators or  $\mathcal{O}(10^{-19})$  from the parity-odd sector (if present). These agree with the lensing shear forecast of [24], though we note that the results have strong dependence on the assumed intercommuting probability  $P$ , with the degeneracy direction  $(G\mu)^2 P^{-3/2}$ . Furthermore, the constraints

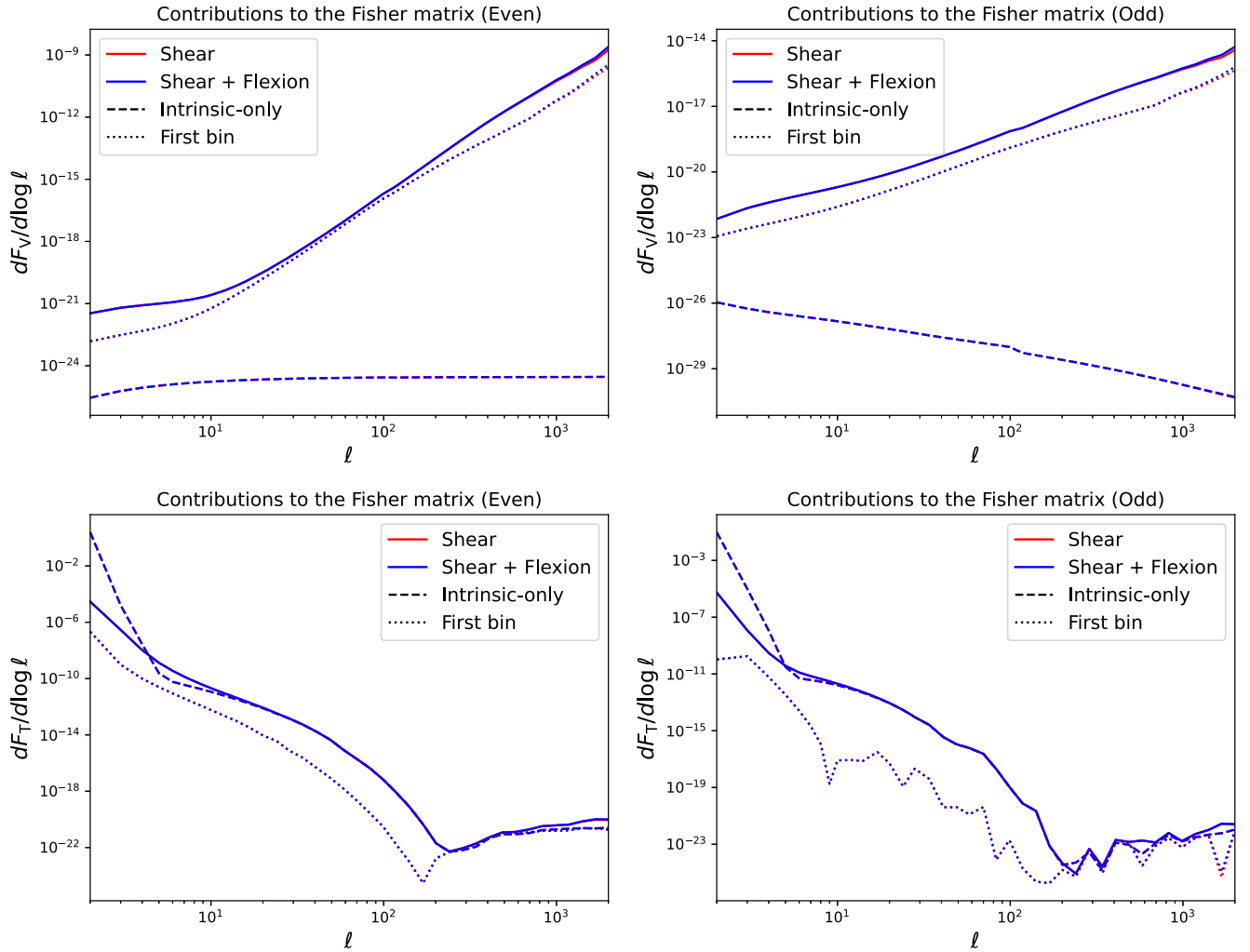


FIG. 4. Constraints on primordial vector (top) and tensor (bottom) amplitudes from parity-even (left) and parity-odd (right) shear and flexion power spectra. In each case, we plot the per- $\ell$  contribution to the Fisher matrix on the amplitude parameter  $r_X$ , motivated by the Cramér-Rao bound  $\sigma_X \geq F_X^{-1/2}$ . Red lines show results using only the shear correlators, whilst blue lines additionally include flexion (and cross-correlations). Dashed lines show the constraints in the absence of weak lensing, whilst the dotted lines show the constraints from only the first redshift bin. We observe that constraints on vector amplitudes are dominated by high- $\ell$ , whilst those on tensor amplitudes depend principally on the largest scales measured.

are of a similar amplitude to the limits from pulsar timing array experiments, with  $G\mu \lesssim 10^{-10}$  (though this statement is inherently model dependent) [44]. Both vector- and tensor-derived constraints show strong scale-dependence, with maximal detection significance at  $\ell \sim 1000$ . As before, this implies that flexion can lead to significantly improved constraints, though all spectra will saturate at high- $\ell$  due to Poisson noise. Here, we find that the overall constraints are dominated by lensing at high redshift, which is rationalized by noting that vector modes decay quickly after their sourcing. As in Fig. 3, we note that string-induced tensors contain significantly less information than vectors, with roughly  $500 \times$  weaker constraints. Overall, the prospect of constraining cosmic strings with galaxy

shapes is promising, particularly when we include all sources of information available.

## VII. SUMMARY AND CONCLUSIONS

Perturbations in the Universe can be decomposed into scalars, vectors, and tensors. To date, only scalar physics has been observed; however, there exist a wealth of cosmological models that could source vector and tensor contributions at early or late times, thus their study can yield strong constraints on the Universe's initial conditions and evolution. In this work, we provide an indepth study of the impact of such modes on galaxy shape statistics. These are a natural place in which to look for new physics since

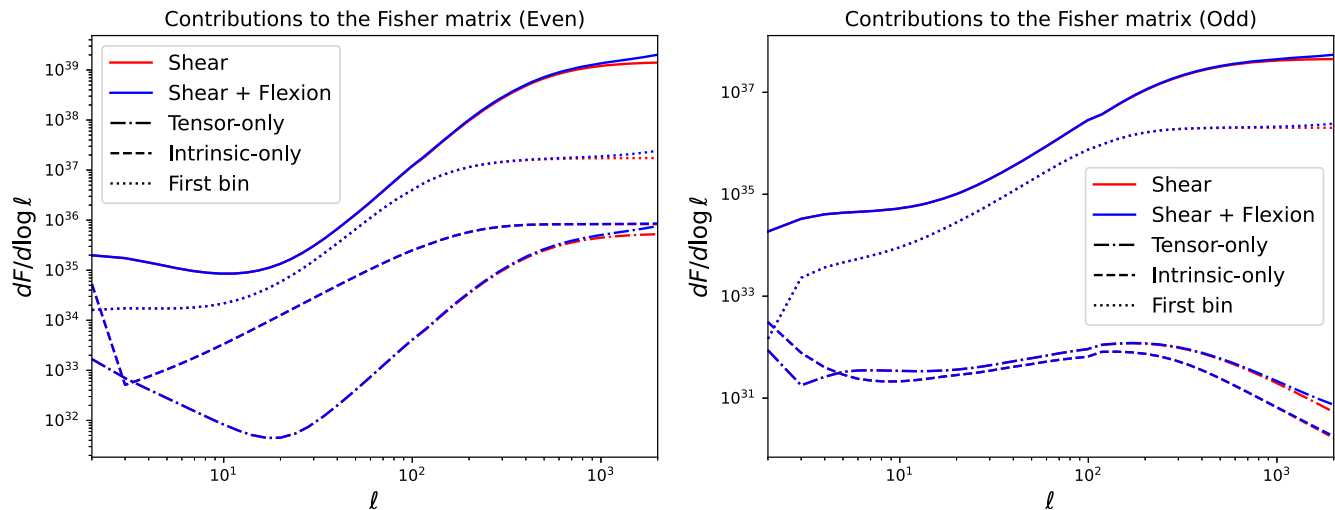


FIG. 5. Constraints on the cosmic string tension parameter  $(G\mu)^2$  from parity-even (left) and parity-odd (right) shear and flexion power spectra. This is analogous to Fig. 4, but displays the joint constraint from vector and tensor modes (with the tensor-only results shown as dot-dashed lines). In this scenario, information is principally sourced by vector lensing correlations and is more equally distributed across scales than for the primordial constraints (Fig. 4). At large  $\ell$  ( $\gtrsim 1000$ ), we find that adding flexion into the analysis can lead to improved constraints.

they are tensorial (and thus respond directly to metric perturbations), and will be observed in great depth in the coming decade.

New physics can distort galaxy shapes both intrinsically (through correlations with the local tidal field (e.g., [12,15,17]) and extrinsically (through weak gravitational lensing e.g., [7,10]). Both effects can be straightforwardly written in terms of derivatives of the metric perturbations, and thus mapped to galaxy shape observables, such as shear and its higher-order generalization, flexion (e.g., [65,66]) (though the scale dependence of such effects may complicate analyses slightly). For scalar perturbations, only shear- $E$  and flexion- $g$  modes are sourced; vector and tensor physics yield signals also in shear- $B$  and flexion- $c$  observables. Spectra of the latter could thus be a natural place to search for new physics without contamination from scalar modes (at leading order); these are additionally free from cosmic variance limitations (though their scalings with  $\ell$  usually differ from the  $E$ - and  $g$ -modes) [e.g., [22]]. In addition, if the Universe contains parity-violating physics, such as chiral gravitational waves,  $EB$  cross-correlations (and beyond) will be sourced (e.g., [25]), which again do not suffer from cosmic variance at leading order. We caution, however, that  $B$  modes are often used as a consistency check in weak lensing analyses (see [104] for a detailed discussion); if a survey finds a nontrivial shear- $B$  power spectrum (in excess of noise), this is usually attributed to systematics effects, and the null tests are said to have failed. Although this could well be the case, new physics could also be hiding in such regimes!

To place these results in quantitative context, we have considered test cases for vector and tensor physics, sourced by primordial and late-time physics, with the latter

involving a network of cosmic strings. For a *Euclid*-like lensing experiment, we concluded that primordial gravitational waves would be very difficult to detect (unless one worked at much higher redshift, as discussed in [22,25], though without flexion), though competitive constraints on cosmic string physics could be possible (as in [24], though without flexion, intrinsic alignments, or tensors). Drawing general conclusions from specific physical models is, in general, difficult; however, we may make the following broad statements:

- (i) Shear and flexion spectra induced by new physics models can have a wide range of scale and redshift-dependencies, due to the large array of possible underlying perturbation power spectra and transfer functions. For example, cosmic strings and primordial vectors source spectra dominant at high- $\ell$ , whilst gravitational waves contribute only on very large scales.
- (ii) Due to their strong scaling with redshift, vector modes sourced in the early Universe will be essentially impossible to detect using galaxy shapes (or any other late-Universe probe). Vector modes sourced at late times could be detectable however, as seen from the cosmic string example.
- (iii) If the new physics contributes significantly on small scales, the addition of flexion correlators can boost signal-to-noise, and may allow various models to be differentiated. This may be of particular relevance for dark matter studies, and may yield significantly tighter constraints on phenomena such as fuzzy dark matter (e.g., [105–110]). If irreducible rank-three tensors also exist in the Universe (e.g., from some modified gravity phenomena, such as torsion), one

might also expect them to show up in flexion spectra.

- (iv) Depending on the type of spectrum and physical model of interest, the shear and flexion correlators could be dominated either by lensing, intrinsic alignments, or their cross-correlation; as such, both effects should always be included in analysis pipelines.
- (v) *BB* and *EB* spectra could be smoking guns of new physics. Whilst their utility depends on noise parameters (since they are not cosmic-shear limited) and systematic contamination, these spectra are not sourced by scalars at leading order (or, for the cross-spectrum, at any order). They could thus be a robust cosmological probe, particularly for parity-violating physics.

Based on the above, the overarching conclusion of this work is clear: if we wish to make full use of the treasure trove of cosmological information provided by upcoming galaxy shape surveys, we must look not just to vanilla  $\Lambda$ CDM physics and simple observables, but also to nonstandard physics and higher-order statistics, such as vectors, tensors, *B*-modes, and flexion.

### ACKNOWLEDGMENTS

We thank Kazuyuki Akitsu, Jo Dunkley, Bhuv Jain, Fabian Schmidt, Uros Seljak, and Risa Wechsler for useful discussions across the years this paper took to write. We are additionally grateful to the anonymous referee for insightful feedback. O. H. E. P is a Junior Fellow of the Simons Society of Fellows. This work was inspired by the creative output of Funkmaster Flex. This project has been partially completed at the Laboratory for Nuclear Science and the Center for Theoretical Physics at the Massachusetts Institute of Technology (MIT-CTP/5613).

### APPENDIX A: TENSORS ON THE TWO-SPHERE

A general rank- $s$  tensor,  $\mathcal{T}$ , on the two-sphere may be written in terms of the  $\mathbf{m}_\pm$  basis vectors defined in (19) as

$$\begin{aligned} \mathcal{T}_{i_1 \dots i_s}(\hat{\mathbf{n}}) &= {}_{+s}\mathcal{T}(\hat{\mathbf{n}})(\mathbf{m}_+ \otimes \dots \otimes \mathbf{m}_+)_{i_1 \dots i_s} \\ &+ {}_{-s}\mathcal{T}(\hat{\mathbf{n}})(\mathbf{m}_- \otimes \dots \otimes \mathbf{m}_-)_{i_1 \dots i_s} \end{aligned} \quad (\text{A1})$$

(e.g., [8,84]). Here,  ${}_{\pm s}\mathcal{T}(\hat{\mathbf{n}})$  is the spin- $\pm s$  component of  $\mathcal{T}$ , which transforms as  ${}_{\pm s}\mathcal{T} \rightarrow e^{\pm is\varphi} {}_{\pm s}\mathcal{T}$  under rotation by  $\varphi$ . Using the basis vector properties outlined in Sec. III B, we may extract the spin- $\pm s$  components from the components of  $\mathcal{T}$  in some arbitrary coordinate chart as

$${}_{\pm s}\mathcal{T}(\hat{\mathbf{n}}) = (m_{\mp}^{i_1} \dots m_{\mp}^{i_s}) \mathcal{T}_{i_1 \dots i_s}(\hat{\mathbf{n}}), \quad (\text{A2})$$

assuming the Einstein summation convention. In a local orthogonal basis  $\{\hat{\mathbf{e}}_1, \hat{\mathbf{e}}_2, \hat{\mathbf{n}}\}$ , the basis vectors can be written

$\mathbf{m}_\pm = (\hat{\mathbf{e}}_1 \mp i\hat{\mathbf{e}}_2)/\sqrt{2}$ , such that the spin components take a simple form. As an example, a vector field has  ${}_{\pm 1}v(\hat{\mathbf{n}}) = (v_1 \pm iv_2)/\sqrt{2}$  locally.

To alter the spin of objects on the two-sphere, we can use the spin-raising and spin-lowering operators,  $\bar{\partial}$  and  $\partial$  (“edth”). These are defined by their action on spin- $s$  functions (for both  $s < 0$  and  $s > 0$ ):

$$\begin{aligned} \partial_s \mathcal{T}(\hat{\mathbf{n}}) &= -(\sin \theta)^s [\partial_\theta + i \csc \theta \partial_\varphi] (\sin \theta)^{-s} \mathcal{T}(\hat{\mathbf{n}}), \\ \bar{\partial}_s \mathcal{T}(\hat{\mathbf{n}}) &= -(\sin \theta)^{-s} [\partial_\theta - i \csc \theta \partial_\varphi] (\sin \theta)^s \mathcal{T}(\hat{\mathbf{n}}) \end{aligned} \quad (\text{A3})$$

(e.g., [8,111,112]), assuming a spherical coordinate chart  $\{\theta, \varphi\}$ . It is straightforward to show that  $\partial_s \mathcal{T}$  has spin  $(s+1)$  and  $\bar{\partial}_s \mathcal{T}$  has spin  $(s-1)$ . In the flat-sky limit, the operators reduce to

$$\begin{aligned} \partial_s \mathcal{T}(\hat{\mathbf{n}}) &\rightarrow -(\partial_1 + i\partial_2)_s \mathcal{T}(\hat{\mathbf{n}}), \\ \bar{\partial}_s \mathcal{T}(\hat{\mathbf{n}}) &\rightarrow -(\partial_1 - i\partial_2)_s \mathcal{T}(\hat{\mathbf{n}}), \end{aligned} \quad (\text{A4})$$

i.e.,  $-\partial$  and  $-\partial^*$  in the complex-valued notation of [65,66]. Furthermore, the derivatives can be written in terms of the covariant derivative  $\nabla$  on the two-sphere:

$$\begin{aligned} \partial[{}_s\mathcal{T}(\hat{\mathbf{n}})] &= -\sqrt{2}(\nabla_k[{}_s f(\hat{\mathbf{n}})]m_\pm^k + s\tau_s \mathcal{T}(\hat{\mathbf{n}})), \\ \bar{\partial}[{}_s\mathcal{T}(\hat{\mathbf{n}})] &= -\sqrt{2}(\nabla_k[{}_s \mathcal{T}(\hat{\mathbf{n}})]m_\mp^k - s\bar{\tau}_s \mathcal{T}(\hat{\mathbf{n}})) \end{aligned} \quad (\text{A5})$$

Reference [8], where  $\tau = \nabla_k m_{+i} m_-^i m_-^k$  accounts for the spatial variation of the basis functions. A particularly useful result is the action of  $s$   $\bar{\partial}$  operators on a spin- $s$  function (with  $s > 0$ ), or  $s$   $\partial$  operators on a spin- $-s$  function. This yields

$$\begin{aligned} \bar{\partial}_s {}_s \mathcal{T}(\hat{\mathbf{n}}) &= \left\{ \partial_\mu + \frac{i\partial_\varphi}{1-\mu^2} \right\}^s (1-\mu^2)^{s/2} {}_s \mathcal{T}(\hat{\mathbf{n}}) \\ \partial_{-s} {}_s \mathcal{T}(\hat{\mathbf{n}}) &= \left\{ \partial_\mu - \frac{i\partial_\varphi}{1-\mu^2} \right\}^s (1-\mu^2)^{s/2} {}_{-s} \mathcal{T}(\hat{\mathbf{n}}), \end{aligned} \quad (\text{A6})$$

where  $\mu \equiv \cos \theta$ .

Much like a scalar on the two-sphere can be written in terms of spherical harmonics, a rank- $s$  tensor can be written in terms of *spin-weighted* spherical harmonics. Explicitly,

$${}_s \mathcal{T}(\hat{\mathbf{n}}) = \sum_{\ell m} {}_s \mathcal{T}_{\ell m s} Y_{\ell m}(\hat{\mathbf{n}}), \quad (\text{A7})$$

where  $\ell$  and  $m$  are integers satisfying  $\ell \geq 0$ ,  $|m| \leq \ell$ . The spin-weighted spherical harmonics may be obtained by applying the spin-raising and spin-lowering operators to the standard spherical harmonics,  $Y_{\ell m}$ :

$$\begin{aligned} \sqrt{\frac{(\ell+s)!}{(\ell-s)!}} {}_s Y_{\ell m}(\hat{\mathbf{n}}) &= \partial^s Y_{\ell m}(\hat{\mathbf{n}}) \\ \sqrt{\frac{(\ell+s)!}{(\ell-s)!}} {}_{-s} Y_{\ell m}(\hat{\mathbf{n}}) &= (-1)^s \bar{\partial}^s Y_{\ell m}(\hat{\mathbf{n}}) \end{aligned} \quad (\text{A8})$$

(for  $s \geq 0$ ). These are orthonormal (for arbitrary  $s$ ):

$$\int d\hat{\mathbf{n}} {}_s Y_{\ell m}(\hat{\mathbf{n}}) [{}_s Y_{\ell' m'}(\hat{\mathbf{n}})]^* = \delta_{\ell\ell'}^K \delta_{mm'}^K, \quad (\text{A9})$$

and obey the relations (e.g., [8])

$$\begin{aligned} \partial_s Y_{\ell m}(\hat{\mathbf{n}}) &= \sqrt{(\ell-s)(\ell+s+1)} {}_{s+1} Y_{\ell m}(\hat{\mathbf{n}}), \\ \bar{\partial}_s Y_{\ell m}(\hat{\mathbf{n}}) &= -\sqrt{(\ell+s)(\ell-s+1)} {}_{s-1} Y_{\ell m}(\hat{\mathbf{n}}). \end{aligned} \quad (\text{A10})$$

Via orthogonality, the coefficients appearing in (A8) can be extracted straightforwardly:

$${}_s \mathcal{T}_{\ell m} = \int d\hat{\mathbf{n}} {}_s \mathcal{T}(\hat{\mathbf{n}}) [{}_s Y_{\ell m}(\hat{\mathbf{n}})]^*. \quad (\text{A11})$$

An additional relation of use is obtained by performing integration by parts on the above expression, and using (A10):

$$\begin{aligned} {}_s \mathcal{T}_{\ell m} &= \sqrt{\frac{(\ell-|s|)!}{(\ell+|s|)!}} \int d\hat{\mathbf{n}} (-\bar{\partial})^s {}_s \mathcal{T}(\hat{\mathbf{n}}) [Y_{\ell m}(\hat{\mathbf{n}})]^* \\ &= \sqrt{\frac{(\ell-|s|)!}{(\ell+|s|)!}} \int d\hat{\mathbf{n}} \bar{\partial}^s {}_{-s} \mathcal{T}(\hat{\mathbf{n}}) [Y_{\ell m}(\hat{\mathbf{n}})]^* \end{aligned} \quad (\text{A12})$$

for  $s > 0$ . To extract the basis functions, one can thus apply spin-lowering or raising operations to the spin components  ${}_{\pm s} \mathcal{T}(\hat{\mathbf{n}})$ , and integrate with respect to a spherical harmonic.

## APPENDIX B: COSMIC STRING TENSOR MODES

Below, we provide a brief derivation of the tensor power spectrum arising from cosmic string sources. This follows [24], whereupon vector perturbations were considered. Starting from (13), the  $ij$  component of the stress-energy tensor from a single string segment can be written

$$\delta T_{ij}(\mathbf{x}, \eta) = \mu \int d\sigma e^{ik \cdot x(\sigma, \eta)} (\dot{x}^i \dot{x}^j - x^{i'} x^{j'}) (\sigma, \eta). \quad (\text{B1})$$

Via the Einstein equation (8), this can be related to the metric perturbation  $h_{ij}$ . Projecting onto the tensor helicity basis (which removes the trace term), we find:

$$\ddot{h}_{\pm}(\mathbf{k}, \eta) + 2 \frac{\dot{a}}{a} \dot{h}_{\pm}(\mathbf{k}, \eta) + k^2 h_{\pm}(\mathbf{k}, \eta) = 16\pi G\mu a^2 \int d\sigma e^{ik \cdot x(\sigma, \eta)} e_{ij}^{(\mp 2)}(\hat{\mathbf{k}}) (\dot{x}^i \dot{x}^j - x^{i'} x^{j'}) (\sigma, \eta), \quad (\text{B2})$$

where, in contrast to the above, dots and primes denote derivatives with respect to  $\eta$  and  $\sigma$  in this section. To proceed we make the simplifying assumption that the source can be considered time-independent (i.e., we assume steady-state behavior), which permits the solution:

$$h_{\pm}(\mathbf{k}, \eta) = \frac{16\pi G\mu a^2}{k^2} \int d\sigma e^{ik \cdot x(\sigma, \eta)} e_{ij}^{(\mp 2)}(\hat{\mathbf{k}}) (\dot{x}^i \dot{x}^j - x^{i'} x^{j'}) (\sigma, \eta), \quad (\text{B3})$$

henceforth disregarding the propagating modes (i.e., gravitational waves). To obtain the shear and flexion predictions, one should properly consider the unequal-time power spectrum of  $h_{ij}$ ; here we follow [24] and make the assumption that  $P_{h_{\pm}}(k, \eta, \eta') \approx \sqrt{P_{h_{\pm}}(k, \eta) P_{h_{\pm}}(k, \eta')}$ . This is not exact, but is appropriate for this rough forecast. The equal-time correlation function can be obtained from (B3):

$$P_{h_{\pm}}(k, \eta, \eta) = \frac{(16\pi G\mu)^2 a^4}{k^4} n_s dV \frac{1}{\mathcal{V}} e_{ij}^{(\mp 2)}(\hat{\mathbf{k}}) e_{kl}^{(\pm 2)}(\hat{\mathbf{k}}) \int d\sigma_1 d\sigma_2 \langle e^{ik \cdot (x(\sigma_1, \eta) - x(\sigma_2, \eta))} (j^i j^j - r^{i'} r^{j'}) (\sigma_1, \eta) (j^k j^l - r^{k'} r^{l'}) (\sigma_2, \eta) \rangle, \quad (\text{B4})$$

for comoving volume element  $dV = 4\pi\chi^2/H$ , string segment number density  $n_s = a^3/\xi^3$ , survey volume  $\mathcal{V}$ , and characteristic string length  $\xi$ . Asserting the isotropic and time-independent correlators  $\langle j^i(\sigma_1, \eta) j^j(\sigma_2, \eta) \rangle = \frac{1}{3} \delta_K^{ij} V_s(\sigma_1 - \sigma_2)$ ,  $\langle r^{i'}(\sigma_1, \eta) r^{j'}(\sigma_2, \eta) \rangle = \frac{1}{3} \delta_K^{i'j'} T_s(\sigma_1 - \sigma_2)$ , with  $\langle e^{ik \cdot (x(\sigma_1, \eta) - x(\sigma_2, \eta))} \rangle = e^{-k^2 \Gamma_s(\sigma_1 - \sigma_2)/6}$  with  $\Gamma_s(\sigma) \approx \sigma^2 T_s(\sigma)$ , we can write

$$P_{h_{\pm}}(k, \eta, \eta) = \frac{2(16\pi G\mu)^2 a^4}{9} \frac{4\pi\chi^2 a^3}{k^4} \frac{1}{H\xi^3} \frac{1}{\mathcal{V}} \int d\sigma_- d\sigma_+ e^{-(1/6)k^2 \sigma_-^2 T_s(\sigma_-)} [V_s^2(\sigma_-) + T_s^2(\sigma_-)], \quad (\text{B5})$$

defining  $\sigma_{\pm} = \sigma_1 \pm \sigma_2$ . As in [24], we assume the correlators have the scale invariant forms  $V_s \approx v_{\text{rms}}^2$ ,  $T_s \approx (1 - v_{\text{rms}}^2)$  on scales  $\sigma < \xi/a$ , and zero else. Noting that  $\int d\sigma_+/\mathcal{V}$  is the length of the string segment per unit volume,  $\approx a^2/\xi^2 \sqrt{1 - v_{\text{rms}}^2}$ , and that  $|\sigma_-| \lesssim \xi/2a \sqrt{1 - v_{\text{rms}}^2}$ , we find

$$P_{h_{\pm}}(k, \eta, \eta) = (16\pi G\mu)^2 \frac{\sqrt{6\pi}}{9(1-v_{\text{rms}}^2)} \frac{4\pi\chi^2 a^4}{H} \left(\frac{a}{k\xi}\right)^5 \text{erf}\left[\frac{k\xi/a}{2\sqrt{6}}\right] [v_{\text{rms}}^4 + (1-v_{\text{rms}}^2)^2]. \quad (\text{B6})$$

### APPENDIX C: INTRINSIC VECTOR SPECTRA

Here, we derive the shear kernels sourced by vector intrinsic alignments, following the methodology of [85]. Starting from (32), and expanding in helicity states using (5), we find

$${}_{\pm 2}\gamma(\mathbf{x}, \chi)|_{V,\text{int}} = b_V(\chi) \int_{\mathbf{k}} e^{i\mathbf{k}\cdot\mathbf{x}} (ik_{\pm}) \sum_{\lambda} \mathcal{I}_V B_{\lambda}(\mathbf{k}, \chi) e_{\pm}^{(\lambda)}(\hat{\mathbf{k}}), \quad (\text{C1})$$

where  $k_{\pm} \equiv m_{\mp}^i k_i$  and  $e_{\pm}^{(\lambda)} \equiv m_{\mp}^i e_i^{(\lambda)}$ . For a single Fourier mode along  $\mathbf{k} = k\hat{\mathbf{z}}$ , the basis definition of (19) implies  $k_{\pm} = -(k/\sqrt{2})\sqrt{1-\mu^2}$ , and  $e_{\pm}^{(\lambda)} = (1/2)(\mu \pm \lambda)e^{-i\lambda\varphi}$  for  $\mu \equiv \cos\theta = \hat{\mathbf{z}} \cdot \hat{\mathbf{n}}$ . Additionally restricting to a single polarization state  $\lambda$ , we find the contribution

$${}_{\pm 2}\gamma(\chi\hat{\mathbf{n}}, \chi; k\hat{\mathbf{z}}, \lambda)|_{V,\text{int}} = \frac{-ik}{2\sqrt{2}} b_V(\chi) \sqrt{1-\mu^2} (\mu \pm \lambda) e^{-i\lambda\varphi} \mathcal{I}_V B_{\lambda}(\mathbf{k}, \chi) e^{ik\chi\mu}. \quad (\text{C2})$$

To obtain the shear harmonic coefficients, it is convenient to first compute the spin-zero quantities  $\bar{\delta}_{+2}^2\gamma$  and  $\delta_{-2}^2\gamma$ . Using relation (A6), these can be written

$$\begin{aligned} \bar{\delta}_{+2}^2\gamma(\chi\hat{\mathbf{n}}, \chi; k\hat{\mathbf{z}}, \lambda)|_{V,\text{int}} &= \frac{-ik}{2\sqrt{2}} b_V(\chi) \mathcal{I}_V B_{\lambda}(\mathbf{k}, \chi) e^{-i\lambda\varphi} \left\{ \partial_{\mu} + \frac{\lambda}{1-\mu^2} \right\}^2 [(1-\mu^2)^{3/2} (\mu + \lambda) e^{ik\chi\mu}] \\ &\equiv \frac{b_V(\chi)}{2\sqrt{2}\chi} \mathcal{I}_V B_{\lambda}(\mathbf{k}, \chi) \sqrt{1-\mu^2} e^{-i\lambda\varphi} \hat{\mathcal{Q}}_{\gamma,V}^{(\lambda)}(x) e^{ix\mu} \\ \delta_{-2}^2\gamma(\chi\hat{\mathbf{n}}, \chi; k\hat{\mathbf{z}}, \lambda)|_{V,\text{int}} &= \frac{-ik}{2\sqrt{2}} b_V(\chi) \mathcal{I}_V B_{\lambda}(\mathbf{k}, \chi) e^{-i\lambda\varphi} \left\{ \partial_{\mu} - \frac{\lambda}{1-\mu^2} \right\}^2 [(1-\mu^2)^{3/2} (\mu - \lambda) e^{ik\chi\mu}] \\ &\equiv \frac{b_V(\chi)}{2\sqrt{2}\chi} \mathcal{I}_V B_{\lambda}(\mathbf{k}, \chi) \sqrt{1-\mu^2} e^{-i\lambda\varphi} \hat{\mathcal{Q}}_{\gamma,V}^{(\lambda)*}(x) e^{ix\mu}, \end{aligned} \quad (\text{C3})$$

where  $x \equiv k\chi$ , and we have defined the operator  $\hat{\mathcal{Q}}_{\gamma,V}^{(\lambda)}(x) = x[4x + (12 + x^2)\partial_x + 8x\partial_x^2 + x^2\partial_x^3] + i\lambda x^2[x + 4\partial_x + x\partial_x^2]$ , which satisfies  $\hat{\mathcal{Q}}_{\gamma,V}^{(\lambda)}(x) = \hat{\mathcal{Q}}_{\gamma,V}^{(-\lambda)}(x)$ . The spin-weighted spherical harmonic coefficients  ${}_{\pm 2}\gamma_{\ell m} \equiv \gamma_{\ell m}^E \pm i\gamma_{\ell m}^B$  can be obtained via the relation

$${}_{+2}\gamma_{\ell m} = \sqrt{\frac{(\ell-2)!}{(\ell+2)!}} \int d\hat{\mathbf{n}} \bar{\delta}_{+2}^2\gamma(\hat{\mathbf{n}}) Y_{\ell m}^*(\hat{\mathbf{n}}), \quad {}_{-2}\gamma_{\ell m} = \sqrt{\frac{(\ell-2)!}{(\ell+2)!}} \int d\hat{\mathbf{n}} \delta_{-2}^2\gamma(\hat{\mathbf{n}}) Y_{\ell m}(\hat{\mathbf{n}}) \quad (\text{C4})$$

Equation (A12). To perform the integral over  $\hat{\mathbf{n}}$ , we use the result proved in Ref. [84] (Appendix A):

$$\int d\hat{\mathbf{n}} Y_{\ell m}^*(\hat{\mathbf{n}}) (1-\mu^2)^{|r|/2} e^{ir\varphi} e^{ix\mu} = \sqrt{4\pi(2\ell+1)} \sqrt{\frac{(\ell+|r|)!}{(\ell-|r|)!}} i^r i^{\ell} \frac{j_{\ell}^r(x)}{x^{|r|}} \delta_{mr}^K \quad (\text{C5})$$

for integer  $r$ ,  $\ell$ , and  $m$ , and spherical Bessel function  $j_{\ell}(x)$ . This leads to the following shear coefficients:

$${}_{+2}\gamma_{\ell m}(\chi; k\hat{\mathbf{z}}, \lambda)|_{V,\text{int}} = i^{\ell-\lambda} \sqrt{4\pi(2\ell+1)} \sqrt{\frac{(\ell-2)! (\ell+1)!}{(\ell+2)! (\ell-1)!}} \frac{b_V(\chi)}{2\sqrt{2}\chi} \mathcal{I}_V B_{\lambda}(\mathbf{k}, \chi) \hat{\mathcal{Q}}_{\gamma,V}^{(\lambda)}(x) \frac{j_{\ell}^{\lambda}(x)}{x} \times \delta_{m(-\lambda)}^K. \quad (\text{C6})$$

The expression for  ${}_{-2}\gamma_{\ell m}$  is analogous, but with  $\hat{\mathcal{Q}}_{\gamma,V}^{(\lambda)}(x)$  replaced with its conjugate. To form the shear power spectrum arising from vector perturbations, we need simply take the expectation of two copies of  $\gamma_{\ell m}^X$  (for  $X \in \{E, B\}$ ), summing over  $\lambda$ , averaging over  $m$ , and integrating over  $\mathbf{k}$ :

$$C_\ell^{r^X r^Y}(\chi, \chi')|_{V, \text{int}} = \frac{1}{2\ell+1} \sum_{m=-\ell}^{\ell} \sum_{\lambda=\pm 1} \int_{\mathbf{k}} \langle Y_{\ell m}^X(\chi; k\hat{\mathbf{z}}, \lambda) |_{V, \text{int}} Y_{\ell m}^{Y*}(\chi'; k\hat{\mathbf{z}}, \lambda) |_{V, \text{int}} \rangle. \quad (\text{C7})$$

By isotropy, this recovers the full spectrum, even though we have only considered  $\mathbf{k} = k\hat{\mathbf{z}}$ . In full, we obtain the spectra

$$C_\ell^{r^X r^Y}(\chi, \chi')|_{V, \text{int}} = \frac{2}{\pi} \int_0^\infty k^2 dk F_\ell^{r^X, V}(k, \chi) F_\ell^{r^Y, V*}(k, \chi') [P_{B_+}(k, \chi, \chi') \pm P_{B_-}(k, \chi, \chi')], \quad (\text{C8})$$

using the correlation properties of  $B_\lambda(\mathbf{k}, \chi)$  (7), where we take the difference of two helicity states if  $X \neq Y$ .<sup>9</sup> From the spectrum, we can read off the kernels (dropping a trivial  $i^\ell$  factor)

$$\begin{aligned} F_\ell^{r^E, V}(k, \chi)|_{\text{int}} &= \sqrt{\frac{(\ell-2)!(\ell+1)! b_V(\chi)}{(\ell+2)!(\ell-1)! 2\sqrt{2}\chi}} \text{Re}[\hat{Q}_{r, V}^{(+1)}(x)] \frac{j_\ell(x)}{x} \mathcal{I}_V \\ F_\ell^{r^B, V}(k, \chi)|_{\text{int}} &= \sqrt{\frac{(\ell-2)!(\ell+1)! b_V(\chi)}{(\ell+2)!(\ell-1)! 2\sqrt{2}\chi}} \text{Im}[\hat{Q}_{r, V}^{(+1)}(x)] \frac{j_\ell(x)}{x} \mathcal{I}_V. \end{aligned} \quad (\text{C9})$$

As discussed in the main text, vectors source both  $E$ - and  $B$  modes (unlike scalar perturbations); moreover, if the spectrum does not conserve parity  $P_{B_+} \neq P_{B_-}$ , and an  $EB$  cross-spectrum will be sourced. These spectra can be promoted to binned form by simply integrating over  $\chi$  and  $\chi'$  via (45).

The flexion kernels can be similarly computed. Restricting our attention to the spin- $\pm 1$  flexion (for brevity), the Fourier-mode expansion of (32) gives

$${}_{\pm 1}\mathcal{F}(\mathbf{x}, \chi)|_{V, \text{int}} = \frac{8\sqrt{2}\chi \tilde{b}_V(\chi)}{27} \int_{\mathbf{k}} e^{i\mathbf{k}\cdot\mathbf{x}} \sum_{\lambda} [(ik_{\pm})^2 e_{\mp}^{(\lambda)}(\hat{\mathbf{k}}) + 2(ik_{\mp})(ik_{\pm}) e_{\pm}^{(\lambda)}(\hat{\mathbf{k}})] \mathcal{I}_V B_\lambda(\mathbf{k}, \chi). \quad (\text{C10})$$

The contribution to  $\bar{\delta}_{+1}\mathcal{F}$  from a Fourier mode  $\mathbf{k} = k\hat{\mathbf{z}}$  and a single helicity state is equal to

$$\begin{aligned} \bar{\delta}_{+1}\mathcal{F}(\chi\hat{\mathbf{n}}, \chi; k\hat{\mathbf{z}}, \lambda)|_{V, \text{int}} &= -\frac{2\sqrt{2}\chi \tilde{b}_V(\chi)}{27} k^2 e^{-i\lambda\varphi} \left\{ \partial_\mu + \frac{\lambda}{1-\mu^2} \right\} [(1-\mu^2)^{3/2} e^{i\lambda\mu} (3\mu + \lambda)] \mathcal{I}_V B_\lambda(\mathbf{k}, \chi) \\ &= -\frac{2\sqrt{2}\tilde{b}_V(\chi)}{27\chi} \mathcal{I}_V B_\lambda(\mathbf{k}, \chi) e^{-i\lambda\varphi} \sqrt{1-\mu^2} \hat{Q}_{r, V}^{(\lambda)}(x) e^{i\lambda\mu}, \end{aligned} \quad (\text{C11})$$

where  $\hat{Q}_{\mathcal{F}, V}^{(\lambda)}(x) \equiv x^2[4 + 12\partial_x^2 + 3x\partial_x(1 + \partial_x^2) + i\lambda x(1 + \partial_x^2)]$ .  $\bar{\delta}_{-1}\mathcal{F}$  takes a similar form but replacing  $\hat{Q}_{\mathcal{F}, V}^{(\lambda)}(x)$  with its conjugate. As before, the spin-zero coefficients can be used to obtain the spherical harmonic decomposition of  $\mathcal{F}$ :

$$\begin{aligned} {}_{+1}\mathcal{F}_{\ell m}(\chi; k\hat{\mathbf{z}}, \lambda) &= -\sqrt{\frac{(\ell-1)!}{(\ell+1)!}} \int d\hat{\mathbf{n}} \bar{\delta}_{+1}\mathcal{F}(\chi\hat{\mathbf{n}}, \chi; k\hat{\mathbf{z}}, \lambda) Y_{\ell m}^*(\hat{\mathbf{n}}) \\ &= i^{\ell-\lambda} \sqrt{4\pi(2\ell+1)} \frac{2\sqrt{2}\tilde{b}_V(\chi)}{27\chi} \mathcal{I}_V B_\lambda(\mathbf{k}, \chi) \hat{Q}_{\mathcal{F}, V}^{(\lambda)}(x) \frac{j_\ell(x)}{x} \times \delta_{m(-\lambda)}^{\mathbf{k}} \end{aligned} \quad (\text{C12})$$

again using (C5). The resulting spectrum takes the same form as (C8), but with the modified kernels

$$\begin{aligned} F^{\mathcal{F}^q, V}(k, \chi)|_{\text{int}} &= \frac{2\sqrt{2}\tilde{b}_V(\chi)}{27\chi} \text{Re}[\hat{Q}_{\mathcal{F}, V}(x)] \frac{j_\ell(x)}{x} \mathcal{I}_V, \\ F^{\mathcal{F}^c, V}(k, \chi)|_{\text{int}} &= -\frac{2\sqrt{2}\tilde{b}_V(\chi)}{27\chi} \text{Im}[\hat{Q}_{\mathcal{F}, V}(x)] \frac{j_\ell(x)}{x} \mathcal{I}_V. \end{aligned} \quad (\text{C13})$$

<sup>9</sup>This arises since  $\text{Re}\hat{Q}^{(-1)}(x) = \text{Re}\hat{Q}^{(+1)}(x)$ , but  $\text{Im}\hat{Q}^{(-1)}(x) = -\text{Im}\hat{Q}^{(+1)}(x)$ .

Derivations for other intrinsic alignment spectra, such as those sourced by scalars and tensors, follow similarly, and make use of the kernels given in Appendix E.

### APPENDIX D: EXTRINSIC VECTOR AND TENSOR SPECTRA

Here, we derive the full-sky power spectrum of shear sourced by vector and tensor lensing, following an analogous procedure to Appendix C (from [22]). The vector contribution can be written

$${}_{+2\gamma}(\chi\hat{\mathbf{n}}, \chi)|_{V,\text{ext}} = - \int_0^\chi d\chi' \int_{\mathbf{k}} e^{ik\chi'k\hat{\mathbf{n}}} \sum_{\lambda} B_{\lambda}(\mathbf{k}, \chi') \left[ \left(1 - 2\frac{\chi'}{\chi}\right) (ik_{\pm}) e_{\pm}^{(\lambda)}(\hat{\mathbf{k}}) + \frac{\chi'}{\chi} (\chi - \chi') (ik_{\pm})^2 e_{\parallel}^{(\lambda)}(\hat{\mathbf{k}}) \right], \quad (\text{D1})$$

where  $e_{\parallel}^{(\lambda)} \equiv \hat{\mathbf{n}}^k e_k^{(\lambda)}$ . Restricting to a single helicity state and Fourier mode with  $\mathbf{k} = k\hat{\mathbf{z}}$ , we find

$${}_{+2\gamma}(\chi\hat{\mathbf{n}}, \chi; k\hat{\mathbf{z}}, \lambda)|_{V,\text{ext}} = \int_0^\chi d\chi' B_{\lambda}(\mathbf{k}, \chi') \frac{\sqrt{1-\mu^2}}{2\sqrt{2}} \left[ ix'(\mu + \lambda) \left(\frac{1}{\chi'} - \frac{2}{\chi}\right) + x'^2(1-\mu^2) \left(\frac{1}{\chi'} - \frac{1}{\chi}\right) \right] e^{-i\lambda\varphi} e^{ix'\mu}, \quad (\text{D2})$$

using that  $e_{\parallel}^{(\lambda)} = (\sqrt{1-\mu^2}/\sqrt{2})e^{-i\lambda\varphi}$  and setting  $x' \equiv k\chi'$ . The spin-zero part,  $\bar{\delta}_{+2\gamma}^2$ , can be obtained with (A6):

$$\begin{aligned} \bar{\delta}_{+2\gamma}^2(\chi\hat{\mathbf{n}}, \chi; k\hat{\mathbf{z}}, \lambda)|_{V,\text{ext}} &= \frac{1}{2\sqrt{2}} \int_0^\chi d\chi' B_{\lambda}(\mathbf{k}, \chi') e^{-i\lambda\varphi} \left\{ \partial_{\mu} + \frac{\lambda}{1-\mu^2} \right\}^2 \\ &\quad \times \left[ ix'(\mu + \lambda)(1-\mu^2)^{3/2} \left(\frac{1}{\chi'} - \frac{2}{\chi}\right) + x'^2(1-\mu^2)^{5/2} \left(\frac{1}{\chi'} - \frac{1}{\chi}\right) \right] e^{ix'\mu}, \\ &\equiv \frac{1}{2\sqrt{2}} \int_0^\chi \frac{d\chi'}{\chi'} B_{\lambda}(\mathbf{k}, \chi') e^{-i\lambda\varphi} \sqrt{1-\mu^2} \left[ \hat{Q}_{\gamma,V,1}^{(\lambda)}(x') + \frac{\chi'}{\chi} Q_{\gamma,V,2}^{(\lambda)}(x') \right] e^{ix'\mu}, \end{aligned} \quad (\text{D3})$$

defining the new operators  $Q_{\gamma,V,1/2}^{(\lambda)}(x)$ , whose forms are given in (E4). The expression for  $\bar{\delta}_{-2\gamma}^2$  is analogous but with all  $\hat{Q}$  operators replaced by their conjugates. As in Appendix C, we proceed by integrating (D3) against a spherical harmonic using (C5) to yield

$${}_{+2\gamma}\ell_m(\chi; k\hat{\mathbf{z}}, \lambda)|_{V,\text{ext}} = \frac{\sqrt{4\pi(2\ell+1)}}{2\sqrt{2}} \sqrt{\frac{(\ell-2)!(\ell+1)!}{(\ell+2)!(\ell-1)!}} i^{\ell-\lambda} \int_0^\chi \frac{d\chi'}{\chi'} B_{\lambda}(\mathbf{k}, \chi') \left[ \hat{Q}_{\gamma,V,1}^{(\lambda)}(x') + \frac{\chi'}{\chi} Q_{\gamma,V,2}^{(\lambda)}(x') \right] \frac{j_{\ell}(x')}{x'}, \quad (\text{D4})$$

if  $m = -\lambda$ , and zero else. Integrating over redshift via (45) gives

$$\begin{aligned} {}_{+2\gamma}\ell_{m,a}(k\hat{\mathbf{z}}, \lambda)|_{V,\text{ext}} &= \frac{\sqrt{4\pi(2\ell+1)}}{2\sqrt{2}} \sqrt{\frac{(\ell-2)!(\ell+1)!}{(\ell+2)!(\ell-1)!}} i^{\ell-\lambda} \\ &\quad \times \int_0^{\chi_H} \frac{d\chi}{\chi} B_{\lambda}(\mathbf{k}, \chi) [m_a(\chi) \hat{Q}_{\gamma,V,1}^{(\lambda)}(x) + (m_a(\chi) - q_a(\chi)) Q_{\gamma,V,2}^{(\lambda)}(x)] \frac{j_{\ell}(x)}{x}, \end{aligned} \quad (\text{D5})$$

exchanging the order of integration and introducing  $q_a$  and  $m_a$  kernels. This yields spectra of the general form (44) with the kernels given in (52).

A similar form may be obtained for the shear spectrum from tensor modes, starting from (41). Here, we implement the  $h_{\pm}(\mathbf{0}, \mathbf{0})$  term by subtracting the  $k \rightarrow 0$  limit of the scalar shear kernel (which is nonzero only for  $\ell = 2$ ), and absorb the  $-\frac{1}{2}h_{\pm}(\chi\hat{\mathbf{n}}, \chi)$  term into the intrinsic tensor shear contribution, redefining  $\mathcal{I}_T h_{ij} \rightarrow (\mathcal{I}_T - 1/2b_T(\chi))h_{ij}$ . For the remaining terms, a procedure analogous to the above

(described in detail in [22]) leads to the kernels given in (52).

### APPENDIX E: BESSEL FUNCTION OPERATORS

Below, we list the various  $\hat{Q}(x)$  Bessel function operators appearing in the full-sky power spectra of Sec. VA. Firstly, the relevant operators for shear sourced by intrinsic scalar, vector, and tensor perturbations (Sec. VA 1) are given by:

$$\begin{aligned}
\hat{Q}_{\gamma,S}^{(\lambda)}(x) &= x^2[4 + 12\partial_x^2 + 8x\partial_x(1 + \partial_x^2) + x^2(1 + \partial_x^2)^2] \\
\hat{Q}_{\gamma,V}^{(\lambda)}(x) &= x[4x + (12 + x^2)\partial_x + 8x\partial_x^2 + x^2\partial_x^3] + i\lambda x^2[x + 4\partial_x + x\partial_x^2] \\
\hat{Q}_{\gamma,T}^{(\lambda)}(x) &= [12 - x^2 + 8x\partial_x + x^2\partial_x^2] + 2i\lambda x[4 + x\partial_x],
\end{aligned} \tag{E1}$$

whilst those for the spin- $\pm 1$  flexion are

$$\begin{aligned}
\hat{Q}_{\mathcal{F},S}^{(\lambda)}(x) &= 3x^3[x + 4\partial_x + x\partial_x^2](1 + \partial_x^2) \\
\hat{Q}_{\mathcal{F},V}^{(\lambda)}(x) &= x^2[4 + 12\partial_x^2 + 3x\partial_x(1 + \partial_x^2) + i\lambda x(1 + \partial_x^2)] \\
\hat{Q}_{\mathcal{F},T}^{(\lambda)}(x) &= x[x + 12\partial_x + 3x\partial_x^2 + 2i\lambda x\partial_x],
\end{aligned} \tag{E2}$$

and for the spin- $\pm 3$  flexion:

$$\begin{aligned}
\hat{Q}_{\mathcal{G},S}^{(\lambda)}(x) &= -x^3[x(x^2 + 18) + 18(x^2 + 4)\partial_x + 3x(x^2 + 36)\partial_x^2 + 12(3x^2 + 10)\partial_x^3 + 3x(x^2 + 30)\partial_x^4 + 18x^2\partial_x^5 + x^3\partial_x^6] \\
\hat{Q}_{\mathcal{G},V}^{(\lambda)}(x) &= -x^2[6(x^2 + 4) + x(x^2 + 66)\partial_x + 24(x^2 + 5)\partial_x^2 + 2x(x^2 + 45)\partial_x^3 + 18x^2\partial_x^4 + x^3\partial_x^5 \\
&\quad + i\lambda x(6 + x^2 + 12x\partial_x + 2(x^2 + 15)\partial_x^2 + 12x\partial_x^3 + x^2\partial_x^4)] \\
\hat{Q}_{\mathcal{G},T}^{(\lambda)}(x) &= x[x(x^2 - 30) - 6(x^2 + 20)\partial_x - 90x\partial_x^2 - 18x^2\partial_x^3 - x^3\partial_x^4 - 2i\lambda x(6x + (x^2 + 30)\partial_x + 12x\partial_x^2 + x^2\partial_x^3)].
\end{aligned} \tag{E3}$$

The scalar, vector, and tensor operators act on  $j_\ell(x)$ ,  $j_\ell(x)/x$ , and  $j_\ell(x)/x^2$  respectively.

The kernels relevant to the extrinsic power spectra (Sec. VA 2) are given by

$$\begin{aligned}
\hat{Q}_{\gamma,V,1}^{(\lambda)}(x) &= -x[x(x^2 + 8) + (11x^2 + 12)\partial_x + 2x(x^2 + 14)\partial_x^2 + 11x^2\partial_x^3 + x^3\partial_x^4 - i\lambda x(x + 4\partial_x + x\partial_x^2)] \\
\hat{Q}_{\gamma,V,2}^{(\lambda)}(x) &= x[x(x^2 + 12) + 12(x^2 + 2)\partial_x + 2x(x^2 + 18)\partial_x^2 + 12x^2\partial_x^3 + x^3\partial_x^4], \\
\hat{Q}_{\gamma,T,1}^{(\lambda)}(x) &= -\frac{x}{2}[x(x^2 + 14) + 2(7x^2 + 20)\partial_x + 2x(x^2 + 25)\partial_x^2 + 14x^2\partial_x^3 + x^3\partial_x^4 \\
&\quad - 2i\lambda(4 + x^2 + 6x\partial_x + x^2\partial_x^2)] \\
\hat{Q}_{\gamma,T,2}^{(\lambda)}(x) &= \frac{1}{2}[24(x^2 + 1) + x^4 + 16x(x^2 + 6)\partial_x + 2x^2(x^2 + 36)\partial_x^2 + 16x^3\partial_x^3 + x^4\partial_x^4].
\end{aligned} \tag{E4}$$

In the large- $\ell$  limit, the action of the  $\hat{Q}$  operators on the spherical Bessel functions simplifies considerably. The intrinsic functions have the following asymptotic forms:

$$\begin{aligned}
\hat{Q}_{\gamma,S}^{(\lambda)}(x)j_\ell(x) &\approx \ell^4 j_\ell(x), & \hat{Q}_{\gamma,V}^{(\lambda)}(x)\frac{j_\ell(x)}{x} &\approx \ell^2 j'_\ell(x) + i\lambda \ell^2 j_\ell(x), & \hat{Q}_{\gamma,T}^{(\lambda)}(x)\frac{j_\ell(x)}{x^2} &\approx \left(\frac{\ell^2}{x^2} - 2\right)j_\ell(x) + 2i\lambda j'_\ell(x), \\
\hat{Q}_{\mathcal{F},S}^{(\lambda)}(x)j_\ell(x) &\approx 3\ell^4 j_\ell(x), & \hat{Q}_{\mathcal{F},V}^{(\lambda)}(x)\frac{j_\ell(x)}{x} &\approx 3\ell^2 j'_\ell(x) + i\lambda \ell^2 j_\ell(x), & \hat{Q}_{\mathcal{F},T}^{(\lambda)}(x)\frac{j_\ell(x)}{x^2} &\approx \left(3\frac{\ell^2}{x^2} - 2\right)j_\ell(x) + 2i\lambda j'_\ell(x), \\
\hat{Q}_{\mathcal{G},S}^{(\lambda)}(x)j_\ell(x) &\approx -\ell^6 j_\ell(x), & \hat{Q}_{\mathcal{G},V}^{(\lambda)}(x)\frac{j_\ell(x)}{x} &\approx -\ell^4 j'_\ell(x) - i\lambda \ell^4 j_\ell(x), & \hat{Q}_{\mathcal{G},T}^{(\lambda)}(x)\frac{j_\ell(x)}{x^2} &\approx -\ell^2 \left(\frac{\ell^2}{x^2} - 2\right)j_\ell(x) - 2i\lambda \ell^2 j'_\ell(x),
\end{aligned} \tag{E5}$$

where  $j'_\ell(x) \equiv \partial_x j_\ell(x)$ . A similar form can be obtained for the extrinsic kernels:

$$\hat{Q}_{\gamma,V,1}^{(\lambda)}(x)\frac{j_\ell(x)}{x} \approx -\frac{\ell^4}{x}j_\ell(x) + i\lambda \ell^2 j_\ell(x), \quad \hat{Q}_{\gamma,V,2}^{(\lambda)}(x)\frac{j_\ell(x)}{x} \approx \frac{\ell^4}{x}j_\ell(x) \tag{E6}$$

$$\hat{Q}_{\gamma,T,1}^{(\lambda)}(x)\frac{j_\ell(x)}{x^2} \approx -\frac{\ell^4}{2x^2}j_\ell(x) + i\lambda \frac{\ell^2}{x}j_\ell(x), \quad \hat{Q}_{\gamma,T,2}^{(\lambda)}(x)\frac{j_\ell(x)}{x^2} \approx \frac{\ell^4}{2x^2}j_\ell(x). \tag{E7}$$

- [1] T. M. C. Abbott, M. Aguena, A. Alarcon, S. Allam, O. Alves *et al.* (DES Collaboration), Dark Energy Survey Year 3 results: Cosmological constraints from galaxy clustering and weak lensing, *Phys. Rev. D* **105**, 023520 (2022).
- [2] T. M. C. Abbott, M. Aguena, A. Alarcon *et al.* (Dark Energy Survey, Kilo-Degree Survey Collaborations), DES Y3 + KiDS-1000: Consistent cosmology combining cosmic shear surveys, *Open J. Astrophys.* **6** (2023).
- [3] M. Asgari, C.-A. Lin, B. Joachimi, B. Giblin, C. Heymans, H. Hildebrandt *et al.*, KiDS-1000 cosmology: Cosmic shear constraints and comparison between two point statistics, *Astron. Astrophys.* **645**, A104 (2021).
- [4] R. Dalal, X. Li, A. Nicola, J. Zuntz, M. A. Strauss, S. Sugiyama *et al.*, Hyper Suprime-Cam Year 3 results: Cosmology from cosmic shear power spectra, *Phys. Rev. D* **108**, 123519 (2023).
- [5] J. Green, P. Schechter, C. Baltay, R. Bean, D. Bennett, R. Brown *et al.*, Wide-Field InfraRed Survey Telescope (WFIRST) final report, [arXiv:1208.4012](https://arxiv.org/abs/1208.4012).
- [6] P. A. Abell, J. Allison, S. F. Anderson, J. R. Andrew, J. R. P. Angel *et al.* (LSST Science Collaboration), LSST science book, version 2.0, [arXiv:0912.0201](https://arxiv.org/abs/0912.0201).
- [7] M. Bartelmann and P. Schneider, Weak gravitational lensing, *Phys. Rep.* **340**, 291 (2001).
- [8] P. G. Castro, A. F. Heavens, and T. D. Kitching, Weak lensing analysis in three dimensions, *Phys. Rev. D* **72**, 023516 (2005).
- [9] M. Kilbinger, Cosmology with cosmic shear observations: A review, *Rep. Prog. Phys.* **78**, 086901 (2015).
- [10] H. Hoekstra and B. Jain, Weak gravitational lensing and its cosmological applications, *Annu. Rev. Nucl. Part. Sci.* **58**, 99 (2008).
- [11] A. Refregier, Weak gravitational lensing by large-scale structure, *Annu. Rev. Astron. Astrophys.* **41**, 645 (2003).
- [12] K. Kogai, K. Akitsu, F. Schmidt, and Y. Urakawa, Galaxy imaging surveys as spin-sensitive detector for cosmological colliders, *J. Cosmol. Astropart. Phys.* **03** (2021) 060.
- [13] F. Schmidt, N. E. Chisari, and C. Dvorkin, Imprint of inflation on galaxy shape correlations, *J. Cosmol. Astropart. Phys.* **10** (2015) 032.
- [14] N. E. Chisari, C. Dvorkin, F. Schmidt, and D. Spergel, Multitracing anisotropic non-Gaussianity with galaxy shapes, *Phys. Rev. D* **94**, 123507 (2016).
- [15] C. M. Hirata and U. Seljak, Intrinsic alignment-lensing interference as a contaminant of cosmic shear, *Phys. Rev. D* **70**, 063526 (2004).
- [16] Z. Vlah, N. E. Chisari, and F. Schmidt, An EFT description of galaxy intrinsic alignments, *J. Cosmol. Astropart. Phys.* **01** (2020) 025.
- [17] J. Blazek, M. McQuinn, and U. Seljak, Testing the tidal alignment model of galaxy intrinsic alignment, *J. Cosmol. Astropart. Phys.* **05** (2011) 010.
- [18] R. G. Crittenden, P. Natarajan, U.-L. Pen, and T. Theuns, Spin-induced galaxy alignments and their implications for weak-lensing Measurements, *Astrophys. J.* **559**, 552 (2001).
- [19] T. Kurita, M. Takada, T. Nishimichi, R. Takahashi, K. Osato, and Y. Kobayashi, Power spectrum of halo intrinsic alignments in simulations, *Mon. Not. R. Astron. Soc.* **501**, 833 (2021).
- [20] J. Shi, T. Kurita, M. Takada, K. Osato, Y. Kobayashi, and T. Nishimichi, Power spectrum of intrinsic alignments of galaxies in IllustrisTNG, *J. Cosmol. Astropart. Phys.* **03** (2021) 030.
- [21] D. Sarkar, P. Serra, A. Cooray, K. Ichiki, and D. Baumann, Cosmic shear from scalar-induced gravitational waves, *Phys. Rev. D* **77**, 103515 (2008).
- [22] F. Schmidt and D. Jeong, Large-scale structure with gravitational waves. II. Shear, *Phys. Rev. D* **86**, 083513 (2012).
- [23] F. Schmidt, E. Pajer, and M. Zaldarriaga, Large-scale structure and gravitational waves. III. Tidal effects, *Phys. Rev. D* **89**, 083507 (2014).
- [24] D. Yamauchi, T. Namikawa, and A. Taruya, Weak lensing generated by vector perturbations and detectability of cosmic strings, *J. Cosmol. Astropart. Phys.* **10** (2012) 030.
- [25] M. Biagetti and G. Orlando, Primordial gravitational waves from galaxy intrinsic alignments, *J. Cosmol. Astropart. Phys.* **07** (2020) 005.
- [26] L. Dai, D. Jeong, and M. Kamionkowski, Seeking inflation fossils in the cosmic microwave background, *Phys. Rev. D* **87**, 103006 (2013).
- [27] E. Dimastrogiovanni, M. Fasiello, D. Jeong, and M. Kamionkowski, Inflationary tensor fossils in large-scale structure, *J. Cosmol. Astropart. Phys.* **12** (2014) 050.
- [28] L. H. Ford, Inflation driven by a vector field, *Phys. Rev. D* **40**, 967 (1989).
- [29] T. Koivisto and D. F. Mota, Vector field models of inflation and dark energy, *J. Cosmol. Astropart. Phys.* **08** (2008) 021.
- [30] P. W. Graham, J. Mardon, and S. Rajendran, Vector dark matter from inflationary fluctuations, *Phys. Rev. D* **93**, 103520 (2016).
- [31] A. Golovnev, V. Mukhanov, and V. Vanchurin, Vector inflation, *J. Cosmol. Astropart. Phys.* **06** (2008) 009.
- [32] S. Alexander, A. Marcianò, and D. Spergel, Chern-Simons inflation and baryogenesis, *J. Cosmol. Astropart. Phys.* **13** (2013) 046.
- [33] E. McDonough and S. Alexander, Observable chiral gravitational waves from inflation in string theory, *J. Cosmol. Astropart. Phys.* **11** (2018) 030.
- [34] S. Alexander, E. McDonough, and D. N. Spergel, Chiral gravitational waves and baryon superfluid dark matter, *J. Cosmol. Astropart. Phys.* **05** (2018) 003.
- [35] S. Alexander, E. McDonough, and R. Sims, V-mode polarization in axion inflation and preheating, *Phys. Rev. D* **96**, 063506 (2017).
- [36] Y. Akrami, F. Arroja, M. Ashdown, J. Aumont, C. Baccigalupi *et al.* (Planck Collaboration), Planck 2018 results. X. Constraints on inflation, *Astron. Astrophys.* **641**, A10 (2020).
- [37] C. Armendáriz-Picón, Could dark energy be vector-like?, *J. Cosmol. Astropart. Phys.* **07** (2004) 007.
- [38] S. Alexander and N. Yunes, Chern-Simons modified general relativity, *Phys. Rep.* **480**, 1 (2009).
- [39] R. Jackiw and S. Y. Pi, Chern-Simons modification of general relativity, *Phys. Rev. D* **68**, 104012 (2003).

- [40] S. Alexander, R. Brandenberger, and J. Froehlich, Tracking dark energy from axion-gauge field couplings, [arXiv:1601.00057](#).
- [41] L. Pogosian and M. Wyman, B-modes from cosmic strings, *Phys. Rev. D* **77**, 083509 (2008).
- [42] G. R. Vincent, M. Hindmarsh, and M. Sakellariadou, Correlations in cosmic string networks, *Phys. Rev. D* **55**, 573 (1997).
- [43] A. Vilenkin and E. P. S. Shellard, *Cosmic Strings and Other Topological Defects* (Cambridge University Press, 2000).
- [44] EPTA Collaboration, The second data release from the European Pulsar Timing Array: V. Implications for massive black holes, dark matter and the early Universe, [arXiv:2306.16227](#).
- [45] D. J. Reardon *et al.*, Search for an isotropic gravitational-wave background with the Parkes Pulsar Timing Array, *Astrophys. J. Lett.* **951**, L6 (2023).
- [46] H. Xu *et al.*, Searching for the nano-hertz stochastic gravitational wave background with the Chinese Pulsar Timing Array Data Release I, *Res. Astron. Astrophys.* **23**, 075024 (2023).
- [47] EPTA Collaboration, The second data release from the European Pulsar Timing Array III. Search for gravitational wave signals, *Astron. Astrophys.* **678**, A50 (2023).
- [48] NANOGrav Collaboration, The NANOGrav 15 yr data set: Evidence for a gravitational-wave background, *Astrophys. J. Lett.* **951**, L8 (2023).
- [49] S. Alexander, Inflationary birefringence and baryogenesis, *Int. J. Mod. Phys. D* **25**, 1640013 (2016).
- [50] H. Abedi, M. Ahmadvand, and S. S. Gousheh, Electro-weak baryogenesis via chiral gravitational waves, *Phys. Lett. B* **786**, 35 (2018).
- [51] O. H. E. Philcox, Probing parity violation with the four-point correlation function of BOSS galaxies, *Phys. Rev. D* **106**, 063501 (2022).
- [52] G. Cabass, M. M. Ivanov, and O. H. E. Philcox, Colliders and ghosts: Constraining inflation with the parity-odd galaxy four-point function, *Phys. Rev. D* **107**, 023523 (2023).
- [53] C. Creque-Sarbinowski, S. Alexander, M. Kamionkowski, and O. Philcox, Parity-violating trispectrum from Chern-Simons gravity, *J. Cosmol. Astropart. Phys.* **11** (2023) 029.
- [54] O. H. E. Philcox, Do the CMB temperature fluctuations conserve parity?, *Phys. Rev. Lett.* **131**, 181001 (2023).
- [55] R. N. Cahn, Z. Slepian, and J. Hou, Test for cosmological parity violation using the 3D distribution of galaxies, *Phys. Rev. Lett.* **130**, 201002 (2023).
- [56] J. Hou, Z. Slepian, and R. N. Cahn, Measurement of parity-odd modes in the large-scale 4-point correlation function of Sloan Digital Sky Survey Baryon Oscillation Spectroscopic Survey twelfth data release CMASS and LOWZ galaxies, *Mon. Not. R. Astron. Soc.* **522**, 5701 (2023).
- [57] A. Lue, L. Wang, and M. Kamionkowski, Cosmological signature of new parity-violating interactions, *Phys. Rev. Lett.* **83**, 1506 (1999).
- [58] Y. Minami and E. Komatsu, New extraction of the cosmic birefringence from the Planck 2018 polarization data, *Phys. Rev. Lett.* **125**, 221301 (2020).
- [59] T. Liu, X. Tong, Y. Wang, and Z.-Z. Xianyu, Probing P and CP violations on the cosmological collider, *J. High Energy Phys.* **04** (2020) 189.
- [60] G. Cabass, S. Jazayeri, E. Pajer, and D. Stefanyzyn, Parity violation in the scalar trispectrum: No-go theorems and yes-go examples, *J. High Energy Phys.* **02** (2023) 021.
- [61] V. Ajani, M. Baldi, A. Barthelemy, A. Boyle, P. Burger *et al.* (Euclid Collaboration), Euclid preparation XXIX: Forecasts for 10 different higher-order weak lensing statistics, *Astron. Astrophys.* **675**, A120 (2023).
- [62] O. H. E. Philcox and M. C. Johnson, Novel cosmological tests from combining galaxy lensing and the polarized Sunyaev-Zel'dovich effect, *Phys. Rev. D* **106**, 083501 (2022).
- [63] T. Kurita and M. Takada, Constraints on anisotropic primordial non-Gaussianity from intrinsic alignments of SDSS-III BOSS galaxies, *Phys. Rev. D* **108**, 083533 (2023).
- [64] C. Fedeli, M. Bartelmann, and L. Moscardini, Constraining primordial non-Gaussianity with cosmological weak lensing: shear and flexion, *J. Cosmol. Astropart. Phys.* **10** (2012) 018.
- [65] D. J. Bacon, D. M. Goldberg, B. T. P. Rowe, and A. N. Taylor, Weak gravitational flexion, *Mon. Not. R. Astron. Soc.* **365**, 414 (2006).
- [66] D. M. Goldberg and D. J. Bacon, Galaxy-galaxy flexion: Weak lensing to second order, *Astrophys. J.* **619**, 741 (2005).
- [67] E. J. Arena, D. M. Goldberg, and D. J. Bacon, Cosmic flexion, *Phys. Rev. D* **105**, 123521 (2022).
- [68] Y. Okura, K. Umetsu, and T. Futamase, A method for weak-lensing flexion analysis by the HOLICs moment approach, *Astrophys. J.* **680**, 1 (2008).
- [69] Y. Okura, K. Umetsu, and T. Futamase, A new measure for weak-lensing flexion, *Astrophys. J.* **660**, 995 (2007).
- [70] E. S. Giesel, B. Ghosh, and B. M. Schaefer, Intrinsic and extrinsic gravitational flexions, *Mon. Not. R. Astron. Soc.* **510**, 2773 (2022).
- [71] D. Munshi, J. Smidt, A. Heavens, P. Coles, and A. Cooray, Higher order statistics of weak lensing shear and flexion, *Mon. Not. R. Astron. Soc.* **411**, 2241 (2011).
- [72] C.-P. Ma and E. Bertschinger, Cosmological perturbation theory in the synchronous and conformal Newtonian gauges, *Astrophys. J.* **455**, 7 (1995).
- [73] H. Kodama and M. Sasaki, Cosmological perturbation theory, *Prog. Theor. Phys. Suppl.* **78**, 1 (1984).
- [74] V. F. Mukhanov, H. A. Feldman, and R. H. Brandenberger, Theory of cosmological perturbations, *Phys. Rep.* **215**, 203 (1992).
- [75] W. Hu and M. White, CMB anisotropies: Total angular momentum method, *Phys. Rev. D* **56**, 596 (1997).
- [76] L. Dai, M. Kamionkowski, and D. Jeong, Total angular momentum waves for scalar, vector, and tensor fields, *Phys. Rev. D* **86**, 125013 (2012).
- [77] W. Hu and M. J. White, CMB anisotropies: Total angular momentum method, *Phys. Rev. D* **56**, 596 (1997).
- [78] K. Ichiki, K. Takahashi, and N. Sugiyama, Constraint on the primordial vector mode and its magnetic field generation from seven-year Wilkinson microwave anisotropy probe observations, *Phys. Rev. D* **85**, 043009 (2012).

- [79] M. Tristram, A. J. Banday, K. M. Górski, R. Keskitalo, C. R. Lawrence, K. J. Andersen *et al.*, Improved limits on the tensor-to-scalar ratio using BICEP and Planck data, *Phys. Rev. D* **105**, 083524 (2022).
- [80] M. Hindmarsh, Small-scale microwave background fluctuations from cosmic strings, *Astrophys. J.* **431**, 534 (1994).
- [81] C. J. A. P. Martins and E. P. S. Shellard, Quantitative string evolution, *Phys. Rev. D* **54**, 2535 (1996).
- [82] K. Takahashi, A. Naruko, Y. Sendouda, D. Yamauchi, C.-M. Yoo, and M. Sasaki, Non-Gaussianity in the cosmic microwave background temperature fluctuations from cosmic (super-)strings, *J. Cosmol. Astropart. Phys.* **10** (2009) 003.
- [83] T. Hamana, M. Shirasaki, S. Miyazaki, C. Hikage, M. Oguri, S. More *et al.*, Cosmological constraints from cosmic shear two-point correlation functions with HSC survey first-year data, *Publ. Astron. Soc. Jpn.* **72** (2020) 16.
- [84] F. Schmidt and D. Jeong, Cosmic rulers, *Phys. Rev. D* **86**, 083527 (2012).
- [85] F. Schmidt, N. E. Chisari, and C. Dvorkin, Imprint of inflation on galaxy shape correlations, *J. Cosmol. Astropart. Phys.* **10** (2015) 032.
- [86] B. Ghosh, R. Durrer, and B. M. Schäfer, Intrinsic and extrinsic correlations of galaxy shapes and sizes in weak lensing data, *Mon. Not. R. Astron. Soc.* **505**, 2594 (2021).
- [87] K. Akitsu, T. Kurita, T. Nishimichi, M. Takada, and S. Tanaka, Imprint of anisotropic primordial non-Gaussianity on halo intrinsic alignments in simulations, *Phys. Rev. D* **103**, 083508 (2021).
- [88] K. Akitsu, Y. Li, and T. Okumura, Quadratic shape biases in three-dimensional halo intrinsic alignments, *J. Cosmol. Astropart. Phys.* **08** (2023) 068.
- [89] K. Akitsu, Y. Li, and T. Okumura, Gravitational wave fossils in nonlinear regime: Halo tidal bias and intrinsic alignments from gravitational wave separate universe simulations, *Phys. Rev. D* **107**, 063531 (2023).
- [90] N. Kaiser, G. Squires, and T. Broadhurst, A method for weak lensing observations, *Astrophys. J.* **449**, 460 (1995).
- [91] E. M. Huff and G. J. Graves, Magnificent magnification: Exploiting the other half of the lensing signal, *Astrophys. J. Lett.* **780**, L16 (2014).
- [92] C. M. Hirata and U. Seljak, Reconstruction of lensing from the cosmic microwave background polarization, *Phys. Rev. D* **68**, 083002 (2003).
- [93] F. Schmidt, E. Rozo, S. Dodelson, L. Hui, and E. Sheldon, Lensing bias in cosmic shear, *Astrophys. J.* **702**, 593 (2009).
- [94] D. N. Limber, The analysis of counts of the extragalactic nebulae in terms of a fluctuating density field, *Astrophys. J.* **117**, 134 (1953).
- [95] P. Lemos, A. Challinor, and G. Efstathiou, The effect of Limber and flat-sky approximations on galaxy weak lensing, *J. Cosmol. Astropart. Phys.* **05** (2017) 014.
- [96] M. LoVerde and N. Afshordi, Extended Limber approximation, *Phys. Rev. D* **78**, 123506 (2008).
- [97] X. Fang, E. Krause, T. Eifler, and N. MacCrann, Beyond Limber: Efficient computation of angular power spectra for galaxy clustering and weak lensing, *J. Cosmol. Astropart. Phys.* **05** (2020) 010.
- [98] M. Kilbinger, C. Heymans, M. Asgari, S. Joudaki, P. Schneider, P. Simon *et al.*, Precision calculations of the cosmic shear power spectrum projection, *Mon. Not. R. Astron. Soc.* **472**, 2126 (2017).
- [99] K. W. Masui, U.-L. Pen, and N. Turok, Two- and three-dimensional probes of parity in primordial gravity waves, *Phys. Rev. Lett.* **118**, 221301 (2017).
- [100] R. Laureijs, J. Amiaux, S. Arduini, J. L. Auguères, J. Brinchmann, R. Cole *et al.*, Euclid definition study report, [arXiv:1110.3193](https://arxiv.org/abs/1110.3193).
- [101] A. Chudaykin and M. M. Ivanov, Measuring neutrino masses with large-scale structure: Euclid forecast with controlled theoretical error, *J. Cosmol. Astropart. Phys.* **11** (2019) 034.
- [102] R. E. Smith, J. A. Peacock, A. Jenkins, S. D. M. White, C. S. Frenk, F. R. Pearce, P. A. Thomas, G. Efstathiou, and H. M. P. Couchman, Stable clustering, the halo model and non-linear cosmological power spectra, *Mon. Not. R. Astron. Soc.* **341**, 1311 (2003).
- [103] M. Tegmark, A. N. Taylor, and A. F. Heavens, Karhunen-Loève eigenvalue problems in cosmology: How should we tackle large data sets?, *Astrophys. J.* **480**, 22 (1997).
- [104] P. Schneider, The consequences of parity symmetry for higher-order statistics of cosmic shear and other polar fields, *Astron. Astrophys.* **408**, 829 (2003).
- [105] E. G. M. Ferreira, Ultra-light dark matter, *Astron. Astrophys. Rev.* **29**, 7 (2021).
- [106] L. Hui, J. P. Ostriker, S. Tremaine, and E. Witten, Ultra-light scalars as cosmological dark matter, *Phys. Rev. D* **95**, 043541 (2017).
- [107] W. Hu, R. Barkana, and A. Gruzinov, Cold and fuzzy dark matter, *Phys. Rev. Lett.* **85**, 1158 (2000).
- [108] P. Mocz *et al.*, Cosmological structure formation and soliton phase transition in fuzzy dark matter with axion self-interactions, *Mon. Not. R. Astron. Soc.* **521**, 2608 (2023).
- [109] T. Dome, A. Fialkov, P. Mocz, B. M. Schäfer, M. Boylan-Kolchin, and M. Vogelsberger, On the cosmic web elongation in fuzzy dark matter cosmologies: Effects on density profiles, shapes, and alignments of haloes, *Mon. Not. R. Astron. Soc.* **519**, 4183 (2022).
- [110] M. A. Amin, M. Jain, R. Karur, and P. Mocz, Small-scale structure in vector dark matter, *J. Cosmol. Astropart. Phys.* **08** (2022) 014.
- [111] J. N. Goldberg, A. J. Macfarlane, E. T. Newman, F. Rohrlich, and E. C. G. Sudarshan, Spin-s spherical harmonics, *J. Math. Phys. (N.Y.)* **8**, 2155 (1967).
- [112] W. Hu, Weak lensing of the CMB: A harmonic approach, *Phys. Rev. D* **62**, 043007 (2000).